POOL BOILING HEAT TRANSFER CHARACTERISTICS OF NANOFLUIDS AND NANOCOATINGS

by

SANG MUK KWARK

Presented to the Faculty of the Graduate School of
The University of Texas at Arlington in Partial Fulfillment
of the Requirements
for the Degree of

DOCTOR OF PHILOSOPHY

THE UNIVERSITY OF TEXAS AT ARLINGTON
December 2009

ACKNOWLEDGEMENTS

I would like to acknowledge the friendship and technical support of my fellow lab members. I especially want to thank Dr. Seung Mun You, who served as my supervisor and counselor through my doctoral research. His dedication has truly helped to motivate and inspire me all the time. Also, I would like to extend my gratitude to Dr. Ratan Kumar, Dr. Gilbert Moreno, Dr. Muguel Amaya, Dr. Choong-un Kim, and material science lab fellows for their advice and help on present study. Most of all, I gratefully acknowledge the support and encouragement of my beloved wife, Yoo Kyoung Song. She always encouraged me during this study not only as a wife but also as a mentor. I will never find the words for a little daughter, Eunseo Kwark. Her smile makes me always feel a full of energy. Finally, I want to thank my parents and parents in law for their support and encouragement.

.

November 19, 2009

ABSTRACT

POOL BOILING HEAT TRANSFER CHARACTERISTICS

OF NANOFLUIDS AND NANOCOATINGS

Sang Muk Kwark, Ph.D.

The University of Texas at Arlington, 2009

Supervising Professor: Seung Mun You

This research is a qualitative and quantitative investigation to understand the behaviors of nanofluids and nanocoated surfaces during pool boiling heat transfer. The pool boiling behavior of low concentration nanofluids, a mixture created by dispersing nanoparticles in pure water, was experimentally studied over a flat heater. A majority of this work was conducted using Al_2O_3 nanoparticles dispersed in water and some minor work was performed with others (CuO and diamond nanoparticles). Results from this study are consistent with those previously reported in demonstrating that boiling of nanofluids produces a nanocoating on the heater surface, and which in turn increases the critical heat flux (CHF). This study also investigates the possible causes responsible for the deposition of nanoparticles on the heater surface. Through experimental, it was shown that microlayer evaporation, during nanofluid boiling, was responsible for the nanoparticle coating formed on the heater surfaces. Subjecting the heater surfaces to extended periods of nanofluid boiling has shown an eventual degradation in BHT that has been attributed to modifications in surface conditions that are continuously being altered through additional nanoparticle deposition. The wetting and wicking characteristics of

the nanocoating are investigated by measuring the apparent contact angle and by conducting vertical dip test. It is found that the CHF enhancement mechanism is dominated by the wetting characteristics of the nanocoating and a relationship between the quasi-static contact angle and the CHF value is provided.

The fundamental pool boiling test of nanofluid exhibited some unique characteristics like an enhanced CHF, transient boiling behaviors, and nanoparticle deposition on the heater surface. After this fundamental study, further investigation was conducted to understand the effects of the nanocoating in pool boiling heat transfer. The thickness and the uniformity of the nanocoating dictated the BHT and the CHF conditions based on this. A methodology for an optimal nanocoating development is provided. The optimal nanocoating provided unique pool boiling characteristics and was generated by controlling the thickness and uniformity of the nanoparticle precipitation on the heater's surface. Parametric tests on pool boiling using this nanocoated surface are investigated. The parametric test involved variations in nanoparticle size, system pressure, heater orientation, and heater size. For this, different Al_2O_3 nanoparticles sizes (75 ± 50, 139 ± 100, and 210 nm ± 200 nm), system pressures (20 ~ 200 kPa), heater orientations (0 ~ 180º), and heater sizes (0.75 × 0.75 ~ 2 cm × 2 cm) were used. Results indicate that the pool boiling performance is dependent on the parameters tested, except the particle size, for both uncoated and nanocoated surfaces. The nanoparticle coated heater consistently showed a dramatic CHF enhancement relative to the uncoated surface at all tested conditions.

TABLE OF CONTENTS

LIST OF ILLUSTRATIONS

LIST OF TABLES

NOMENCLATURE

A	area, [m^2]
BHT	boiling heat transfer
Bo	bond number
CHF	Critical Heat Flux
c_p	specific heat, [J/kgK]
C_{sf}	fluid-surface combination coefficient
d_d	bubble departure diameter, [m]
f	frequency, [1/s]
g	gravitational acceleration, [m/s]
h	heat transfer coefficient, [W/m^2K]
h_{fg}	latent heat of vaporization, [J/kg]
Ja	jakob number
k	thermal conductivity, [W/mK]
L	length, [m]
L’	dimensionless length
N_j	number of vapor jets
Pr	prandtl number
q”	heat flux, [kW/m^2]
t	time, [sec.]
ΔT_{sat}	wall superheat, $T_w - T_{sat}$ (P_{sys})

Greek symbols

μ	dynamic viscosity, [kg/ms]
ν	kinematic viscosity, [m^2/s]
ρ	density, [kg/m^3]
σ	surface tension, [N/m]
θ	angle, [deg.]

Subscripts

d	diameter
g	vapor
H	heater
l	liquid
w	heater surface (wall)
sat	saturated

CHAPTER 1

INTRODUCTION

The critical need to create new materials with advanced thermal properties has generated a lot of interest in nanofluids. Research on nanofluids, a colloidal mixture consisting of nanosized particles dispersed in a fluid medium, has provided a glut of information about the thermal properties for this potentially promising cooling fluid. Results from these studies have reported enhancements to the thermal properties, particularly the thermal conductivity. Recently, nanofluids have been used for two phase (boiling) heat transfer and they have shown a dramatic critical heat flux (CHF) enhancement over the base fluid. It is well known that two phase heat transfer is highly efficient mode of heat dissipation but its implementation can be restricted as a result of the critical heat flux (CHF) phenomenon. CHF essentially limits the heat flux dissipation potential of two phase (boiling) heat transfer and exceeding this CHF limit may result in component damage. This makes nanofluids a great candidate for high heat flux applications. Ever since the seminal work by You et al. [1] in reporting a CHF enhancement of almost 200%, there have been several publications to confirm and explain this augmentation. To make a fair analysis of this experimental study, a literature review of the thermal studies on nanofluids is discussed below.

1.1 Thermo-physical Properties of Nanofluids (Literature Review)

Conventional heat transfer fluids have inherently poor heat transfer properties compared to most solids. Recent research into nanofluids has shown an impressive gain in some thermal properties. Thermal properties like thermal conductivity, viscosity, and surface tension have received both theoretical as well as experimental attention.

1.1.1 Thermal Conductivity

Metallic solids possess an order of magnitude higher thermal conductivity than fluids. It is, therefore, expected that the thermal conductivity of fluids containing suspended solid metallic or nonmetallic particles would be significantly higher than those of pure heat transfer fluids. Through the last decade, numerous studies on nanofluids have shown that an enhancement in its thermal conductivity can be produced by varying the nanoparticles concentration, material, particle size, and shape as well by altering the base fluid, temperature, additive, and acidity. In one of the earliest nanofluid experimental studies, Masuda et al. [2], reported 20% ~ 30% enhancement in the thermal conductivity of water by adding 13 nm Al_2O_3 nanoparticles (~ 4.3% vol.) at 32°C ~ 66°C. They reported that the enhancement was a function of the concentration and this trend is further supported by Lee et al. [3]. Similarly, Xie et al. [4] observed that thermal conductivity enhancement using Al_2O_3 nanoparticles with water, ethylene glycol, and pump oil as base fluids were ~21%, ~30%, and ~38%, respectively, over the pure base fluid. They concluded that the enhancement ratio of the thermal conductivity of the nanofluid to that of pure fluid is reduced with increasing thermal conductivity of the base fluid. Das et al. [5] investigated the temperature effect on the thermal conductivity enhancement of nanofluids (water-based Al_2O_3 - 38.4 nm and CuO - 28.6 nm). Their experimental results showed that the thermal conductivity increased with an increase in temperature. Similar results were further reported by other researchers [6, 7] who used different conditions. Recently, Kim et al. [8] showed that there

is very little thermal conductivity change of nanofluid at the low volume concentration (≤ 0.1% vol.).

Analytical models were also developed to predict the effective thermal conductivity of solid particle suspension [9-13] in a liquid. However, such classical models were unable to predict the anomalously high thermal conductivity of nanofluids. Recently, an improved model was developed by Leong et al. [14] that included both the static and the dynamic mechanisms such as particle size, nanolayer, particle movement, particle surface chemistry, and interaction potential. Although their model appears to fit better with their experimental results, it is not valid for a wide range of previously reported results.

1.1.2 Viscosity

Viscosity is another critical thermo-physical property of fluids. It affects the wetting characteristic of liquid on the heated surface during the boiling heat transfer. Masuda et al. [2] performed a viscosity measurement of water-based TiO_2 nanofluid. They reported that viscosity increases with increasing nanoparticle concentration by as much as ~60% using a 4.3% volumetric loading. Similar results have been further reported by several researchers [15-17]. Prasher et al. [16] have studied the effects of particle size and fluid temperature and reported that the viscosity is largely independent of the diameter of nanoparticles and does not vary significantly with temperature. For the relatively low concentration of nanoparticles (≤ 0.1% vol.), Kim et al. [8] reported that there is practically no viscosity change.

Analytical studies on the effective viscosity of the particle-liquid mixtures are almost as extensive as the ones on the effective thermal conductivity. Einstein [18] was the first to calculate the effective viscosity of a suspension of spheres on the basis of the phenomenological hydrodynamic equations. Since Einstein's work, researchers have made progress in extending the theory [17, 19-21]. However, theoretical predictions have not yet clearly explained the anomalous viscosity increase of nanofluids.

1.1.3 Surface Tension

Surface tension has a significant influence on the boiling process since bubble departure and interfacial equilibrium depends on it. However, there are just a few studies available on the surface tension of nanofluids. Jeong et al. [6] observed that surface tension decreases as the concentration of the nanofluid increases (0.5 ~ 4% vol. of Al_2O_3). However, Kim et al. [8] reported that the surface tension did not show a significant change at room temperature using Al_2O_3, ZrO_2, and SiO_2 nanoparticles (up to 0.1% vol.). Recently, Golubovic et al. [22] further supported this insensitivity of the surface tension at the very low Al_2O_3 concentration (≤ 0.01 g/l).

1.2 Pool Boiling in Nanofluids (Literature Review)

One of the unique characteristics of nanofluid is that it can enhance the critical heat flux (CHF) by 200 ~ 300% [1, 23]. This makes nanofluids a potential candidate for high heat flux boiling since CHF is known to be a limiting factor for heat dissipation in two phase boiling heat transfer. You et al.'s [1] initial study reporting a 200% CHF enhancement using alumina-water nanofluids was quickly followed by a similar study by Vassallo et al. [25] who also reported significant CHF enhancement using silica-water nanofluids. Since these initial findings, many other studies have also reported CHF enhancement using nanofluids composed of various nanoparticles types and base fluids. A majority of the pool boiling studies using nanofluids have looked at parameters like the boiling heat transfer (BHT) coefficient and the CHF values. Table 1.1 provides a synopsis of the various studies performed involving pool boiling of nanofluids.

Table 1.1 Boiling heat transfer of nanofluids.

Author	Nanofluid(s)	Heater	Concen-tration.	Max. CHF Enhanced	BHT Coeff-icient.
You et al. [1], (2003)	Al_2O_3-water, 32 nm	1 cm x 1 cm	0.001 ~ 0.05 g/l	200% 160%	same
Kim et al. [8], (2007)	Al_2O_3-water, 110 ~ 210 nm ZrO-water, 110 ~ 250 nm SiO_2-water, 20 ~ 40 nm	SST OD 0.381 mm, L 12 cm	10^{-3} ~ 10^{-1}% vol.	52% 75% 80%	Decreased
Milanova & Kumar [23], (2005)	SiO_2-water, 10/20 nm	NiCr wire OD 0.32 mm	15/40 % wt	300%	same
Yang & Maa [24], (1984)	Al_2O_3-water, 50/300/1000nm	SST wire OD 3.2 mm	0.1 ~ 0.5% wt.	N/A	Increased
Vassallo et al. [25], (2003)	Silica-water, 15/50/3000 nm	NiCr Wire OD 0.4 mm	0.5% vol.	60%	same
Kim & Kim [26], (2007)	TiO_2-water, 85 nm Al_2O_3-water, 47 nm SiO_2-water, 90 nm TiO_2 coated in water	NiCr wire OD 0.2 mm	10^{-5} ~ 10^{-1}% vol.	100% 60% 160% 160%	N/A
Milanova & Kumar [27], (2008)	SiO_2-water, 18.8/22.5 nm	NiCr wire OD 0.32 mm	0.5% vol.	200%	Marginal
Kim et al. [28], (2004)	Al_2O_3-water, 32 nm	1 cm x 1 cm, Pt wire OD 390μm	0.001 ~ 0.05 g/l	200%	same
Moreno et al. [29], (2005)	Al_2O_3-water, 32 nm ZnO-water, 24 ~ 71 nm	1 cm x 1 cm	0.001 ~ 0.5 g/l	180% 240%	same
Das et al. [30], (2003)	Al_2O_3-water, 38 nm	Cartridge OD 20 mm	0.1 ~ 4% vol.	N/A	Decreased
Bang & Change [31], (2005)	Al_2O_3-water, 47 nm	0.4 cm x 10 cm	0.5 ~ 4% vol.	32%	Decreased
Das et al. [32], (2003)	Al_2O_3-water, 58.4 nm	Tube OD 4/6.5 mm	1 ~ 4% vol.	N/A	Decreased
Bang et al. [33], (2008)	Al_2O_3-Ethanol, 118.2 nm	ITO 24 mm x 10 mm	10^{-2} % vol.	10%	Decreased
Liu & Liao [34], (2008)	CuO-water, 50 nm SiO_2-water, 35 nm CuO-alcohol, 50 nm SiO_2-alcohol, 35 nm	Cond. OD 20 mm flat	0.2 ~ 2% wt.	27% 18% 20% 20%	Marginal Decreased Marginal Decreased
Chopkar et al. [35], (2008)	ZrO_2-water, 20 ~ 25 nm ZrO_2-Surfactant-water	Cond. OD 50.8 mm L110 mm	$5x10^{-3}$ ~ $1.5x10^{-1}$% vol.	N/A	Varied Varied
Tu et al. [36], (2004)	Al_2O_3-water, 38 nm	26 mm x 40 mm, glass heater	0.037 g/l	67%	Increased
Wen & Ding [37], (2005)	Γ- Al_2O_3-water, 167.5 nm	OD 150 mm ring heater	0.32 ~ 1.25% wt	N/A	Increased
Park & Jung [38], (2007)	CNT-R22, OD20/L1000 nm CNT-water,OD20/L1000 nm	Tube(internal) OD 19 mm L152 mm	1% vol.	N/A	Increased
Johnathan & Kim [39], (2008)	Al_2O_3-Alcohol,45 nm Al_2O_3-Alcohol, 45 nm Al_2O_3-Alcohol, 45 nm Al_2O_3-Water, 45 nm	Glass (0.9 cm^2) Cond. Cir. 2 cm^2 Oxidized copper Copper (10 g/l) Copper (0.525 g/l)	0.001 ~ 10 g/l	None 40% 25% 37%	No change Varied Increased Marginal
Sefiane [40], (2006)	Al_2O_3-Ethanol, 10/20 nm	PTFE	1 ~ 5% wt.	N/A	N/A

1.2.1 Nanofluid Pool Boiling with Wire Heater

Historically, Yang and Maa [24] were among the first researchers to perform the boiling experiments with nanofluids as working fluids. They tested three different sizes of Al_2O_3 particles (50 nm, 300 nm, and 1000 nm) in water with varied concentrations (0.1 ~ 0.5% wt.) over a 3.2 mm (OD) stainless steel wire heater at 1atm. They reported no differences in the natural convention region (< 70 kW/m^2) between the nanofluid and pure water. However, they observed a better heat transfer coefficient for nanofluids in the nucleate boiling region. As the concentration increased to 0.5% wt., the boiling heat transfer coefficient increased by ~100% when compared to pure water. In addition, the heat transfer enhancement was more effective when the smaller particle size was used at 0.1% wt. concentration, but the size effect disappeared with 0.5% wt. nanofluid. They attributed this to the disturbance in the thermal boundary layer due to nanoparticle movement. Vassallo et al. [25] reported interesting results, showing ~60% CHF enhancement using silica-water nanofluids (0.5% vol.) without any change in the heat transfer on a OD 0.4 mm NiCr wire heater. Results similar to those obtained by Vassallo et al. [25], were also obtained by Milanova and Kumar [23] who tested with SiO_2 (10 / 20 nm) nanoparticles dispersed in water with a NiCr wire heater (0.32 mm OD). They reported ~300% CHF enhancement in nanofluids without change of heat transfer coefficient. Higher pH levels (up to 12.3) were observed to increase CHF while acidic solutions lowered CHF. While the degree of reported CHF enhancement has varied, several studies have confirmed the nanofluid's ability to increase CHF remarkably [8, 26, 27]. Kim et al. [8] investigated the role played by the nanoparticle deposition on the heater surface and the CHF enhancement that is brought about by enhancing the wetting characteristics. They explored prevailing CHF theories to indicate a positive relationship between the CHF value and the wettability of the heater surface (measured by the static contact angle over the heater surface). However, they observed that the boiling heat transfer coefficient deteriorated (~20% at 1000 kW/m^2) with the addition of nanoparticles (10^{-3} ~ 10^{-1}% vol.). They attributed the CHF enhancement and nucleate boiling

deterioration to a deposited layer of nanoparticles that developed during boiling experiments. This layer played an important role in enhancing the surface wettability and increasing the thermal resistance. Similar results obtained by Kim et al. [8] were reported by Kim and Kim [26] using water-based TiO_2, Al_2O_3, and SiO_2 nanofluids with concentrations from 10^{-5} to 10^{-1}% vol. They observed nanoparticle deposition on the heated surface and a significant CHF enhancement up to ~160%. Interestingly, when the nanocoated wire heater was then tested in the boiling of pure water, the CHF increased by up to two fold, demonstrating CHF enhancement is caused by surface modification. Furthermore, they reported that nanofluids could actually have a lower CHF than the pure fluids given the appropriate surface treatment.

1.2.2 Nanofluid Pool Boiling with Flat Heater

Only a few studies have been performed for pool boiling experiments on flat heater surface (Table 1). You et al. [1] and Kim et al. [28] were among the first to study nanofluid boiling with a flat square heater (1 cm x 1 cm). They dispersed 0.025 g/l of Al_2O_3 in water and reported ~200% enhancement in the CHF of nanofluid with no significant change in the boiling heat transfer (BHT) at T_{sat}=60°C. Moreno et al. [29] reported similar trends in higher CHF (240%) by adding zinc oxide (ZnO) nanoparticles to water. They also reported a 120% increase in the CHF of an aqueous ethylene glycol-based Al_2O_3 nanofluid with a 0.025 g/l concentration at T_{sat}=60°C.

1.2.3 Nanofluid Pool Boiling with Other Heater Geometries

Nanofluid boiling experiments utilizing various heater geometries such as cartridge, tube, glass, ring, thin-long, and conduction heater have also been conducted. A majority have shown a CHF enhancement with nanofluids. However, BHT results are inconsistent (decrease/no-change/increase). Most studies have shown a degradation of the heat transfer rate with nanofluids [30-34]. Das et al. [30] investigated the effect of Al_2O_3-water nanofluids on the cylindrical cartridge heater. They observed a deterioration in BHT with the addition of

nanoparticles (0.1 ~ 4% vol.) and claimed that it could be due to the surface smoothening of heaters by the nanoparticle deposition on them. They inferred that during the boiling process nanoparticles deposit on the heater surface and block out the nucleation sites. Bang and Chang [31], Bang et al. [33], and Liu and Liao [34] have also shown the performance decrease of BHT on the 0.4 cm x 10 cm, ITO (Indium Tin Oxide) 24 mm x 10 mm, OD 20 mm conduction heater, respectively. The studies [30-34] mentioned above have reported sizable CHF enhancement, and indicated that the nanoparticle deposition is responsible for that enhancement. This observation is supported by Kim et al. [8] in stating that the deposition layer is working as both a thermal resistance layer and a better wetting surface.

On the other hand, Chopkar et al. [35] observed that the BHT increased by ~100% at low concentration of nanoparticles (0.005% vol. of ~20 nm ZrO_2). They also reported that the BHT performance of water and nanofluids increased with the addition of an ionic surfactant due to a decrease in bubble size. However, they observed that the BHT decreased as the concentration of nanopaticles further increased. Like Das et al. [30], they attributed this to surface smoothening which results in a decrease in the number of nucleation sites. A BHT enhancement trend using nanofluids has been further reported by Tu et al., [36], Wen and Ding [37], and Park and Jung [38]. Their experiments used various nanoparticles and heaters: Al_2O_3 (38 nm), γ- Al_2O_3, and CNT (OD 20 nm/ L 1000 nm) on a 26 mm x 40 mm glass heater, OD 150 mm ring heater, and OD 19 mm tube heater, respectively. Most recently, Johnathan and Kim [39] conducted boiling experiments with two different working fluids, Al_2O_3-water and Al_2O_3-alcohol. They found that performance was highly dependent on both the nanoparticle concentration and fluid/surface wetting characteristics. The CHF enhancement mechanism with nanofluids appears to be an improvement in the ability of the fluid to wet the surface. Poorly wetting systems (e.g. water on polished copper) enhanced CHF (~37%) by the addition of nanoparticles, whereas better wetting systems (e.g. ethanol on glass) showed no improvement or a larger degradation on CHF.

1.3 Parametric Effects of Pool Boiling Heat Transfer (Literature Review)

One of the important fundamental tests that are typically performed during the investigation of pool boiling of any fluid or fluid mixture is the effect of system variables. However, a parametric study of the pool boiling study of water using a nanoparticle coated heater has not been performed. Such a study has been done in this work and to make an analysis, a literature review of the role played by the selected parameters during boiling of pure liquid is discussed below.

1.3.1 Effect of Pressure

The effect of pressure on the pool boiling of fluids has long been established. Pressure affects both the BHT and the CHF by influencing the vapor density, the latent heat of vaporization, and the surface tension of the working fluid. Numerous researches report an increase in the BHT coefficient and the CHF with increased pressure. Cichelli and Bonilla [41] studied the effects of the pressure on the BHT using various fluids including water, ethanol, benzene, and propane over the flat surface. With increased pressure, they observed the boiling curve to shift to the left in the nucleate boiling regime and an increase of CHF value. Similar results were obtained with the circular flat heater using various refrigerants (Freon, R11, R113, R21, and R114) by Nishikawa et al. [42]. They attributed this behavior to an increased range of cavity radius that may be activated at a given wall superheat with increased pressure (increased active nucleation site density). They explained that the poorer performance of the heat transfer mechanisms at low pressure could be attributed to a lower vapor densities and larger bubbles. The lower pressure increases the critical site radius on a surface. This tends to decrease the number of active bubble nucleation sites and increases the wall superheat which allows bubbles to depart from the surface. This is further supported for various fluids by other literature [43-46]. Like the BHT enhancement, the CHF value also shows an increasing trend with increased pressure, as reported in many studies [44-48]. Mudawar and Anderson [46] observed that an

increase in pressure results in higher CHF values using water as a working fluid. They attributed this primarily to the increase in the vapor density. An increase in the density of the vapor allows more energy to be removed from the surface for the same volume of vapor departing. Kazakova [49] found that the CHF value continues to increase with pressure till 40% of the critical pressure of the liquid and decreases beyond that critical value.

1.3.2 Effect of Orientation

The heater surface inclination has also shown to affect both the BHT and the CHF. Several researchers [50-53] have observed that heat transfer rate, for a given wall superheat, increases when the heating surface is rotated from horizontal to vertical. Marcus and Dropkin [51] attributed this to increased agitation of the superheated boundary region due to the increased path length of the departing bubbles along the surface. Githinji and Sabersky [52] hypothesized that after a certain heat flux the heat transfer coefficient would not be affected by the orientation and Nishikawa et al. [54] confirmed the existence of this transition heat flux. However, Jung et al. [55] and Beduz et al. [56] have shown an angular independence of BHT for enhanced surfaces. Chang and You [53] further supported this insensitivity of the inclination using a microporous surface in FC-72 and attributed this to the higher number of active nucleation sites provided by the surface microstructure. Githinji and Sabersky [52] studied the effect of inclination angle on CHF. Using long-thin heater (10.16 cm x 0.32 cm), they found that CHF increased from 0° to 90° and then decreased drastically from 90° to 180°. This trend has also been the observed and reported in other literature [53, 57].

1.3.3 Effect of Heater Size

The effect of heater size on pool boiling performance has been investigated by many researchers. Baker [58] observed that the BHT increased with a decrease of heater size. On the other hand, Park and Bergles [59] reported that the BHT was insensitive to the heater size.

Kutateladze and Gogonin [60] conducted experiments by varying the heater size to estimate the effect on CHF of ethanol at an orientation of 0° (horizontal, facing upwards) and 180° (facing downwards). They reported that CHF is insensitive to the heater size at an inclination angle of 0°. However, CHF decreased with increased heating area at the facing downwards orientation. Similar reduction in CHF for water was reported by Ishigai et al. [61] at 180º angle using water as a test fluid. Lienhard et al. [62] experimented with various fluids and showed both experimentally and analytically that CHF decreases with increase in heater size up to a point after which the reduction in CHF is less affected by heater size. They attributed this decrease in CHF to the number of “vapor jets” that can be present on the heater’s surface area. In addition, Park and Bergles [59] also found that CHF was affected by changes in heater height and width which is similar to those observed by Saylor et al. [63].

1.4 Objectives

The general objective of this present study is to further the understanding of thermal behavior of nanofluids and nanocoatings during pool boiling heat transfer. The literature review provided ahead, shows a strong interest in this area and several studies have been conducted to understand the BHT and the CHF during nanofluid pool boiling. Almost all such pool boiling studies with nanofluids have attributed an enhanced CHF to a significant nanoparticle deposition on the heater. However, the fundamental mechanisms behind the CHF enhancement and the BHT variation are not fully understood. The current work is motivated to carry out a comprehensive study to understand this phenomenon. It is based on the premise that only very low concentration nanofluids (water based, 0.001 ~ 1 g/l) have shown maximum CHF enhancements. At these low concentrations the thermo-physical properties of nanofluid, including thermal conductivity, viscosity, and surface tension, show very little change from the properties of its base fluid. As such the focus of the investigation is on the nanoparticle deposition and how it affects the BHT and CHF. The mechanism responsible for the

nanoparticle deposition and the corresponding wetting behavior of the deposited layer are studied. Nanocoating optimization study is also undertaken that shows the best boiling performance (BHT and CHF). Finally, a parametric investigation (involving variation in particle size, pressure, orientation, and heater size) is performed with the nanocoated surface in pure water. To summarize, the salient objectives are listed below:

- Measure nanofluid's thermo-physical properties
- Conduct experiments to observe nanofluid pool boiling characteristics
- Understand cause of BHT variation and CHF enhancement during nanofluid boiling
- Study nanoparticle deposition and its effect on the heater surface wetting performance
- Correlate wetting and pool boiling performance of nanocoatings
- Construct a methodology for nanocoating optimization
- Perform parametric tests to observe effects on the pool boiling with nanocoated surfaces

CHAPTER 2

EXPERIMENTAL APPARATUS AND PROCEDURES

2.1 Nanofluid Preparation and Properties

A majority of the experiments were conducted using Al_2O_3 nanoparticles supplied by Nanophase Inc. However, a portion of this study also used CuO (from Nanophase Inc.) and diamond (from Nanoamor Inc.) nanoparticles in powder form. To prepare the nanofluids, each nanoparticle was dispersed into distilled water and sonicated in a bath using ultrasound for two hours. The nanoparticles as supplied from the distributors are in powder form and average grain sizes given in the manufacturer's specification were ~32 nm, ~40 nm, and ~4-25 nm for Al_2O_3, CuO, and diamond, respectively. To confirm this average grain size, Transmission Electron Microscopy (TEM) images were employed to determine the individual grain sizes when in powder form. A TEM micrograph of a particle population captured for ~32 nm Al_2O_3 nanoparticles with a 4 megapixel image intensified CCD camera is shown in Fig. 2.1. In this image, individual nanoparticle grain sizes ranging from approximately 10 nm to 100 nm can be observed. The average grain size of the particles was determined to be 27 nm ± 16 nm. This value is slightly lower but in good agreement with the ~32 nm given in the manufacturer's specifications. The particle size distribution when dispersed into solution was determined using a Nanotrack particle size analyzer by Microtrac Inc. (Fig. 2.2). This device utilizes dynamic light scattering (DLS) to determine the average diameter of dispersed particles and aggregates.

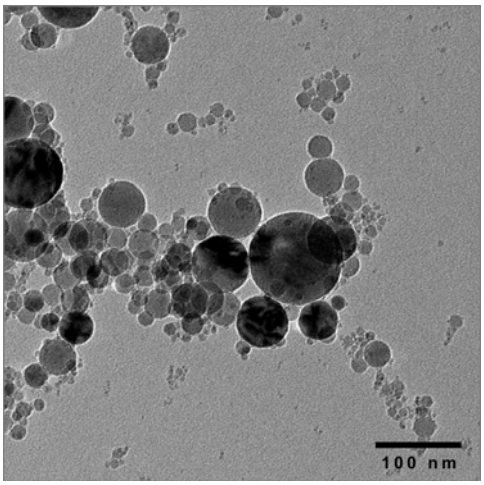

Fig. 2.1 TEM micrograph of ~32 nm Al_2O_3 powder provided by the manufacturer at 50,000X (200KV accelerating voltage).

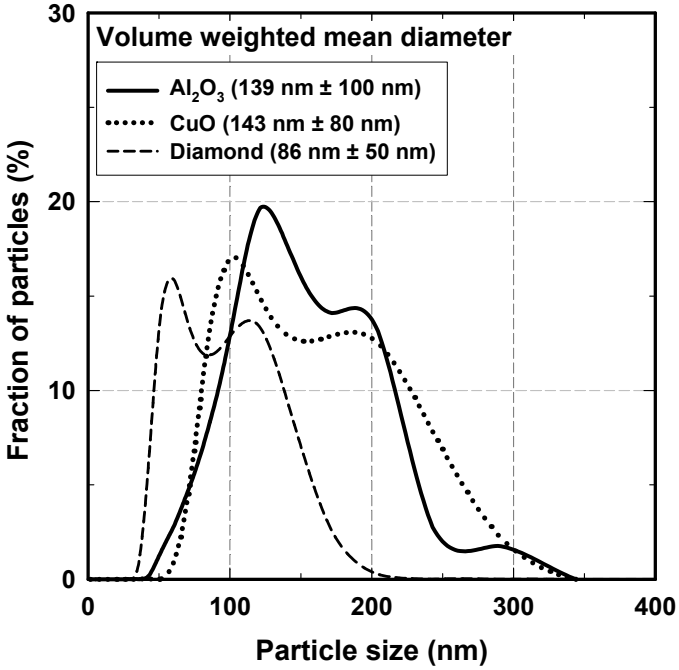

Fig. 2.2 Particle size distribution histogram for various nanofluids (volume weighted mean diameter).

After processing, the DLS data yielded a volume weighted particle size distribution of 139 nm ± 100 nm corresponding to the 27 nm ± 16 nm dry powder size. Based on the large difference between the size as determined by DLS and the average measured with TEM, a large percentage of the particles in solution consist of aggregates. Two additional nanoparticles (CuO and diamond) were also evaluated. The average volume weighted particle sizes distributions (in solution) were 143 nm ± 80 nm and 86 nm ± 50 nm for provided ~40 nm and ~4-25 nm respectively. It should be noted that there is a considerable particle aggregation when the nanoparticles are dispersed into solution.

The working nanofluids are prepared by weighing appropriate quantities of nanoparticles using an Acculab VI-1mg precision balance and then dispersing them into 500 ml of deionized-distilled water. This nanoparticle solution is then subjected to an ultrasonic bath for two hours. A Cole Palmer Ultrasonic Cleaner Model 08849-00 is used to accomplish this process. After this, the 500 ml of the nanofluid is added to 3 liters of base fluid to make a total of 3.5 liters. This 3.5 liters of nanofluid was used as the working fluid for the pool boiling experiments. The isoelectric points (IEP), which serves as a critical indicator for the particle agglomeration and setting in colloids, are determined for each nanofluid. In order to avoid agglomeration and sedimentation, the pH value of the nanofluid should be far from its IEP point. The measured pH values for Al_2O_3, CuO, and diamond nanofluids were 6.3, 5.4, and 4.9, respectively. The corresponding IEP values are 8-9, 9-9.5, and 1-2 for the respective nanofluids. A similar discussion on IEP was reported by Kim et al. [8] and Wen and Ding [37]. No significant nanoparticle sedimentation and agglomeration was observed during nanofluid boiling experiments in the present study. Therefore, the nanofluids used in the present study are assumed to be colloidally stable.

2.2 Pool Boiling Test Facilities and Heaters

2.2.1 Test Vessel

A schematic of the test vessel that was used for the pool boiling tests is shown in Fig. 2.3(a). The test vessel has two reinforced glass windows on the front and back as view ports. The dimension of the apparatus is 20 cm (wide) × 20 cm (high) × 17 cm (depth). Two half-inch diameter (1000 W) cartridge heaters were mounted in the vessel for a rapid heating and degassing process. Band heaters were externally attached to the test vessel to maintain the saturation temperature of the working fluid during experiments. There are two Swagelok valves, ne on the top (degassing) and one at the bottom (draining). The top valve is connected to an external condenser to minimize loss of the working fluid during the degassing procedure. T-type thermocouples are used to measure liquid, vapor, and test heater temperatures. A pressure transducer, Omega PX202, attached to top plate is used to measure the system pressure. An adjustable heater stand was mounted in the vessel for various orientation tests.

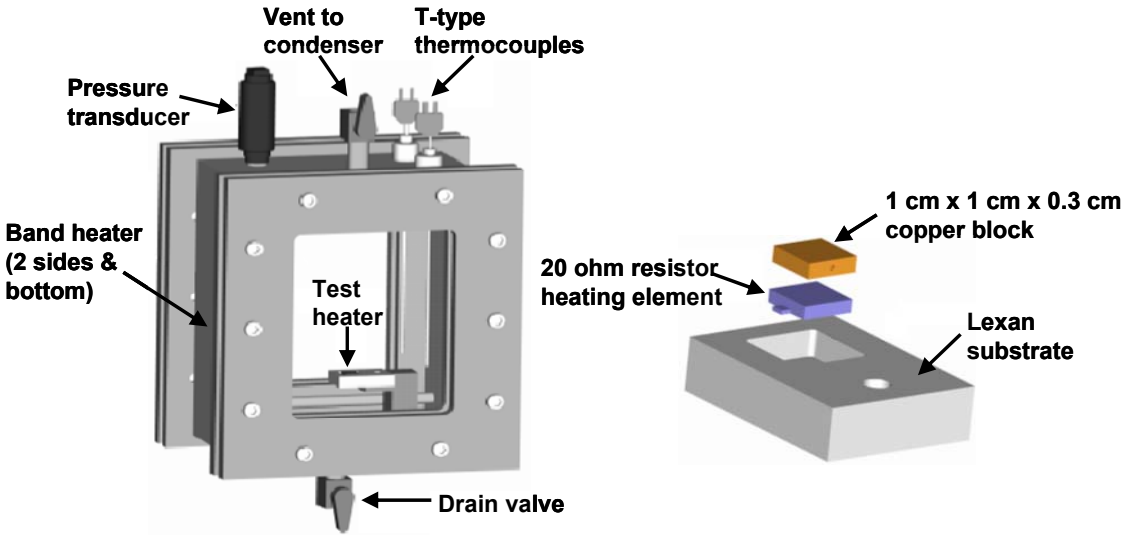

Fig. 2.3 Schematics of (a) test facility (b) test heater assembly.

2.2.2 Test Heater

A schematic of the heater assembly used for the pool boiling tests is shown in Fig. 2.3(b). The test heater consists of a square copper block, a heating element, lexan substrate, epoxy, and wires. A 1 cm x 1 cm resistor (20 Ω) is soldered to the copper block (1 cm × 1 cm × 0.3 cm). The copper block and the resistor assembly are then placed in a polycarbonate substrate, copper side up. 3M® 1838 Scotch-Weld Epoxy is then spread around the perimeter of copper block except for the top of copper surface. Both the epoxy and the substrate also functioned as insulators by preventing heat loss through the sides and bottom. A T-type thermocouple implanted in the copper block provides test heater temperature measurements and two copper wire leads provides power to the heating resistor. The thermocouple is located 1.5 mm below the heater surface and surface temperature is calculated assuming one-dimensional steady-state conduction.

To fabricate different size of heaters, the 1 cm × 1 cm x 0.3 cm copper block is replaced with 0.75 cm × 0.75 cm × 0.3 cm, 1.5 cm × 1.5 cm × 0.3 cm, and 2 cm × 2 cm × 0.3 cm copper blocks. The resistor is also replaced with equivalent sizes to copper blocks. All the other steps to prepare the heater remained the same.

2.3 Experimental Procedures

The pool boiling test on nanofluid is performed by using the apparatus and heater shown in Fig. 2.3. Before each boiling test of nanofluid, the test vessel is thoroughly washed using distilled water. Then pure water boiling test is performed and the boiling curve is compared to the reference curve of water. This ensures that the experimental vessel is not contaminated by nanoparticles from the previous test. After this pre-test, the prepared nanofluid is poured into the test vessel. The top plate of the test section is then attached to the body of the vessel. Once the vessel is tightly sealed, the two cartridge heaters are turned on and the valve on the top of the vessel is opened to release the dissolved non-condensable gasses from the working fluids.

The system temperature is increased till the liquid temperature reaches its saturation temperature and is maintained for 30 min. to remove any non-condensable gas in the test liquid. The condenser, located above the test section, allows any non-condensable gasses to escape while simultaneously condensing any vapor back into the vessel to maintain the original nanoparticle concentration. The top valve is then closed and cartridge heaters are turned off. The saturated test liquid is cooled or heated to the required saturation conditions. Once it reaches the desired system temperature, the internal pressure of the test vessel corresponds to the saturation pressure. At this point, a temperature controller which is connected to external band heaters is activated to control the system temperature. Tests are started after allowing the nanofluid temperature to level off at a constant temperature. An HP6032 power supply is used to power the heater. An HP 3852A data acquisition system is used to record pressure, temperature, and power. The power supply and data acquisition system are controlled using a program written in LabView. Tests are conducted by increasing the heat flux at constant increments till the CHF condition is reached. The program evaluates the heater temperature for steady state equilibrium at each applied heat flux before increasing the heat flux to the next programmed increment. The program assumes that the CHF condition is reached when the temperature of the heater increases by 20°C above the previously recorded temperature. The power to heater is then shut down and all data including temperatures, pressure, and heat flux are saved.

2.4 Uncertainty

The experimental uncertainties for this study were estimated using Kline and McClintock method [64]. By considering the errors due to voltage, surface area of the heater, and the current applied, the nucleate boiling heat flux uncertainty was estimated to be less than 5%. The uncertainty in measuring the CHF value is around 10% and temperature measurements were estimated to have less than ± 0.5°C error considering calibration error. The

net uncertainty in concentration of nanoparticles in base fluid was estimated to be less than ± 0.0005 g/l.

CHAPTER 3

NANOFLUID PROPERTY MEASUREMENT

The thermal properties of the working fluid play a critical role in boiling heat transfer performance. It is, therefore, important to know what effect the dispersed nanoparticles have on nanofluid properties. Although research has shown that nanofluids enhance thermal conductivity, the majority of this work has been conducted using nanofluids with relatively high concentrations (i.e. concentrations greater than those used in this study) [2, 3, 10, 12]. Therefore, the thermo-physical properties including thermal conductivity, viscosity, and surface tension of the nanofluids have been measured as part of this research for concentrations of interest (0.001 ~ 1 g/l). All equipment used for property measurements is included in Appendix A. Each data point is an average value of five measurements and the measurement uncertainties ranges within ± 3%.

3.1 Thermal Conductivity

A KD2-pro, Decagon Device Inc., was used to measure thermal conductivity at different temperatures for various nanofluids (Al_2O_3, CuO, and diamond). The device has a thermal conductivity measurement range of 0.02 ~ 2 W/mK with a 50 ~ 150°C operating temperature and a precision of ± 2.5%. A measurement qualification of thermal conductivity was made with pure water and the result is shown in Fig. 3.1. From the results, the measured thermal conductivity of pure water is well matched with text [65] values (< ± 3% error). Then, the thermal

conductivity measurement of nanofluids was conducted and Fig. 3.2 summarizes the results obtained.

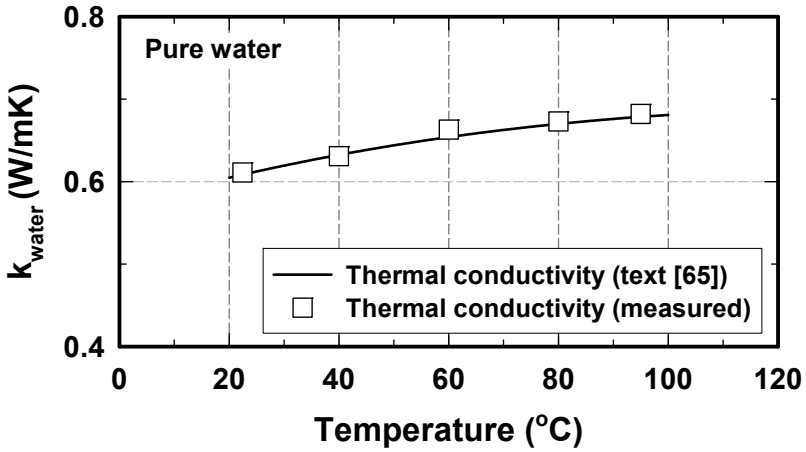

Fig. 3.1 Thermal conductivity of pure water at different temperatures (text vs. measured values).

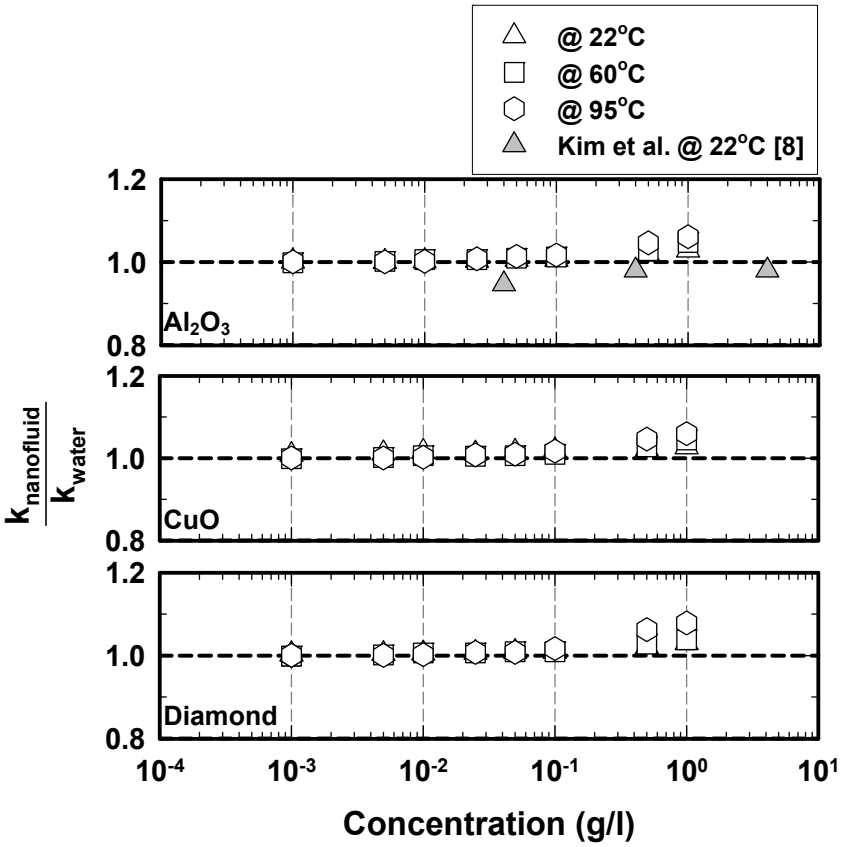

Fig. 3.2 Thermal conductivity enhancement of various nanofluids (effects of concentration and temperature).

No significant change in thermal conductivity is observed at room temperature for all tested concentrations of the nanoparticle (0.001 ~ 1 g/l). From the 0.5 g/l concentration onwards, it seems that the thermal conductivity increases with an increase in temperature (up to ~5% with 1 g/l at 95^{o}C). In general, results from current studies appear to follow the prevailing trend of previous researchers that the thermal conductivity is proportional to concentration [2-4] and temperature [5-7]. As both the concentration and the temperature are increased, the thermal conductivity of the nanofluids is increased. However, in present concentration range of nanofluids, it exhibits a relatively low or marginal thermal conductivity enhancement (up to ~5%), which is similar to results from Kim et al. [8]. Results on other nanofluids, CuO and diamond, show about the same conductivity enhancement trend (Fig. 3.2)

3.2 Viscosity

A Canon-Ubbelohde glass capillary viscometer was used to measure the kinematic viscosity of water and nanofluids. Fig. 3.3 illustrates that viscosity measurements of pure water are very well matched with tabulated text [65] values for various temperatures with less than 3% error.

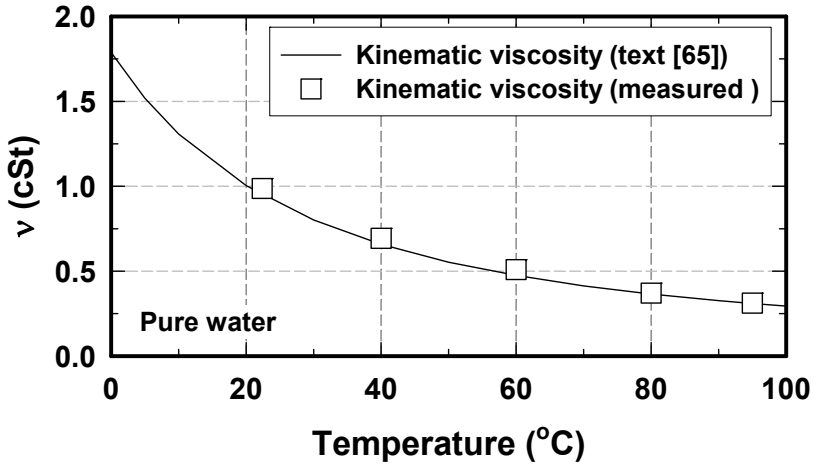

Fig. 3.3 Viscosity of pure water at different temperatures (text vs. measured values).

The following equation was used to calculate kinematic viscosity of the fluid.

$$\nu = Ct \tag{1}$$

where ν is kinematic viscosity, C is the viscometer constant which involves capillary and gravity force, 0.002668, and t is the duration of the measurement. Measurement ranges of the instrument include a 200°C maximum operating temperature and a viscosity range of 0.1 ~ 100,000 cSt. The kinematic viscosity can be converted to dynamic viscosity by using the following relationship between kinematic and dynamic viscosity.

$$\mu = \rho\nu \tag{2}$$

where μ is the dynamic viscosity and ρ is the density of fluid.

Fig. 3.4 shows measured kinematic viscosities of nanofluids at 0.001 ~ 1 g/l concentration. Even though some articles have emphasized the significance of investigating the viscosity of nanofluids, a few have actually measured them. Masuda et al. [2] showed that viscosity is significantly increased with an increase in nanoparticle concentration. This effect has been also reported by later researchers [15-17]. However, no significant viscosity change was observed with concentrations up to 1 g/l nanofluids over the viscosity of pure water. Similar results are reported by Kim et al. [8] at a comparable concentration with the present study. A possible primary reason could be the low concentration since other researches have performed the experiments with very high concentration (1 ~ 5% vol.) compared to the current research (2.7×10^{-5} ~ 2.7×10^{-2} % vol.).

Like Prasher et al. [16], no significant temperature effect on viscosity of nanofluids was observed. This behavior differs from the behavior of the thermal conductivity with increasing temperature. Other nanofluids (CuO-water and diamond-water) also showed about the same trend of the viscosity changes as that exhibited by the Al_2O_3 nanofluids. To conclude, the viscosity change is not significant for the range of concentration of the current study for boiling

experiments (≤ 1 g/l). Also, results showed negligible effect of temperature on viscosity of nanofluids.

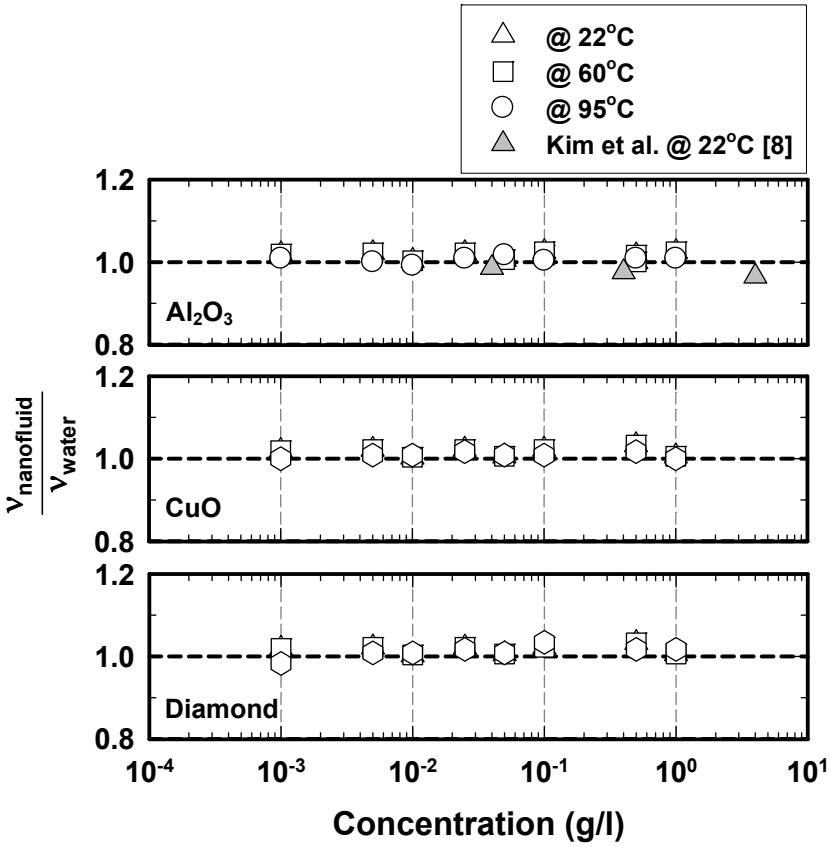

Fig. 3.4 Kinematic viscosity enhancement of various nanofluids (effects of concentration and temperature).

3.3 Surface Tension

Surface tension plays a critical role in boiling heat transfer and therefore the surface tension of nanofluids was investigated. An FTA 1000 optical device, First Ten Angstroms (precision: ±0.5 mN/m), was used to measure the surface tension of nanofluids. The FTA 1000 is equipped with a camera, frame grabber, and analysis software. The Laplace-Young equation was used as a governing equation to calculate the surface tension of sample fluids, water and nanofluids (eq. (3)).

$$\Delta\rho gh = \gamma(1/R_1 + 1/R_2) \quad (3)$$

where $\Delta\rho$ is the difference in densities between liquid and air, h is the height of the drop, γ is the surface tension, R_1 and R_2 are radii of curvature, and g is the acceleration due to gravity. As seen in eq. (3), the surface tension can be determined by only the geometrical shape of the droplet. From the Fig. 3.5, it can be seen that nanofluids over all the concentrations show a slightly lower surface tension than those for pure water. However, the variations in surface tension were within equipment uncertainty and thus this conclusion is not evident. All three nanofluids (water-based Al_2O_3, CuO, and diamond) behaved in a similar manner, showing marginal change in the surface tension up to 1 g/l concentration of nanofluids at room temperature. A similar observation was reported by previous researchers [8, 22].

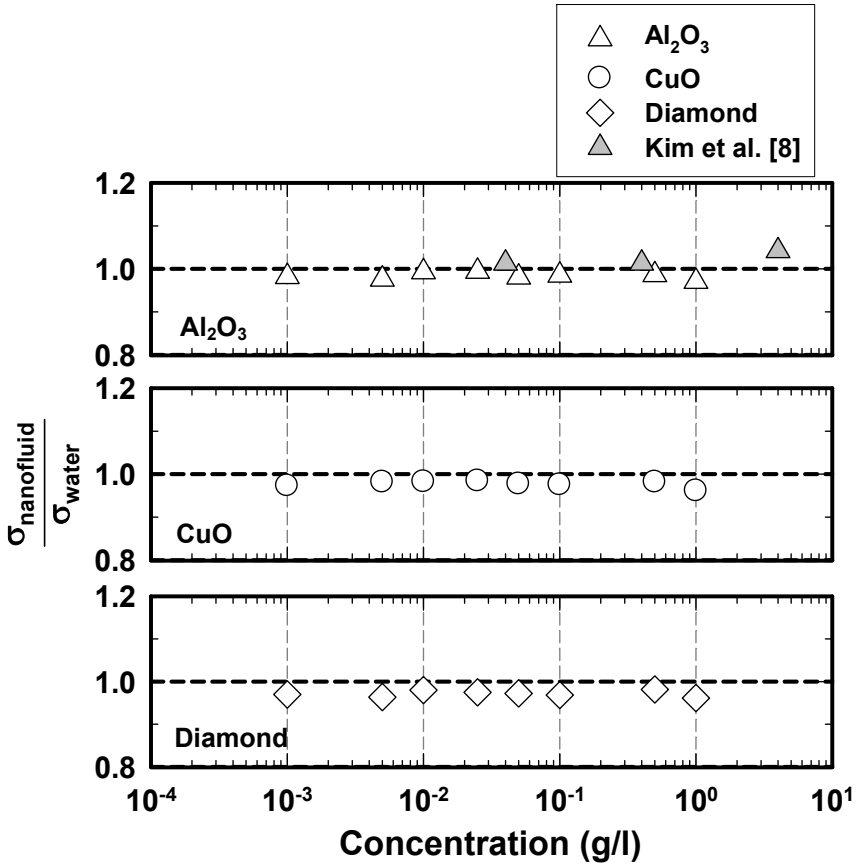

Fig. 3.5 Surface tension enhancement of various nanofluids (effects of concentration at room temperature, ~22°C).

CHAPTER 4

POOL BOILING CHARACTERISTICS OF LOW CONCENTRATION NANOFLUIDS

Inspite of numerous works performed on the pool boiling of nanofluids, the current work is motivated to carry out a comprehensive study based on the fact that only very low concentration nanofluids have shown a trend of CHF enhancement. You et al. [1] had made use of these low concentration nanofluids, with their experiments being performed at T_{sat} = 60^{o}C (~20 kPa). A majority of the studies in this area, on the other hand, were performed at T_{sat} = 100^{o}C (~101 kPa) and utilized non-flat heaters. The experimental tests in this study have been carried out over a square heater at 1 atm. The justification for using low concentration nanofluid and a flat heater surface is provided below.

Use of Low Concentration nanofluid:

Past studies on the pool boiling of nanofluids have included experiments with low as well as high concentration nanofluids. Most studies dealing with high concentrations showed the BHT deterioration. Only a few studies [1, 28, 29] have made use of low concentration nanofluids and shown its unique characteristics. They have reported that there is a distinctive trend in the CHF and the BHT as the particle concentration increases and this cannot be observed at higher concentrations. By varying the concentration of the nanoparticle in the base fluid, a critical concentration is achieved around 0.025 g/l, where one obtains a maximum enhancement in the

CHF value without compromising the BHT coefficient. This chapter will later discuss this phenomenon in detail.

Use of Flat Heater:

The literature survey, as shown in Table 1.1, indicates that several landmark studies in nanofluid boiling have been carried out over a wire heater or a cylindrical cartridge heater. Generally, a heater's curvature gives rise to non-uniform BHT distribution. Pioro et al. [66] reported that the average BHT rate, in that case, is highly dependent on thermocouple location. Very thin-wire heaters, on the other hand, can have a relatively small variation in heat transfer but their size change may become significant when experiments are carried up to the CHF values. The size of a cylindrical heater's diameter controls both the CHF value and the BHT. Lienhard and his coworkers [67, 68] showed that the CHF is related to the dimensionless radius of the cylinder, which in turn is dependent on the cylinder's diameter. Also, the bubble sizes are dependent on the wire diameter [28] and bubble sizes and rate dictate the BHT. This size change issue is of concern when the same wire is used to repeat experiments such as done by Kim and Kim [26]. Tachibana and Akiyama [69] have found that the CHF value is dependent on the heater thickness, which should be at least 1 mm thick. In conclusion, Pioro et al. [66] through their literature survey indicate that a flat heater with no special surface treatment would serve as an optimum heater to conduct fundamental pool boiling studies. Also, the boiling mechanism is highly dependent on the surface wetting and flat heaters lend themselves well to wetting characteristics measurements (like surface contact angle). The salient observations from the pool boiling study of low concentration nanofluid are being described next.

4.1 A Critical Nanoparticle Concentration

The pool boiling experiments were first conducted with Al_2O_3-water nanofluid at nanoparticle concentrations ranging from 0.001 to 1 g/l (2.7×10^{-5} ~ 2.7×10^{-2}% vol.). Different

heaters were used for each experiment and against various concentrations of the nanofluid. This allowed one to take the SEM image of the particle deposition after each experiment. Due to the overwhelming amount of data, the pool boiling curves for all nanofluid concentrations are presented in two different figures (Fig. 4.1 and Fig. 4.2). Fig. 4.1 shows the pool boiling curves for nanofluids with concentrations up to 0.025 g/l.

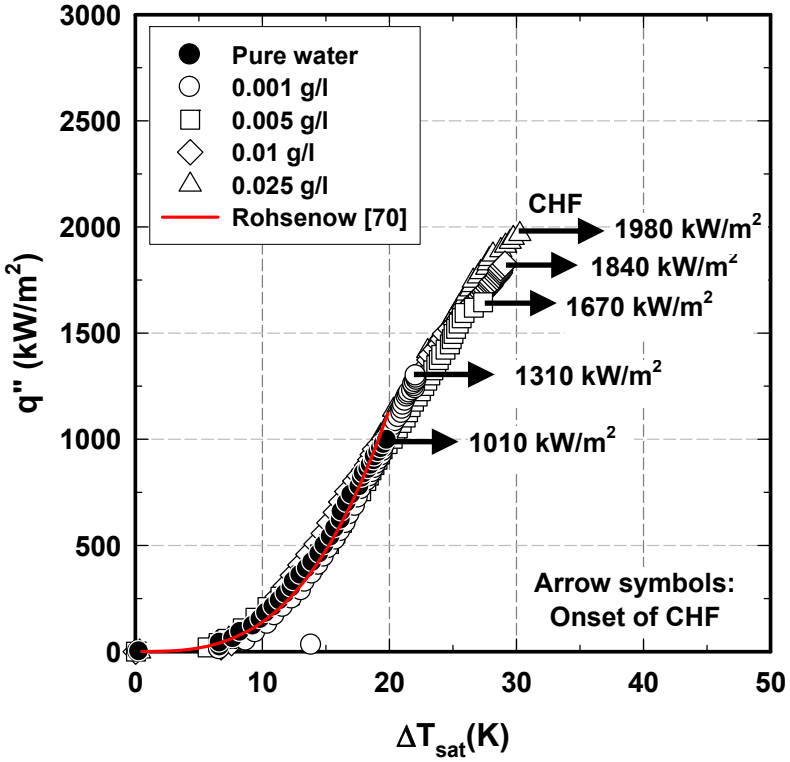

Fig. 4.1 Pool boiling curves for Al_2O_3-water nanofluids (0.001 ~ 0.025 g/l).

Experimental data are presented as symbols while the solid line displays values obtained from Rohsenow's [70] correlation given by:

$$\frac{C_{pl}[T_{wall} - T_{sat}]}{h_{fg}\,\mathrm{Pr}_l^s} = C_{sf}\left[\frac{q''}{\mu_l h_{fg}}\sqrt{\frac{\sigma}{g(\rho_l - \rho_v)}}\right]^r \tag{4}$$

with property values for the nucleate boiling of pure water and surface factor constant, C_{sf} = 0.0128 [71], for polished copper with pure water. r and s are constants whose values are 0.33 and 1.0 respectively, as suggested by Rohsenow [70]. Zuber's [72] correlation given by:

$$q''_{CHF} = 0.131\,\rho_g^{0.5}\,h_{fg}\left[\sigma\, g\,(\rho_l-\rho_v)\right]^{0.25} \quad (5)$$

predicts the CHF value and serves as the termination point for Rohsenow's [70] line. It should be noted that the boiling curve for pure water, as found in this study, is essentially identical to that predicted by the Rohsenow's [70] correlation (eq. (4)). Additionally, the experimental CHF of pure water (1,010 kW/m^2) matches well with the value predicted by Zuber's [72] CHF correlation (1,110 kW/m^2 by eq. (5)) for pure water at 1 atm.

Fig. 4.1 shows that as the nanoparticle concentration increases, the CHF also increases but the pool boiling curves closely follow the boiling curve for pure water. This indicates that at these concentrations (i.e. up to 0.025 g/l), the BHT of the nanofluids and that of pure water are almost identical. The CHF, on the other hand, increases with increased nanoparticle concentration until eventually leveling off at a value of ~1980 kW/m^2. Thus these nanofluids are providing a CHF increase which is about 80% greater than that predicted by Zuber's [72] correlation (eq. (5)) without degrading the BHT.

Fig. 4.2 displays the pool boiling curves for nanofluid concentrations beyond 0.025 g/l. At these relatively higher concentrations, the CHF value remains roughly the same as that obtained at 0.025 g/l nanofluid concentration but the pool boiling curves break away from the boiling curve of pure water. This separation increases with increasing nanoparticle concentration and thereby indicates a marked decrease in BHT. Thus it seems that the optimal Al_2O_3 nanofluid concentration, where both CHF enhancement is maximized and BHT is not deteriorated, is at nanoparticle concentrations of about 0.025 g/l (0.0007% vol.). To support this observation using other nanofluids, additional pool boiling experiments were conducted using CuO-water and diamond-water nanofluids. Almost identical pool boiling behaviors to those observed in Al_2O_3-water nanofluids were obtained and the results are shown in Fig. 4.3.

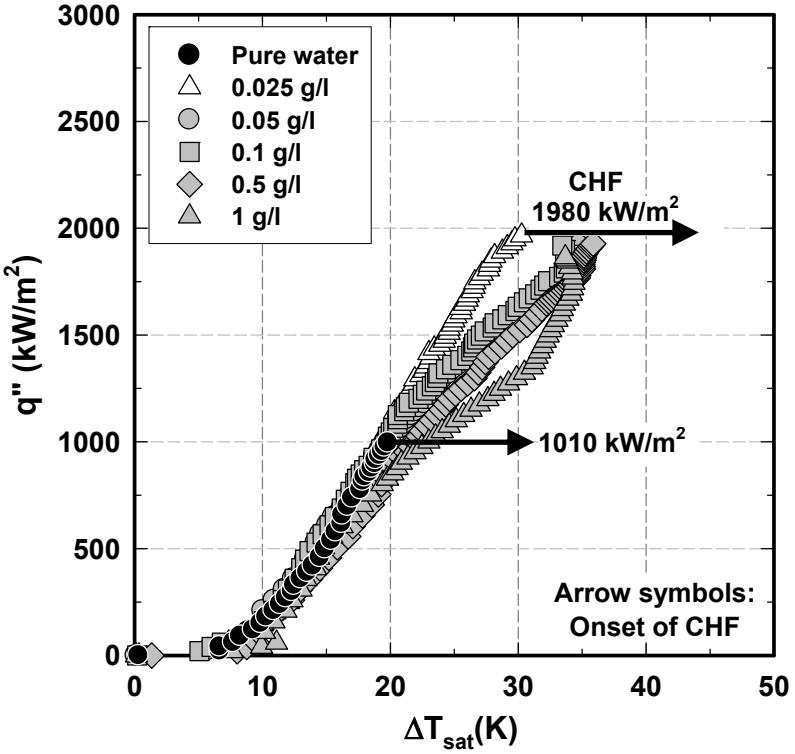

Fig. 4.2 Pool boiling curves for Al_2O_3–water nanofluids (0.025 ~ 1 g/l).

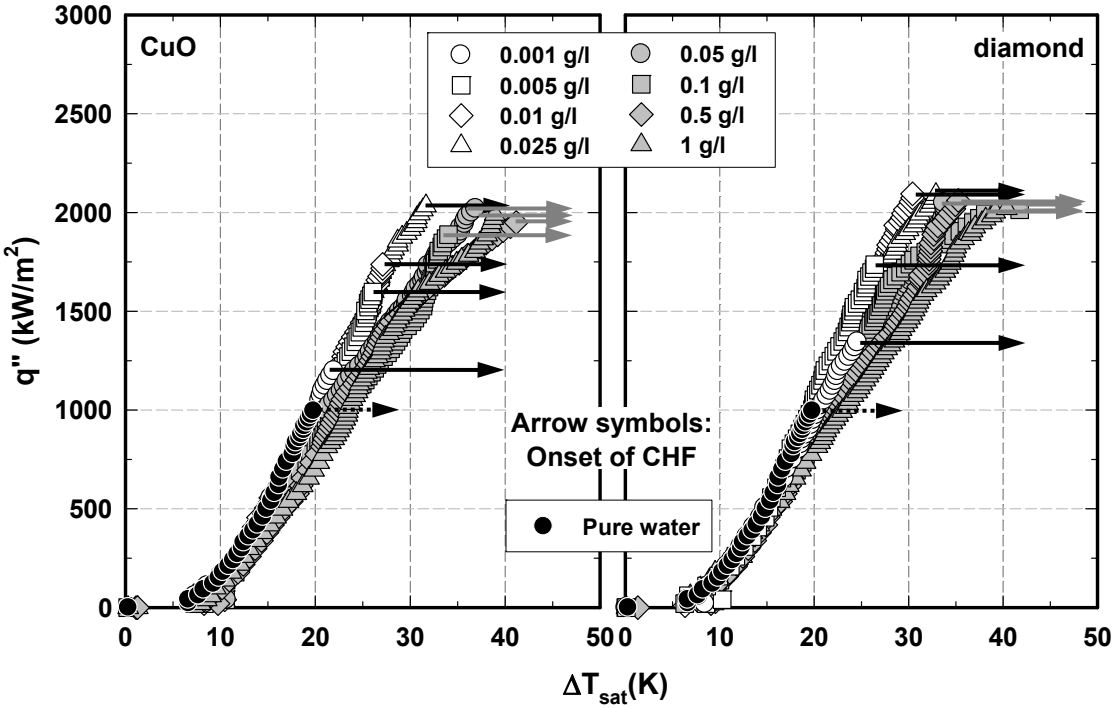

Fig. 4.3 Pool boiling curves for CuO (left) and diamond (right) nanofluids (0.001 ~ 1 g/l).

Fig. 4.4 illustrates the CHF enhancement, which is defined as the ratio of the nanofluid CHF (at various concentrations) over the pure water CHF as predicted by Zuber's [72] correlation (eq. (5)), for the tested nanofluids.

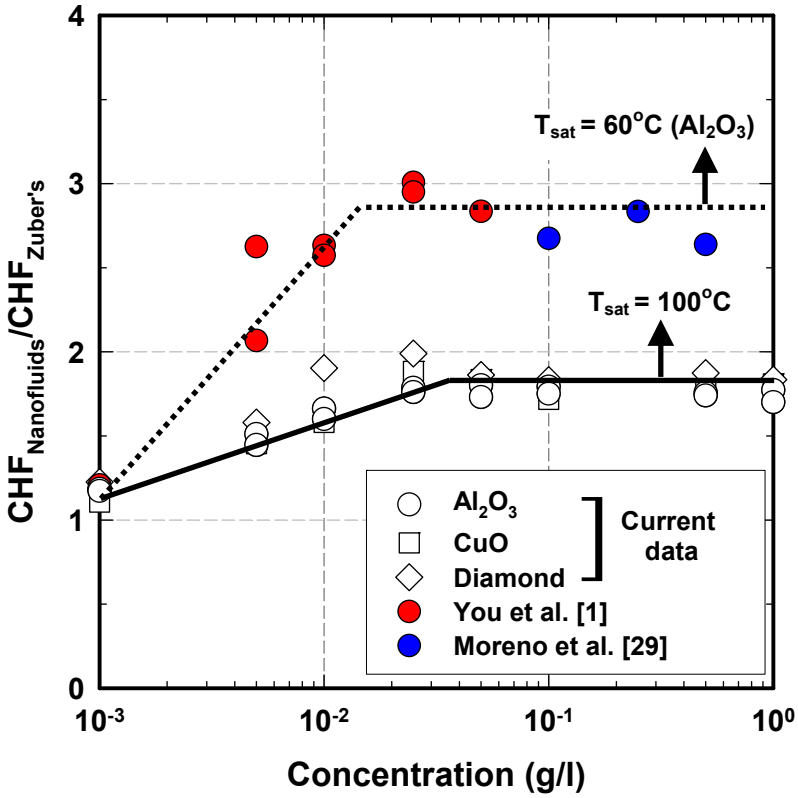

Fig. 4.4 CHF enhancement of nanofluids for tested concentrations.

Results show that both the CHF vs. nanoparticle concentration trend and the magnitude of the CHF enhancement are about the same for all three nanofluids. That is to say, increasing the nanoparticle concentration, for all three nanofluids, increases CHF until a concentration of about 0.025 g/l. Thereafter, CHF remains fairly constant and is about 80% greater than that produced using pure water. This comparable performance between the three nanofluids indicates that nanoparticle material has minimal effect on nanofluid boiling performance, and this is consistent with the findings of Moreno et al. [29]. Also, the observed CHF enhancement trend is similar to that of the Al_2O_3 nanofluids that was tested at a lower saturation temperature of T_{sat} =

60°C (P_{sat}= 20 kPa), and as reported by [1, 29]. The current nanofluid experiments conducted at atmospheric pressures are found to enhance CHF by ~80% whereas those conducted at lower pressures of P_{sat} = 20 kPa were reported to increase CHF by ~200%. Therefore it seems that the nanofluid CHF enhancement decreases with increasing saturation pressure.

The boiling characteristic of these nanofluids can be explained in the following manner. Past works in this area have shown that a significant deposition of nanoparticles on the heater surface is observed after the nanofluid pool boiling experiments. This deposition increases with increased nanoparticle concentration. Fig. 4.5 shows SEM pictures of the heater surface displaying an increased deposition with increased nanoparticle concentration.

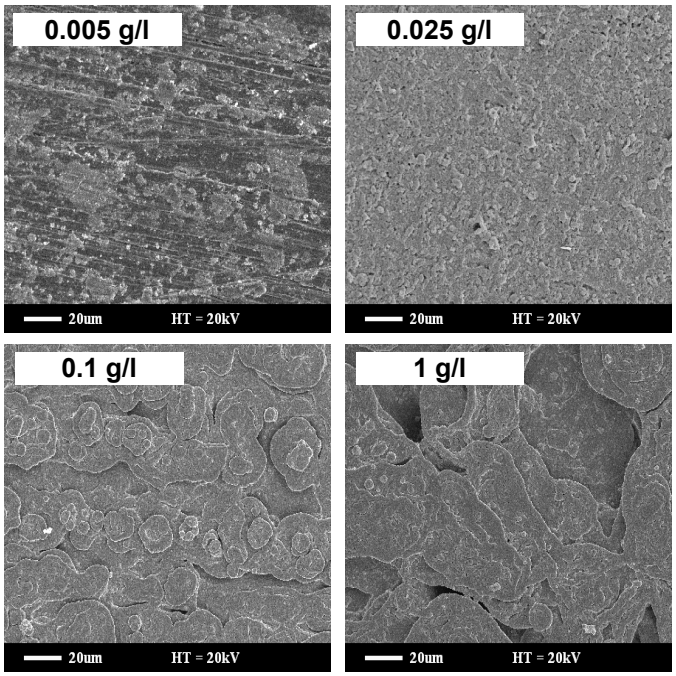

Fig. 4.5 SEM images of nanoparticle deposition after experiments at the various Al_2O_3–water nanofluid concentrations.

The decrease in the BHT coefficient with increased nanoparticle concentration can be attributed to the corresponding thicker coating created on the heater surface and which in turn offers increased thermal resistance. CHF, on the other hand, is dictated not by the nanoparticle coating thickness, but by the wettability of the nanocoating generated over the heater surface [8,

26]. As the nanoparticle deposition increases, the wettability (measured through goniometry) of the heater surface increases and which in turn increases CHF. Once a critical coating condition is reached the wetting on the surface attains a maximum limit and this is reflected by a constant CHF value (Fig. 4.4). Additional layers of nanoparticle coating increase the coating thickness but perhaps do nothing to dramatically change the wetting characteristics of the heater surface. Due to this phenomenon, there exists an optimal nanofluid concentration at which one observes maximum CHF enhancement without any degradation of the BHT. Results from this study and those of previous studies by [1, 28, 29] indicate that the optimal nanofluid concentration is about 0.025 g/l (0.0007% vol.).

4.2 Transient Characteristics During Pool Boiling

The pool boiling performance for a pure fluid is ideally time-independent. Therefore, pool boiling experiments of liquids do not dwell upon how the heat flux is varied with time from the beginning of the boiling process till the CHF condition is obtained. However, the present study and previous nanofluid boiling studies [8, 26, 30-32, 40] have shown that during the boiling process the heater gets coated with nanoparticles. The dynamic growth of this layer keeps modifying the heater surface and this in turn makes the nanofluid boiling process exhibit transient characteristics.

To investigate the transient nature of nanofluid boiling, nanofluid pool boiling tests were repeated 3 times at the same concentration (0.005, 0.025, 0.1, and 1 g/l) without taking out the heater from the experimental chamber. A plain (uncoated) heater was immersed in the nanofluid and boiling experiments were repeated (up to CHF) three successive times in the same nanofluid bath. Results from these consecutive boiling tests are shown in Fig. 4.6 (for 0.005 g/l) and Fig. 4.7 (for 0.025 g/l). Both these figures show nearly similar results, in showing consistently ~50% (for 0.005 g/l) and ~80% (for 0.025 g/l) CHF enhancement with no change in BHT.

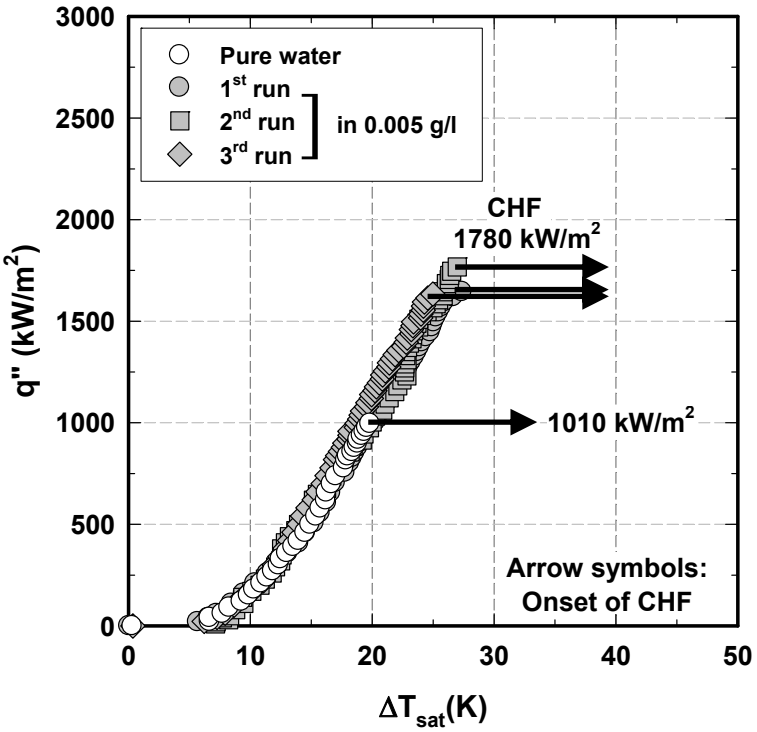

Fig. 4.6 Pool boiling curves of the Al_2O_3-water nanofluid for 3 runs in 0.005 g/l.

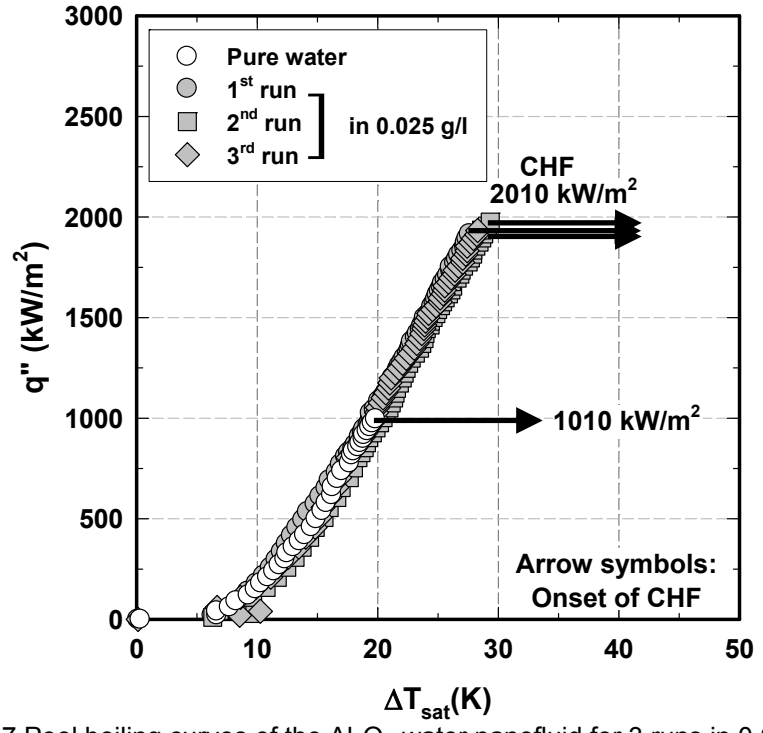

Fig. 4.7 Pool boiling curves of the Al_2O_3-water nanofluid for 3 runs in 0.025 g/l.

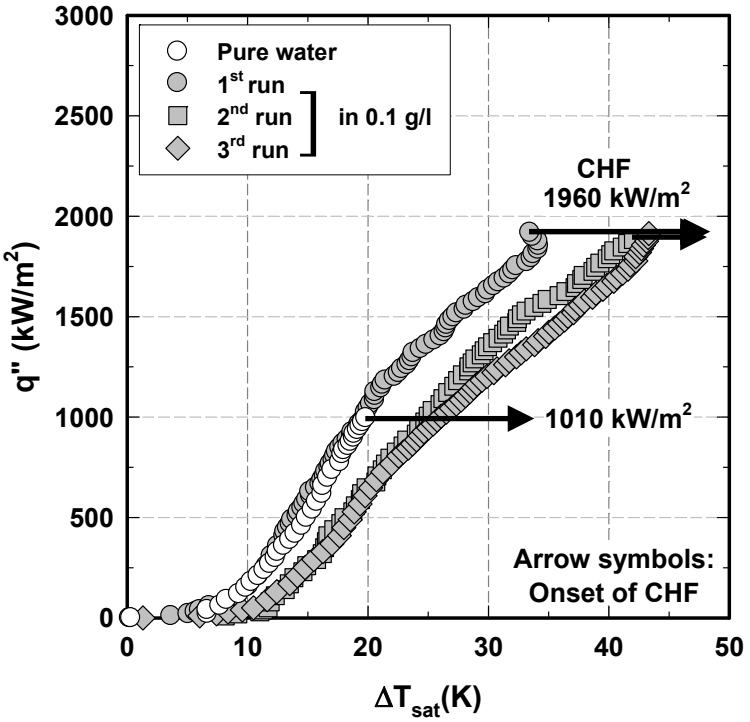

Fig. 4.8 Pool boiling curves of the Al_2O_3-water nanofluid for 3 runs in 0.1 g/l.

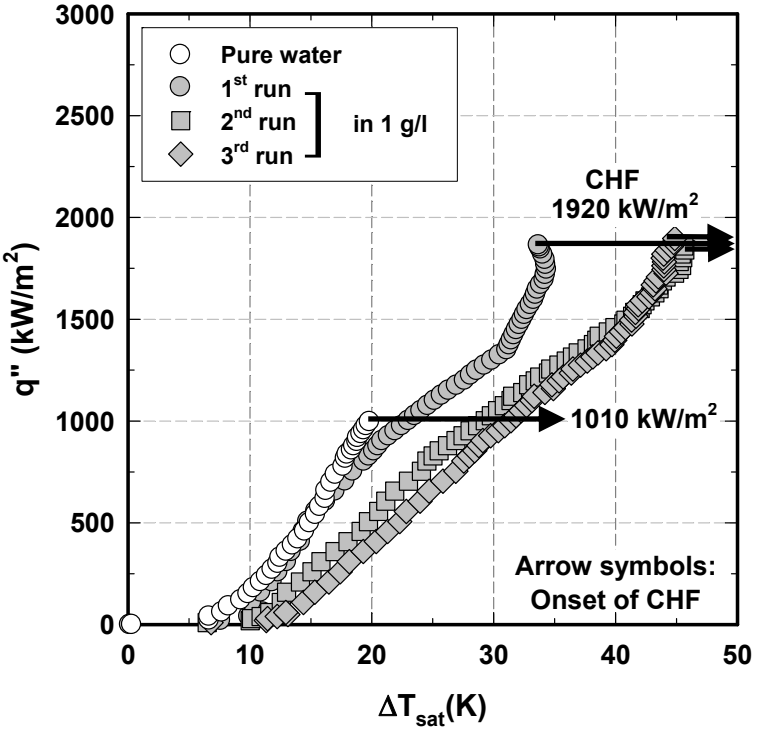

Fig. 4.9 Pool boiling curves of the Al_2O_3-water nanofluid for 3 runs in 1 g/l.

On the contrary, in Fig. 4.8 (for 0.1 g/l) and Fig. 4.9 (for 1 g/l), repeated tests (2nd and 3rd tests) show consistent CHF enhancements but a degradation in the BHT. This BHT degradation indicates that the longer the heater surface is subjected to boiling in nanofluids, the thicker is the nanoparticle coating and this in turn creates an additional thermal resistance. SEM images (Fig. 4.10) taken after 1st run and 3rd run in 0.025 g/l and 0.1g/l nanofluids clearly show that the nanoparticle deposition becomes thicker during these repeated tests.

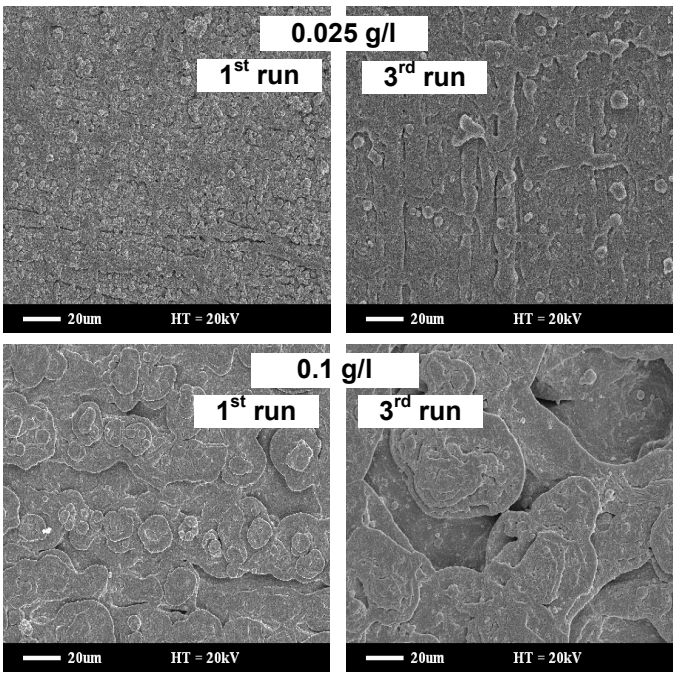

Fig. 4.10 SEM images after 1st and 3rd run in 0.025 g/l and 0.1 g/l.

It should be noted that up to 0.025 g/l concentration, the nanoparticle deposition rate is not as fast as that of relatively higher concentrations (0.1 and 1 g/l). Thus 3 repeated boiling runs are not enough to show a degradation of BHT. From these experiments, it is believed that the nanofluid BHT will eventually deteriorate with sufficient boiling time. The CHF value on the other hand, increases up to ~ 2000 kW/m^2 and retains that value through repeated tests. These experiments show that the heater surface conditions are continuously being modified during nanofluid boiling tests and this results in transient nanofluid boiling characteristics.

The evidence from experiments suggests that the nanofluid boiling performance is affected by the thickness and structure of the nanoparticle deposited layer. Since this coating is primarily dictated by heat flux and the boiling duration, the effect of changing these parameters (i.e. heat flux increments and boiling duration) on the boiling performance was investigated.

4.2.1 Effect of Varying Heat Flux Increment

Two experiments were conducted using two different methods and are denoted as Method 1 and Method 2. Experiments in Method 1 and Method 2 were conducted under identical conditions. The only difference being in the manner in which the heat flux was incremented during nanofluid boiling experiments. In Method 1, the heat flux was incremented by 20 kW/m^2 until onset of nucleate boiling (up to ~ 60 kW/m^2), incremented by 40 kW/m^2 (up to ~800 kW/m^2), and incremented by 20 kW/m^2 thereafter until CHF was reached. It took about 45 min. to complete the boiling tests using this method. In Method 2, the heat flux increments were kept constant (10 kW/m^2) from the start till the CHF condition was reached. This approach took about 120 min.

The results from these two experiments are shown in Fig. 4.11 and are found to be dependent on the nanofluid concentration. At 0.025 g/l concentration, a marginal change in the CHF and the BHT was observed for Method1 and Method2. Incidentally, this is about the same result that was obtained with repeated test experiments (Fig. 4.7). It seems that, at 0.025 g/l concentration, the nanoparticle deposition rate is slow so it may require longer boiling duration for a given heat flux to show the BHT deterioration behavior (will be discussed in Chapter 4.2.2). At 1 g/l concentrations, in contrast, Method 2 shows degradation in the BHT coefficient. With time, there is more deposition taking place on the heater surface and this leads to a decrease in the BHT coefficient while the CHF value remains unaffected.

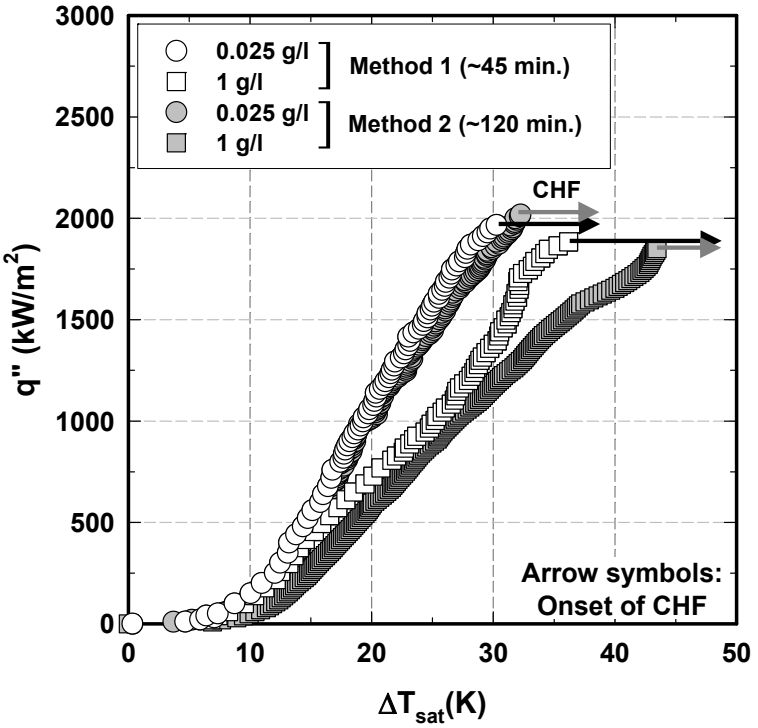

Fig. 4.11 Transient behavior of the nanofluid boiling
(Al_2O_3 nanofluid at 0.025 g/l and 1g/l with Method 1 and Method 2).

4.2.2 Effect of Prolonging a Specific Heat Flux

Another means to demonstrate the transient nature of nanofluid boiling and its dependence on the heat flux is by holding a heat flux value constant for an extended period of time. In these experiments, nanofluid (0.025 g/l) pool boiling tests were carried out by incrementing the heat flux at constant increments until it reached a heat flux of 1000 kW/m^2. The heat flux was then held constant (1000 kW/m^2) for 30, 60, and 120 min. After this wait time had elapsed, the tests were allowed to proceed to CHF condition by incrementing the heat flux. Pool boiling curves, from these tests, are shown in Fig. 4.12 alongside the reference pool boiling curves for this nanofluid that had no extended boiling time at 1000 kW/m^2 imposed (shown as opened symbols). Before the extended boiling wait time is imposed, all boiling curves are essentially identical, as expected. The 30 min. wait time is found to have no significant effect on the boiling performance. However, the longer wait times (60 and 120 min.) are found to affect the performance as is seen in the right-shift in the pool boiling curves. These

experiments demonstrate that a combination of imposed heat flux and its duration cause different thickness of nanoparticle coatings and this is responsible for the degradation in BHT.

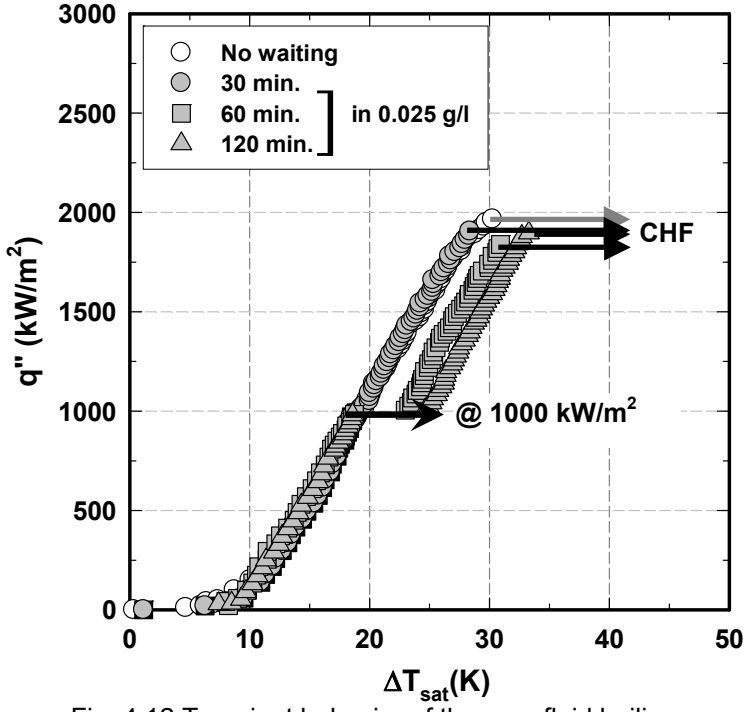

Fig. 4.12 Transient behavior of the nanofluid boiling
(0.025 g/l Al_2O_3-water nanofluid), showing a time dependency.

Pool boiling experiments were also conducted to demonstrate how the nanofluid boiling performance was dependent on heat flux values. Nanofluid pool boiling tests were conducted by incrementing the heat flux up to a heat flux of 500 kW/m^2, where it was held constant for 2 hours. After this wait time the boiling continued up to CHF. Similar experiments with the same waiting time of 2 hours were performed at higher heat fluxes of 1000 kW/m^2 and 1500 kW/m^2. The results obtained are displayed in Fig. 4.13. For all three cases (500, 1000, and 1500 kW/m^2), the effect of prolonging the imposed heat flux is found to degrade BHT. The higher the imposed heat flux the greater the BHT degradation. Therefore, it seems that higher heat fluxes are more conducive to generating thicker nanoparticle coatings. These experiments show that the nanoparticle deposition during the experiments is a function of time, nanoparticle concentration, and the applied heat flux and it could deteriorate the BHT. It is reiterated that

transient changes of heat flux does not bring about any difference in the boiling curve of pure water.

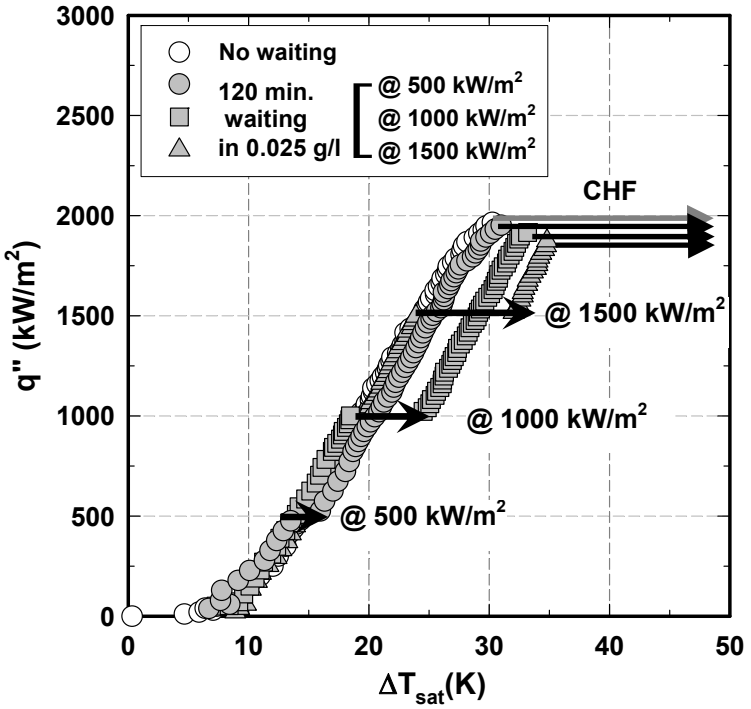

Fig. 4.13 Transient behavior of the nanofluid boiling
(0.025 g/l Al_2O_3-water nanofluid), showing a heat flux dependency.

4.3 A Critical Thickness for Nanoparticle Deposition

The present study shows that the BHT performance of nanofluids eventually deteriorates with time. The magnitude of this BHT degradation is significant at higher concentrations and at higher heat fluxes. The rate at which this deterioration occurs can be observed from Fig. 4.8 and Fig. 4.9, which shows that degradation is relatively less between the 2^{nd} - 3^{rd} trials as compared to the 1^{st} - 2^{nd} trials. The relatively less degradation of BHT during subsequent boiling tests makes the author believe that the deposition on the heater surface approaches a limit beyond which the transient effect is greatly mitigated. In other words, there might be a critical deposition thickness beyond which the nanoparticles do not remain strongly attached. Once this critical thickness is reached, the BHT coefficient ceases to decrease with

time. To verify this, experimental tests were carried out by varying the heat flux with time under a situation that can quickly facilitate nanoparticle deposition onto the heater surface.

It has been previously observed that the amount of nanoparticle deposition is directly dependent on the heat flux and the nanoparticle concentration with an increase in either resulting in greater deposition. Therefore, to investigate if there is indeed a limit to the nanoparticle coating thickness, nanofluid boiling experiments were conducted to maximize the coating thickness. This was accomplished by boiling in a high concentration nanofluid (1 g/l) while imposing a relatively high heat flux (1500 kW/m^2). The heat flux was incremented up to 1500 kW/m^2, where the power was held constant for different waiting times (0, 30, 60, 120, 180, and 240 min.). Fig. 4.14 shows the result obtained from these experiments.

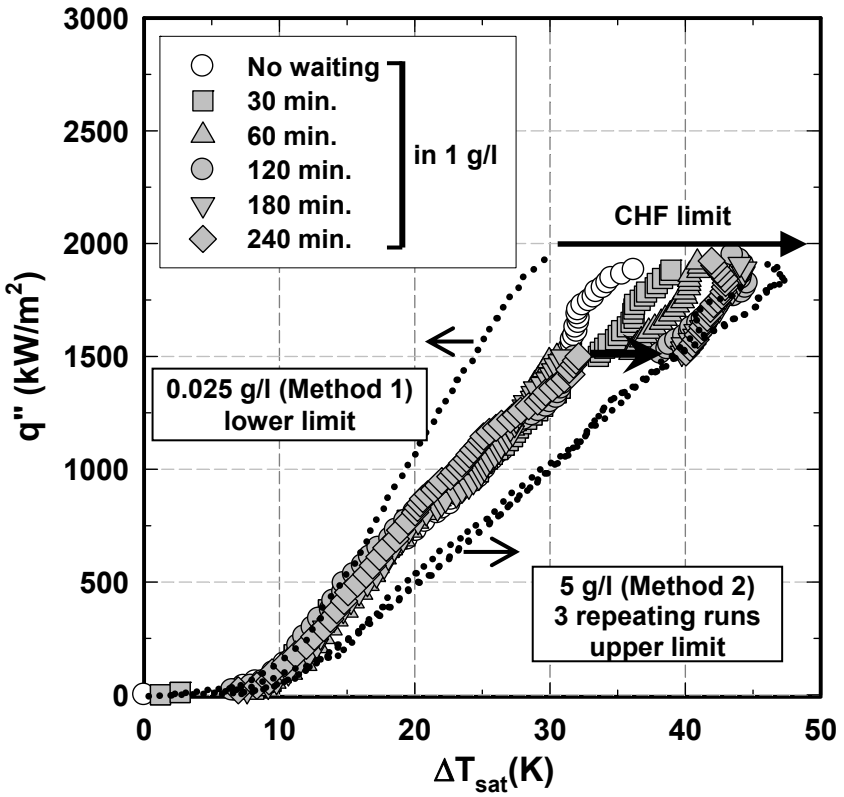

Fig. 4.14 Transient behavior of the nanofluid boiling (CHF and BHT limit).

It is seen that the BHT performance degrades with increasing wait time (until about 120 min. wait time) indicating that the nanoparticle layer grows with increasing time. However, no

further BHT degradation is observed by prolonging the waiting time from 120 min. to 240 min. A critical deposition is finally reached and this results in no further BHT performance deterioration with increasing wait time. As a further confirmation, additional tests were conducted using even higher concentration nanofluids (5 g/l) with Method 2 increment (10 kW/m^2). In fact, these tests were repeated 3 times using the same heater submerged in the same 5 g/l nanofluid solution and all boiling curves from these tests were found to collapse to a single line. Boiling curves from these tests confirm that there is an upper limit to the nanoparticle coating formed on the surface (Fig. 4.14).

This leads to an interesting feature that is observed during the pool boiling of nanofluids over a flat heater. The pool boiling for all concentrations between 0.001 g/l to 5 g/l, displays a lower and upper bound for the boiling curves. This finding, to the authors' knowledge, is being reported for the first time. It should be noted that for all these tests CHF value remains about the same.

CHAPTER 5

STUDY OF NANOPARTICLE DEPOSTION

It is widely accepted that the nanoparticle deposition during pool boiling of nanofluids causes a change in the heater surface characteristics in terms of wettability and its roughness. Past studies have discussed the nanoparticle deposition thickness, wetting characteristics, and surface roughness using nanofluids with relatively high nanoparticle concentrations [8, 23, 26, 30-32, 34, 39]. However, it has been shown that it only requires low concentrations of nanofluids to achieve maximum CHF enhancement with no detriment to the BHT [1, 28, 29]. It is, therefore, important to investigate the surface characteristics of the nanocoated heaters produced by these relatively low concentration nanofluids. Preliminary experiments were carried out to investigate the effects of the nanoparticle deposition on pool boiling heat transfer. An extensive study was also conducted to identify possible factors responsible for the nanoparticle deposition on the heater surface during the boiling process and how this deposition changes the heater's wetting characteristics. In addition, a proper method is proposed to measure apparent contact angles that eliminates the effects of secondary particle deposition by the external evaporation.

5.1 Effects of Nanocoated Surface During Pool Boiling

Kim and Kim [26] demonstrated that the nanoparticle coating deposited on the heater surface, following nanofluid boiling tests, can itself enhance CHF when tested in pure water. Using NiCr wire heaters, their study showed that, when tested in pure water, these nanocoated

surfaces provide even greater (1.35 times) CHF enhancement than that produced with nanofluids. However, these tests require repeating experiments using the same thin wire heaters, once to produce the coating using nanofluids and the second time to test the nanocoated surface in pure water. Therefore, any wire deformations/elongations experienced during CHF in the initial test could affect results in the subsequent test. It is, therefore, believed that such boiling tests are best conducted using flat heater geometries as they will not experience significant size deformation and are more suitable for conducting fundamental pool boiling investigations [66].

To investigate the effect of the nanocoated surfaces on pool boiling performance, two sets of tests were conducted at two different nanoparticle concentrations (0.025 and 1 g/l). Each set of tests consisted of two pool boiling experiments. The first test was conducted with a plain (uncoated) heater in Al_2O_3 nanofluids and the second test was conducted using a nanoparticle coated heater in pure water. Therefore, the first test built up the nanoparticle coating on the heater surface and the second test investigated the effect of this coating on boiling performance in pure water. From here on, the nanocoating produced during 0.025 g/l nanofluid experiments will be defined as ”0.025 g/l nanocoating” and the nanocoating produced during the 1 g/l nanofluid experiments will be designated at “1 g/l nanocoating”.

Some researchers, investigating the mechanism responsible for nanofluid CHF enhancement, have examined the effect of the nanoparticle coatings formed during nanofluid boiling tests. In most every case, the performance of nanocoated heaters is evaluated after the heaters are removed from the nanofluid bath following a nanofluid boiling test and allowed to air dry. Experiments have shown that if a heater is allowed to air dry, any nanofluid droplets remaining on the heater’s surface will eventually evaporate and leave behind additional nanoparticle coating deposits. These additional nanoparticle formations could then influence the boiling performance of these nanocoated heaters and therefore these surfaces are not a true representative of the actual heater surface conditions during nanofluid boiling tests. To better

capture the actual nanoparticle coatings formed during nanofluid boiling tests, the nanoparticle coated heaters used in this study are removed from the nanofluid bath and immediately subjected to a pool boiling test in pure water. This process allows only those nanoparticles that are securely bonded to the heater surface during nanofluid boiling tests to influence boiling performance. These procedures are used when evaluating the pool boiling performance of all the nanoparticle coated heaters. Results from these tests are shown in Fig. 5.1.

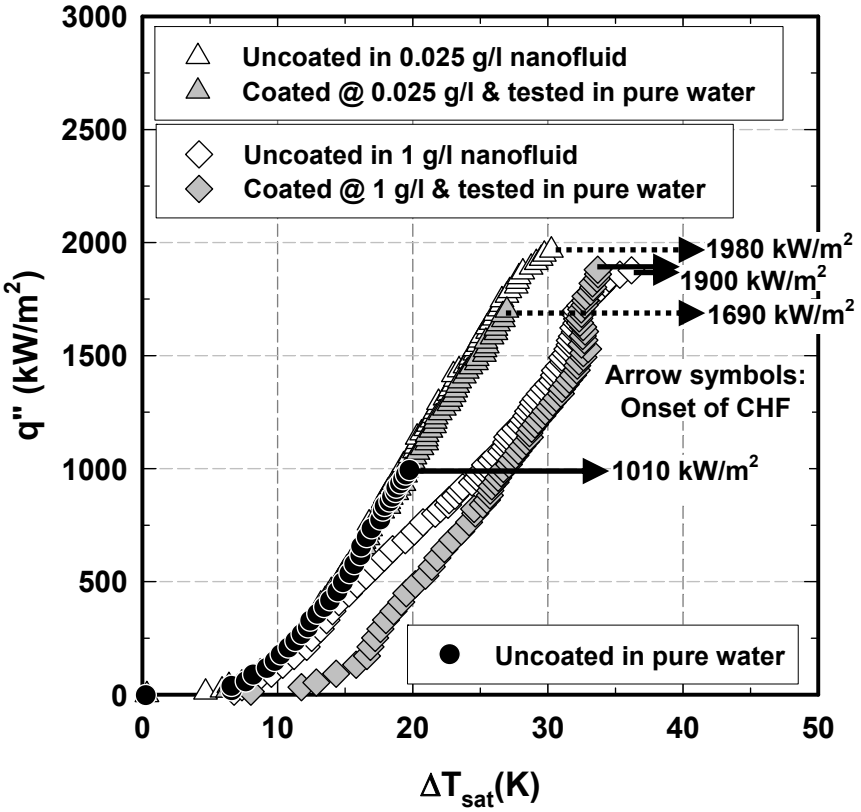

Fig. 5.1 Effects of the nanocoated surfaces for pure water pool boiling.

The CHF versus nanoparticle concentration plot shown in Fig. 4.4 shows that nanoparticle concentrations of about 0.025 g/l are just enough to produce the maximum CHF enhancement. Thus the nanocoating produced using 0.025 g/l nanofluids should be sufficiently thick enough to produce a similar CHF enhancement. However, results show that, when tested in pure water, the CHF for the 0.025 g/l nanocoated heater is lower (~20%) than the initial CHF

obtained with an uncoated heater in 0.025 g/l nanofluid. This indicates that when the nanocoated heaters are tested in pure water, boiling on the heater surface may detach some of the nanocoating from the surface. This in turn causes CHF to decrease for the 0.025 g/l nanocoated heater as compared to the CHF produced with 0.025 g/l nanofluids. However, at a higher concentration (1 g/l), the CHF values are about the same between the clean heater tested in nanofluids and the 1 g/l nanocoated heater tested in pure water. This implies that the 1 g/l nanocoating is thicker and thus any nanocoating removed during boiling has minimal effect on CHF. This coating detachment was optically observed using 1 g/l nanocoating. Fig. 5.2 shows the nanocoating images taken before and after pure water boiling tests. Some parts of the nanocoating were detached during the boiling experiment with pure water (1 g/l nanocoating) – see circled areas in the after picture. Therefore, this makes the author believe that there is a possible detachment on 0.025 g/l nanocoating during pool boiling experiments in pure water as well, resulting in less CHF enhancement. And these experiments indicate that there is a minimum nanoparticle coating thickness required to produce maximum CHF enhancement. Any detachment from this minimum critical coating decreases the CHF value.

Fig. 5.2 Nanocoating detachment before and after pure water boiling experiments.

Unlike Kim and Kim [26], who reported that nanoparticle coated heaters alone (i.e. coated heater tested in pure water) produce higher CHF than that achieved with nanofluids, the current experiments show that the CHF enhancement with a nanocoated heater can at best match that produced with nanofluids. It should also be noted that at low heat fluxes (< 500 kW/m^2), the pool boiling curves for pure water and 1 g/l nanofluid are about the same. However, as discussed earlier, higher heat fluxes are more conducive towards the formation of the nanocoating. This results in an increased nanocoating growth rate (i.e. increased thermal resistance) and a deterioration of the BHT, as indicated by the deviation of the 1 g/l nanofluid boiling curve from that of pure water at higher heat fluxes. On the other hand, since the 1 g/l nanocoated heater (tested in pure water) starts off with a relatively thick nanoparticle coating, its boiling curve is deteriorated from the start.

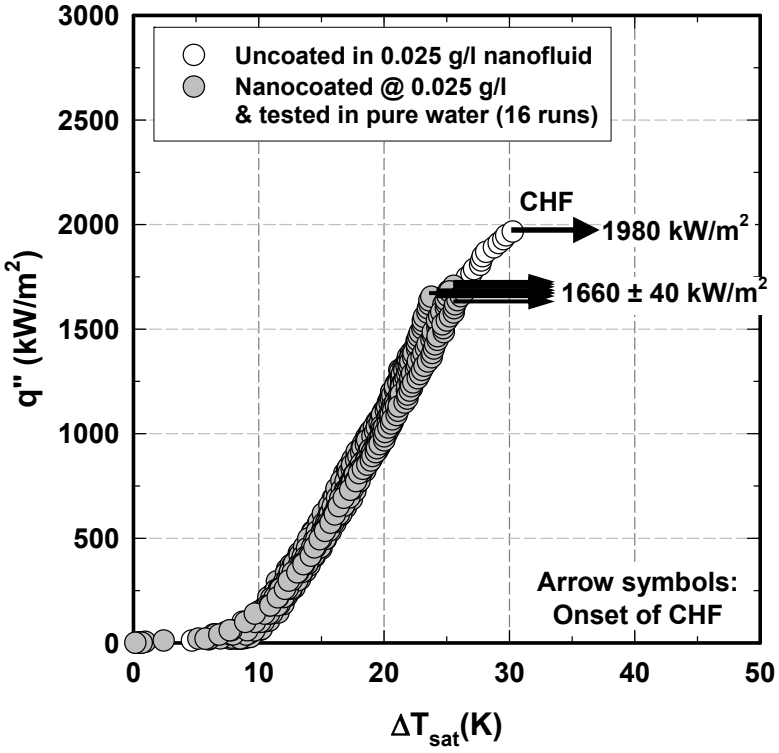

Fig. 5.3 Reliability test of the nanocoated heater (16 runs in pure water).

Additional experiments were conducted with the 0.025 g/l nanocoated heater to determine the reliability of the nanocoating. Reliability is defined as the coating's ability to remain attached to the surface and to enhance CHF. Sixteen consecutive pool boiling tests were conducted with the 0.025 g/l nanocoated heater in pure water and results are shown in Fig. 5.3. Nearly identical pool boiling performance in both BHT and CHF, for the 16 tests, indicates that the coating generated has good bonding to the surface even after repetitive testing.

5.2 Cause of Nanoparticle Deposition

Although studies have been carried out using nanocoated surfaces [26], the factors responsible for the nanoparticle deposition have not been investigated. This section experimentally tries to determine the cause behind this nanoparticle deposition. Four different factors that can potentially generate nanoparticle coatings were investigated. These factors are gravity (natural nanoparticle precipitation), natural convection (low heat flux), an applied electric field, and boiling. Each of these parameters can potentially generate coatings of varying thicknesses and qualities. SEM images, apparent contact angle measurements, and pool boiling performance were used to gauge the effect of these factors on the coatings produced. Also, since the actual boiling experiment lasted around an hour, all parameters affecting the nanoparticles deposition were tested for the same duration.

To investigate the nanoparticle coating formed as a result of only gravitational deposition, a clean heater was left in the nanofluid for 1 hour with no power. For the natural convection role in nanocoatings formation, a heat flux of 10 kW/m^2 was applied to the heater while it was left in the nanofluid for 1 hour. The effect of an electrical field was investigated by applying a 10 volt potential between the heater and a copper block centered 4 mm above the heater. The heater was left in this condition with no power for 1 hour in the nanofluid. For reference, the electrical leakage from the heater during actual experimentation was measured to be ~ 4 mV with the same test configuration. Therefore, it was assumed that the voltage field

of 10 volt should be high enough to demonstrate the effect of the electrical field produced in actual tests. For all tests, Al_2O_3 nanofluids at 0.025 g/l concentration and 1 cm x 1 cm heaters were used.

In the course of 1 hour, the heater experienced varying amounts of nanoparticle deposition for each of the three cases (gravity, natural convection, and electrical field). After 1 hour the nanocoated heaters are removed from the nanofluid bath and pool boiling tests were immediately performed with the nanocoated heaters in pure water. This process allowed only the nanoparticles that are strongly attached on the heater surface to influence the pool boiling performance while the weakly adhered nanoparticles dispersed in pure water. Fig. 5.4 displays the pool boiling curves for these tests. For reference, the pool boiling curve pertaining to the 0.025 g/l nanocoated heater coated during 0.025 g/l nanofluid pool boiling experiments is also shown.

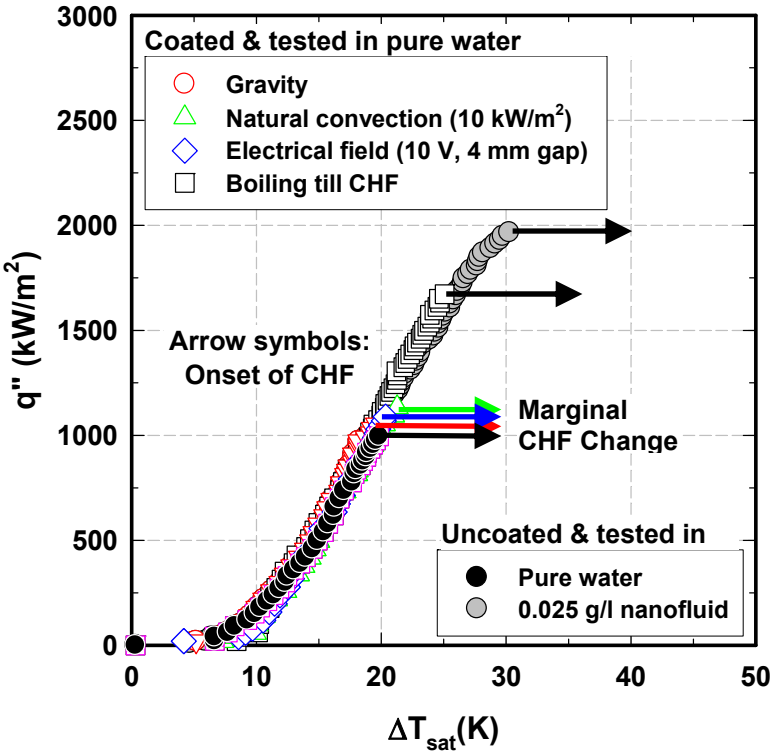

Fig. 5.4 Pool boiling curves of various nanoparticle coated surfaces (gravity, natural convection, electrical field, and boiling).

SEM images of the various nanoparticle coated heaters produced for all cases, taken after pool boiling tests in pure water, are provided in Fig. 5.5. These SEM images show that the nanocoatings produced by means of gravity, natural convection, and electric field, show minimal nanoparticle deposition. Also, the pool boiling performance (Fig. 5.4) in pure water shows that these coatings have negligible effect on the CHF and the BHT. Both pool boiling performance and SEM images indicate neither gravity, natural convection nor electric field methods are capable of producing nanocoatings thick enough to affect the CHF and the BHT.

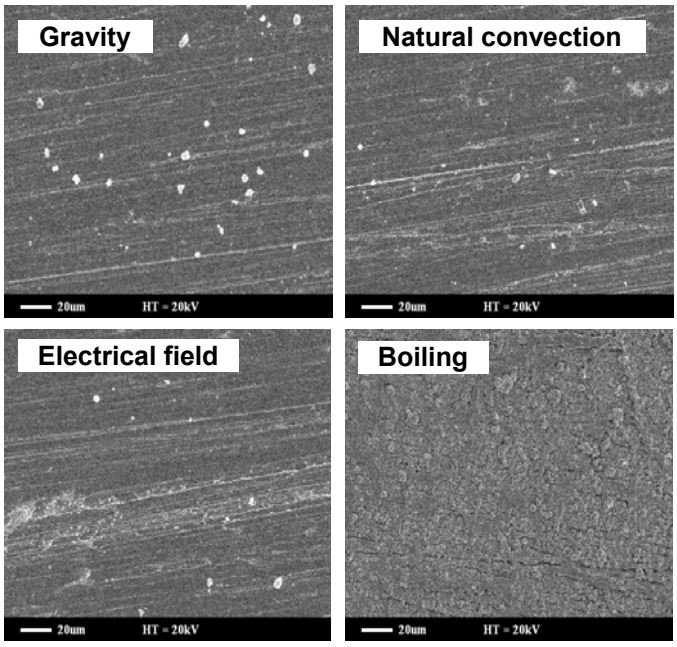

Fig. 5.5 SEM images of the nanoparticle deposits/coatings formed on the heater surface (gravity, natural convection, electric field, and boiling).

Therefore, experimental evidence suggests that boiling itself appears to be the primary mechanism responsible for the nanoparticle coating formation. This is consistent with Kim et al. [8] who hypothesized that the nanocoatings formed during nanofluid boiling are created as the vapor bubbles' microlayers evaporate. As vapor bubbles grow, the evaporating liquid in the microlayer leaves behind nanoparticles which then concentrate at the base of the bubble. The nanoparticles then bond to the hot heater surface (Fig. 5.6).

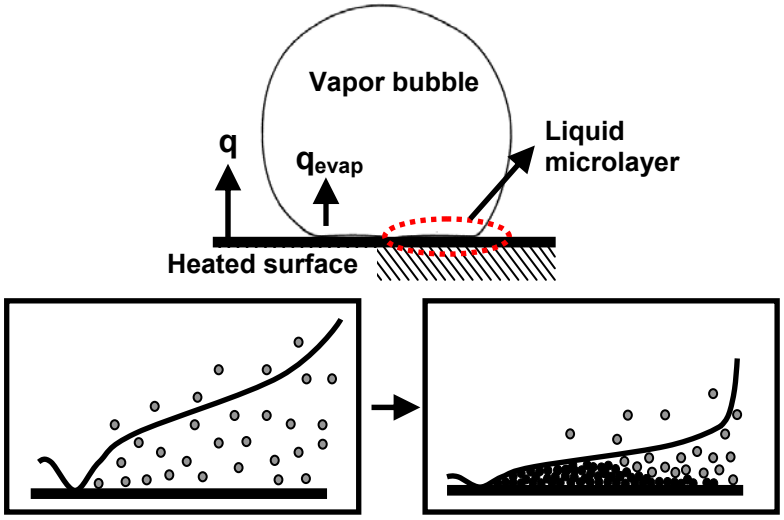

Fig. 5.6 Mechanism of the nanoparticle deposition during the boiling process (microlayer evaporation).

To test this theory, a simple experiment was conducted using a copper heater submerged in Al_2O_3 nanofluid (1 g/l). Power to the heater was slowly increased until a single nucleation site was generated at the heater surface. This power was then maintained constant and the single active nucleation site was allowed to undergo several boiling cycles. After about 2 min., the power to the heater was shut off and the heater was removed from the nanofluid bath. The heater surface is then observed to have a single circular nanoparticle coating formed at the exact active nucleation site location and nowhere else (Fig. 5.7).

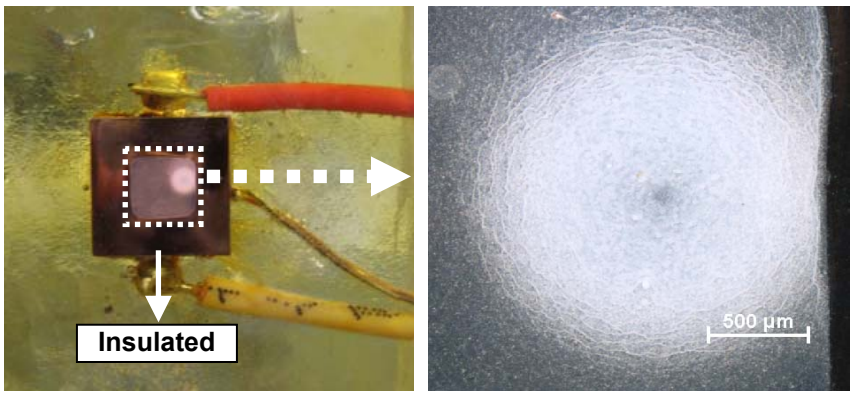

Fig. 5.7 Images of the nanoparticle coating generated on the heater surface from a single bubble.

This test demonstrates that boiling (microlayer evaporation) is responsible for producing the nanoparticle coatings that are observed after nanofluid boiling experiments. While Kim at al. [8] hypothesized this deposition process, this study has experimentally confirmed it. To summarize, boiling (through microlayer evaporation) of low concentration (≤ 0.025 g/l) nanofluids produce a nanoparticle coating on the heater surface and this coating then enhances the surface wetting characteristics which then increases the CHF. The increase of the wettability due to nanocoating is discussed next. It should be noted that using higher concentration nanofluids can also enhance CHF but at the expense of degrading BHT.

5.3 Surface Wettability of Nanocoating

The heater surface wettability plays a key role during the pool boiling of liquids [8, 26, 39]. To investigate the wettability of various coatings (produced through gravity, natural convection, electric field, and boiling), contact angle measurements were carried out for the various nanocoated surfaces. As was the case with SEM images, apparent contact angle measurements were taken for all nanocoated surfaces after these surfaces had been tested in pool boiling with pure water. This then eliminates the influence of any additional nanocoating formations which may occur as the nanofluid liquid droplets (attached to the heater as it is removed from the nanofluid bath), resting on the heater surface, are allowed to dry in ambient conditions. Also, the nano/micro structures of the nanocoatings can potentially wick fluid and thus make static contact angle measurements inadequate in measuring what could be a dynamic situation. Therefore, apparent contact angle measurements in this study are plotted as a function of time (4 min. time span) for the various coatings (Fig. 5.8).

The lack of a substantive nanoparticle coating (generated through gravity, natural convection, and electric field) is evident in their relatively high apparent contact angle measurements which are not much different than those of a plain (uncoated) surface. On the other hand, the thicker nanoparticle coatings formed during pool boiling in nanofluids have

significantly better wetting characteristics (lower contact angle) and which in turn increases the CHF. An observation made through this study is that there seems to be a relationship between the apparent contact angle and CHF value. The contact angles measured on the various coatings were observed to decrease with time (likely a result of evaporation and spreading of liquid) which complicates the issue of selecting one representative contact angle value. Nevertheless, it was decided to use the quasi-static contact angle measurement taken at 60 sec. since it appears to be relatively stable compared to initial value (strong dynamic stage) and the last value (noticeable evaporation in ambient).

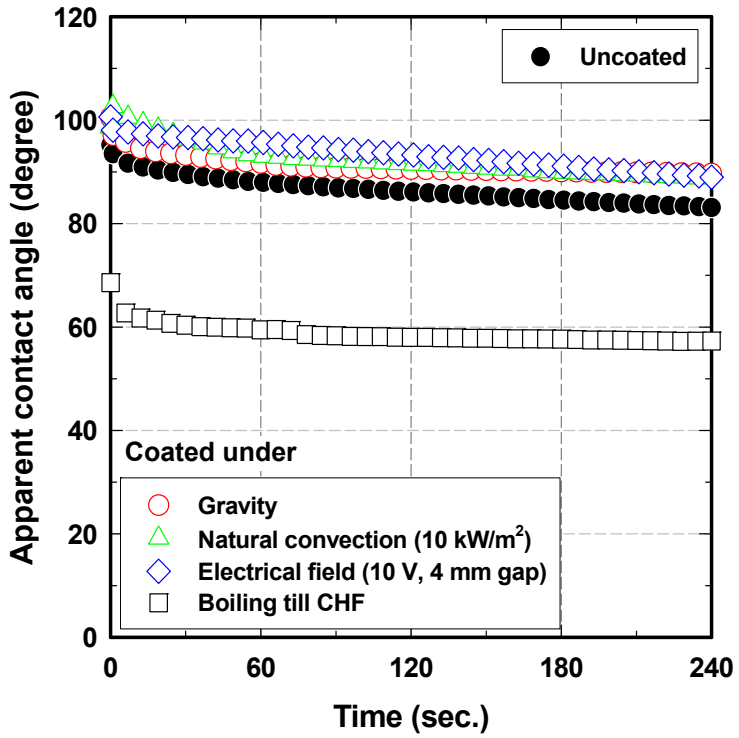

Fig. 5.8 Apparent contact angle measurement for various nanocoatings.

Fig. 5.9 shows that there is a linear-like relationship between CHF and the quasi-static contact angle, in which CHF increases with decreasing contact angle. This strongly indicates that the wettability of the heater surface is closely related with CHF enhancement. This relationship will be further discussed in the next chapter.

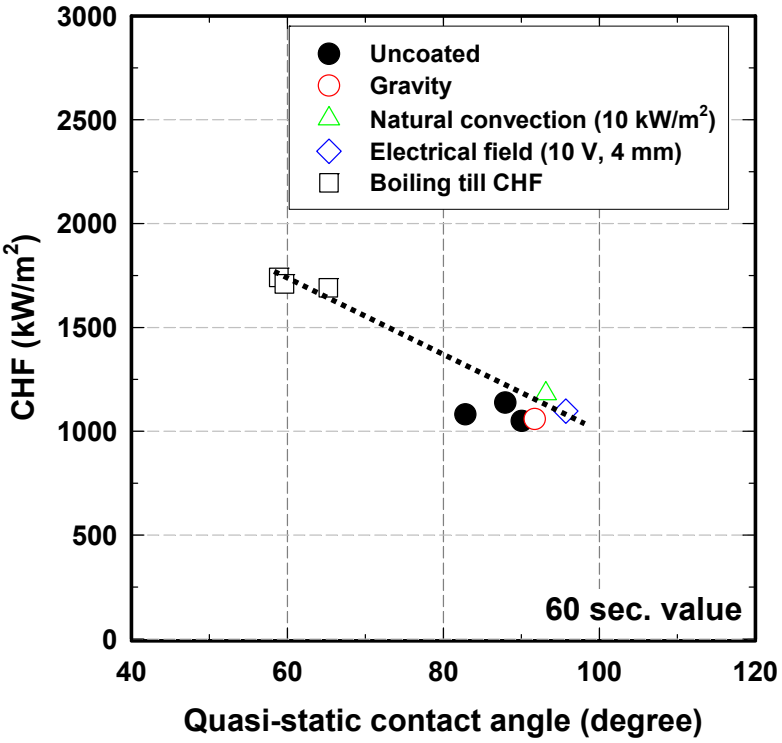

Fig. 5.9 Relationship between CHF value and quasi-static contact angle.

CHAPTER 6

NANOCOATING DEVELOPMENT AND OPTIMIZATION

This section discusses a method to optimally coat a heater surface with nanoparticles which then can provide an enhanced pool boiling characteristics. Prior chapters have confirmed that nanoparticle coatings are the source of the dramatic CHF enhancement and a change in the BHT. Since nanoparticle coatings can be formed during the nanofluid boiling process, an attempt was made to maximize the effectiveness of the coatings by varying the boiling parameters (i.e. imposed heat flux, boiling duration, nanoparticle concentration, and base fluid) to generate coatings of varying structures and/or thicknesses. In this manner, the nanoparticle coatings could be optimized to provide the maximum CHF enhancement without degrading BHT.

6.1 Nanocoating Development in Al_2O_3-Water Nanofluids

Various nanoparticle coatings or nanocoatings were first developed in Al_2O_3-water nanofluids. These coatings were generated by submerging a 1 cm × 1 cm heater in saturated nanofluid, applying power to the heater and leaving it in this condition for a given time. These experiments were then repeated by varying the imposed heat flux, boiling duration, and nanoparticle concentration to create nanocoatings of varying structures and/or thicknesses. The test matrix used to develop the various coatings is provided in Table 6.1.

For example, six nanocoatings are developed in 0.025 g/l concentration of Al_2O_3 water nanofluid by varying developing duration from 5 min. to 120min. at a heat flux of 1000 kW/m^2

(2^{nd} row and 2^{nd} column in Table 6.1). The boiling performance of these coatings was then evaluated by conducting pool boiling tests of the nanocoated heaters in pure water. Results from these experiments are compared and discussed in this section.

Table 6.1 Nanocoating development for various durations (min.) at various heat fluxes and concentrations in water-based nanofluids.

	0.025 g/l	0.1 g/l	1 g/l
1000 kW/m^2	5, 15, 30, 45, 60, 120	2, 5, 10, 15	0.5, 1, 2, 5
500 kW/m^2	20, 40, 60	5, 10, 15	1, 2, 5
250 kW/m^2	60, 80, 120	10, 20, 30	1, 1.5, 2

To demonstrate the effect of the nanocoatings, Fig. 6.1 displays the pool boiling curves for only two nanocoated heaters (15 min. and 120 min.) that were tested in pure water (selection made from 2^{nd} row and 2^{nd} column in Table 6.1. See Fig. B1 in Appendix B for pool boiling results of all other durations). The nanocoating on the two heater surfaces were generated using Al_2O_3 nanofluid at 0.025 g/l concentration while applying a constant power to the heater (1000 kW/m^2). The only difference being that one of nanocoatings was developed by sustaining the heater power for 15 min. while the other was generated by sustaining the heater power for 120 min. Included in Fig. 6.1 is the boiling curves for an uncoated heater as a reference.

Results show that the nanocoatings enhance CHF by 50% and 70% compared to the Zuber's [72] CHF value (eq. (5)) for the 15 and 120 min. nanocoatings, respectively (Fig. 6.1). In addition, the coating generated over a 120 min. period is found to degrade BHT while the coating generated over a shorter 15 min. period is found to have minimal effect on BHT. These differences in performance can be attributed to the differences in the thickness of the nanoparticle coating on the heater surface. From the optical and SEM pictures, it is clear that nanoparticle deposition is a function of heating duration where longer durations result in more nanoparticle deposition (Fig. 6.2). The 15 min. nanocoating is found to have more of a patchy nanoparticle coating leaving some surface areas seemingly uncoated.

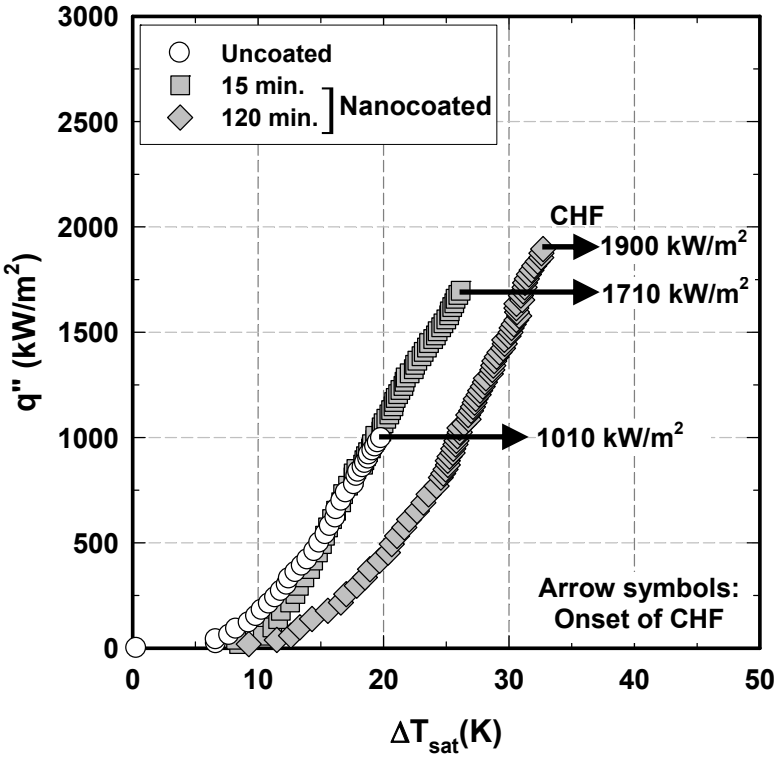

Fig. 6.1 Pool boiling curve of pure water with nanocoatings developed in 0.025 g/l water-based nanofluid for 15 and 120 min. at 1000 kW/m^2.

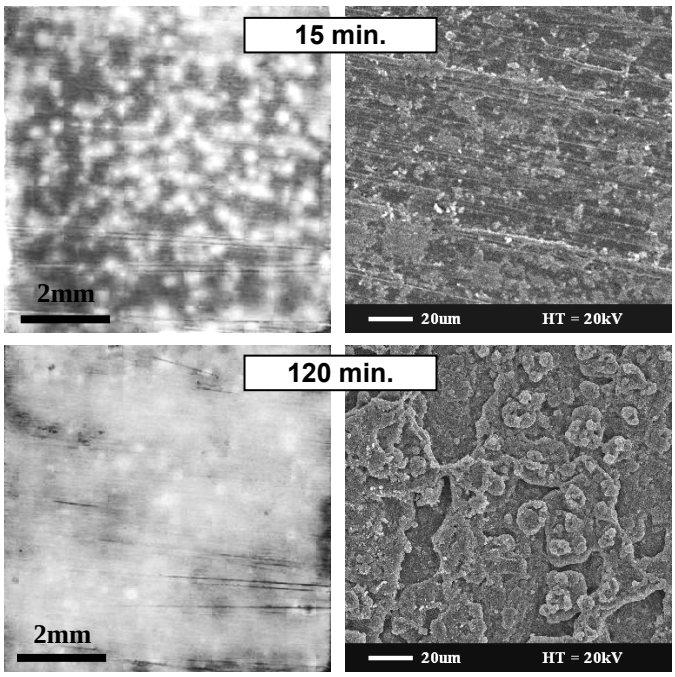

Fig. 6.2 Optical (left) and SEM (right) images of nanocoatings developed in 0.025 g/l water-based nanofluid for 15 (top) and 120 min. (bottom) at 1000 kW/m^2.

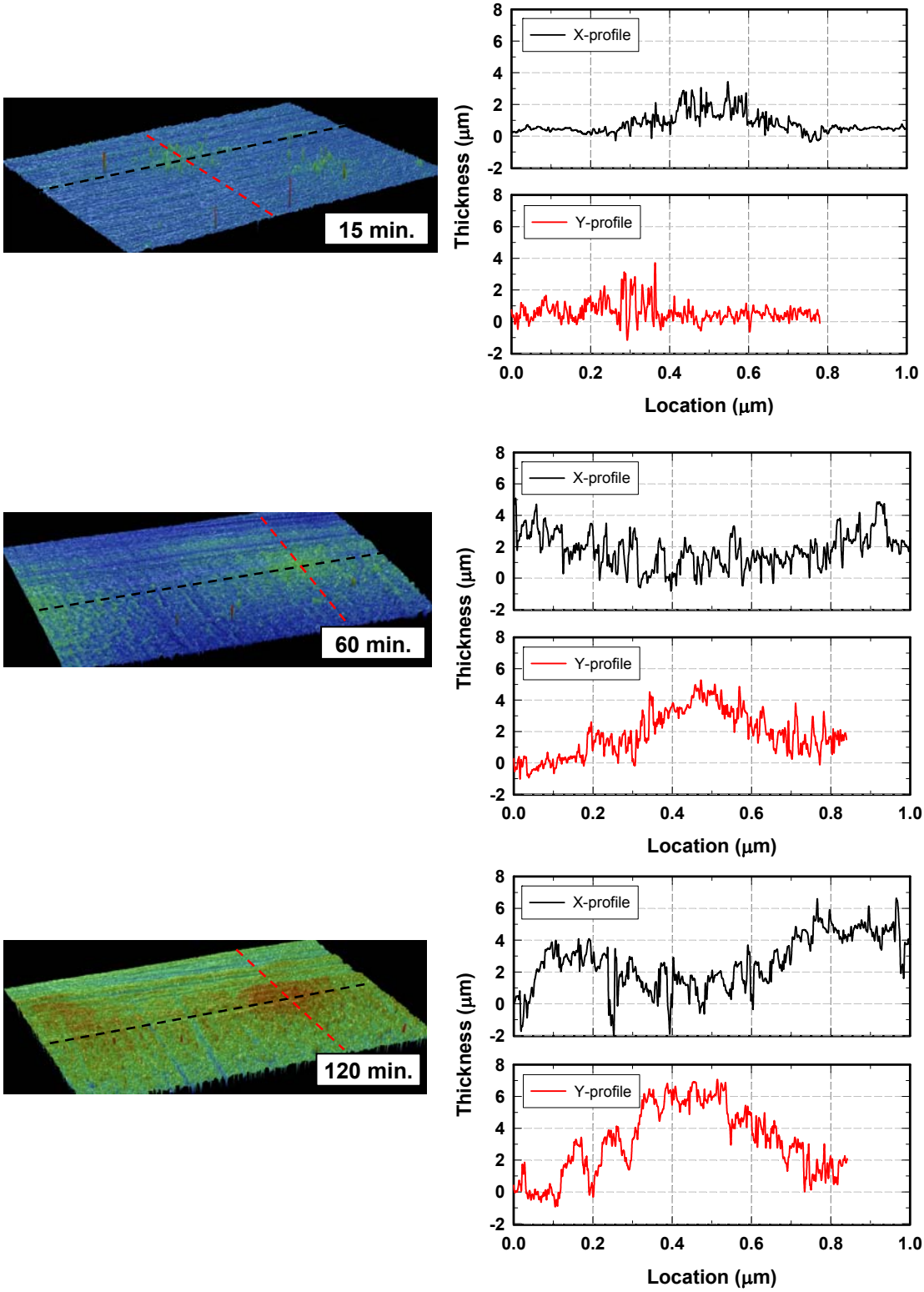

Fig. 6.3 Surface profile measurement of nanocoatings developed for 15, 60, and 120 min. at 1000 kW/m^2.

To further investigate this coating thickness, surface profile measurements of nanocoated layers were taken and their average thicknesses were measured using an optical profilometer. The surface profiles obtained for 15, 60, and 120 min. are shown in Fig. 6.3. The average thickness of nanocoatings were measured to be ~1, ~2, and ~3 μm for the 15, 60, and 120 min., respectively (Fig. 6.4). The results are consistent with SEM images and boiling performance results which indicate that the longer the nanofluid boiling duration, the thicker the nanoparticle deposition. The nanocoating thickness increases the thermal resistance and this is the reason why the thicker 120 min. nanocoating degrades BHT whereas the thinner 15 min. nanocoating does not.

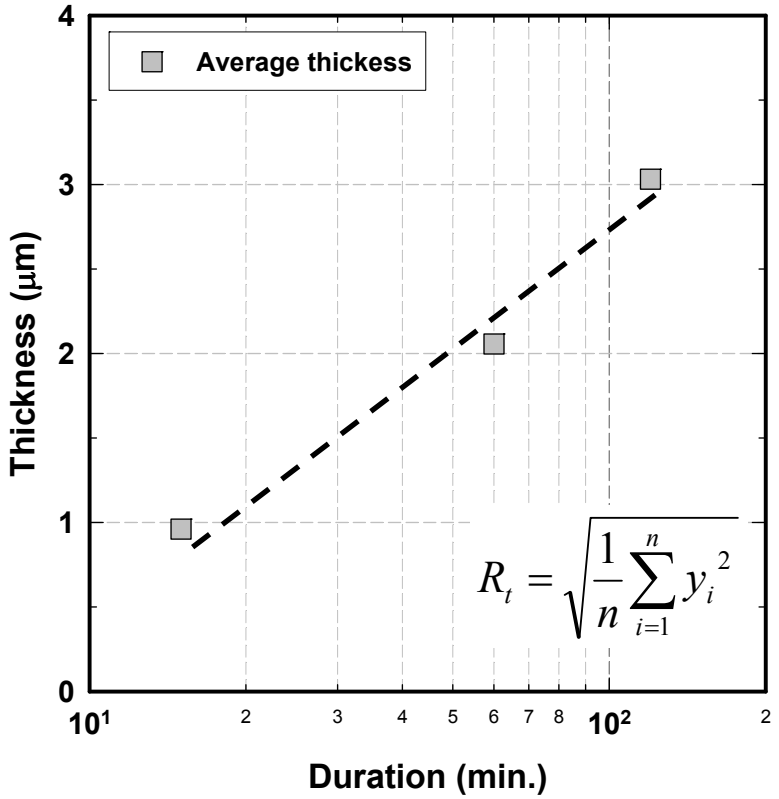

Fig. 6.4 Average thickness of the developed nanocoatings over developing duration (15, 60, and 120 min.).

Due to the large quantity of data gathered, it is not possible to discuss each nucleate boiling performance and SEM image obtained from all the nanocoatings listed in Table 6.1. All experimental results shown in Table 6.1 are included in Appendix B. A summary of the CHF and BHT values for the nanocoatings generated through nanofluid boiling at a heat flux of 1000 kW/m^2 (all nanocoatings listed in the 2nd row in Table 6.1) is provided in Fig. 6.5. The effect of both nanoparticle concentration and nanofluid boiling duration on performance is summarized in this figure. Results show that CHF increases with increasing nanofluid boiling duration which is consistent with the results provided in Fig. 6.1. However, CHF is not found to increase without bound, instead CHF increases with increasing duration until it reaches its maximum value of about 2000 kW/m^2, where it remains unchanged even if boiling duration is increased. In fact, the CHF for any of the nanocoated heaters created never exceeds ~2000 kW/m^2 at the tested 1 atm pressure condition.

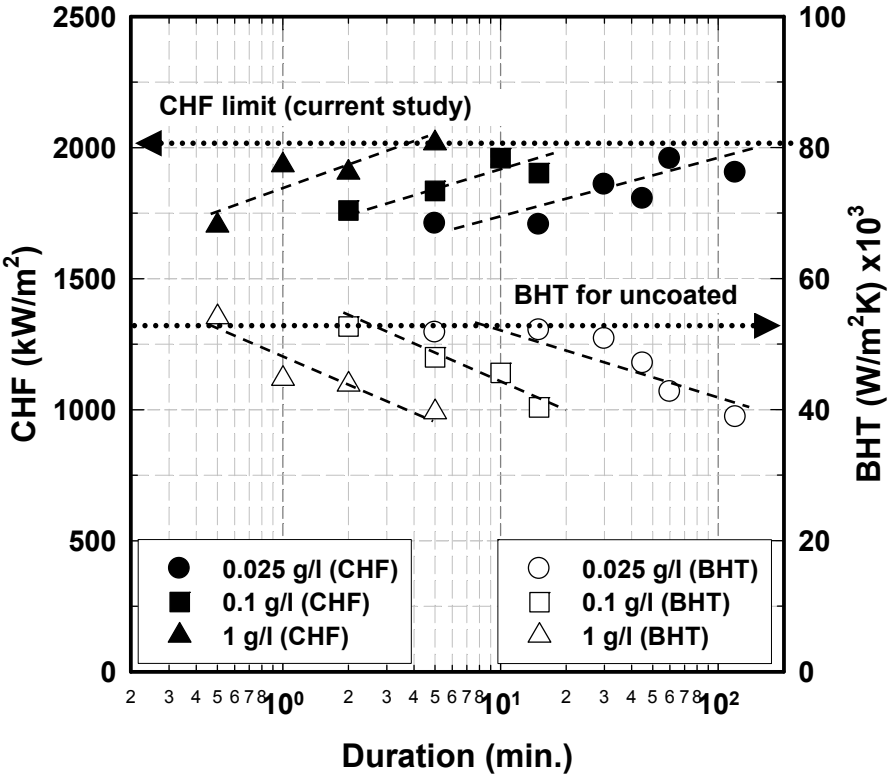

Fig. 6.5 CHF (closed symbols) and BHT (opened symbols, values at 1000 kW/m^2) comparison of developed nanocoatings at 1000 kW/m^2 over durations.

Since the CHF enhancement of nanofluids has been attributed to an increase in surface wettability (decrease of the apparent contact angle), then it might be possible that the limit on CHF enhancement observed in this study could be a result of a limit on the surface wettability. In other words, the surface wettability characteristics change with increasing nanocoating thickness resulting in an increase in CHF. However, beyond a certain nanocoating thickness and/or structure, there is no further change to the surface wetting and thus no further CHF enhancement can be observed. The BHT performance, on the other hand, deteriorates as duration increases that leads to increasing nanocoating thickness (Fig. 6.5).

Experimental results also indicated that the nanocoating film on the heater surface grew at a faster rate using higher concentration nanofluids. For example, a one minute coating development time in the 1 g/l nanofluid created a nanocoating thick enough to degrade BHT (Fig. 6.5). In contrast, it takes a significantly longer (~45 min.) development time to generate a nanocoating thick enough to degrade BHT in 0.025 g/l nanofluid. Other nanocoatings developed at different heat fluxes (500 and 250 kW/m^2) tabulated in 3^{nd} and 4^{th} row of Table 6.1 also show almost identical trend with the nanocoatings generated at 1000 kW/m^2. Fig. 6.6 includes the CHF and the BHT performance of all the nanocoatings listed in Table 6.1.

All nanocoatings discussed above were generated using water-based nanofluids. Although these nanocoatings were successful at enhancing CHF, they tended to be patchy and non-uniform (Fig. 6.2). As discussed earlier, microlayer evaporation is thought to be responsible for the nanoparticle deposition on the heater surface. This suggests that the size of nucleating bubbles could affect the structure of the nanocoating. It is then hypothesized that the relatively large bubbles of water may be responsible for the non-uniformity of the nanocoatings produced using water-based nanofluids. This leads to the idea of using ethanol-based nanofluids, which produce smaller bubble sizes as the result of its lower surface tension, and thus can generate a more uniform nanocoating.

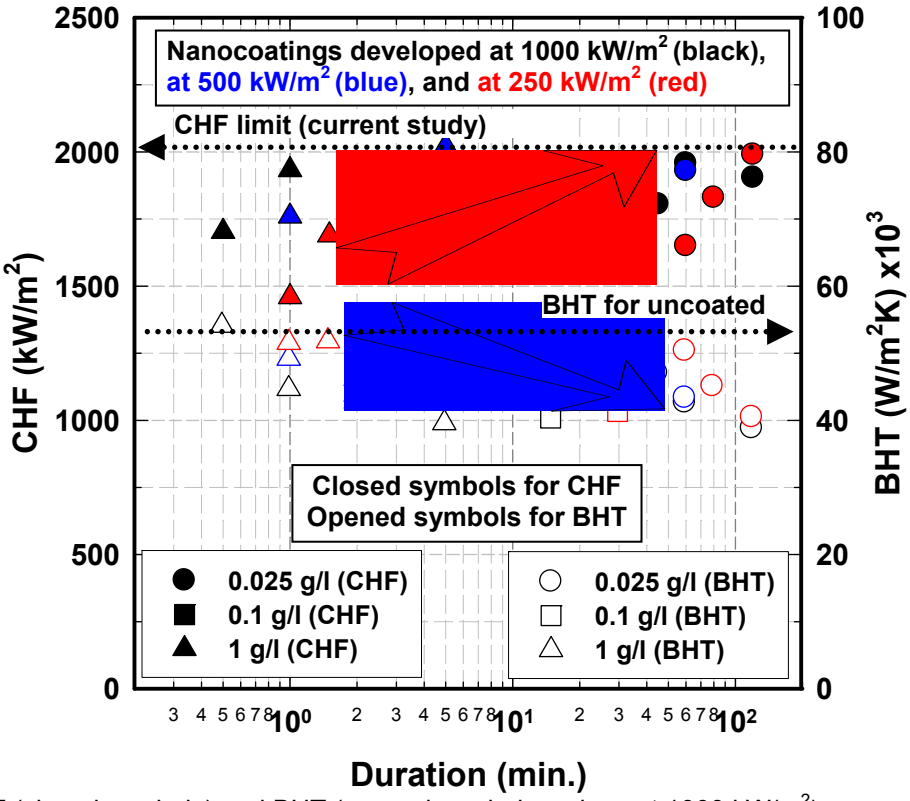

Fig. 6.6 CHF (closed symbols) and BHT (opened symbols, values at 1000 kW/m^2) comparison of developed all nanocoatings listed in Table 6.1 over durations.

6.2 Nanocoating Development in Al_2O_3-Ethanol Nanofluids

Ethanol nanofluids were prepared by dispersing 2 grams Al_2O_3 nanoparticles into 2 liters of ethanol. The solution was then subjected to an ultrasonic bath for two hours which produced the ethanol-based nanofluids which was then used to create the nanocoatings. Flat heaters were immersed into the 1 g/l ethanol nanofluid and a constant heat flux of 500 kW/m^2 was applied to them. Various nanocoatings were created by varying the coating development time or boiling duration (0.5 ~ 5 min.). Once the coating was developed, the heater is flushed with pure ethanol and dried using compressed air. Pool boiling experiments in pure water were then performed using the nanocoated heaters to evaluate the performance of the coatings.

Microscopic images of the nanocoatings created using the ethanol nanofluids for 2 and 5 min. (Fig. 6.7) show a more uniform nanocoating. This is in sharp contrast to the nanocoatings

generated using water-based nanofluids where the coatings tended to have more of a patchy, non-uniform consistency (Fig. 6.2). Since microlayer evaporation is believed to be responsible for depositing and bonding the nanoparticles to the surface, then it is possible that the smaller nucleation bubble sizes of ethanol, as compared to water, is the reason for the uniformity of these coatings.

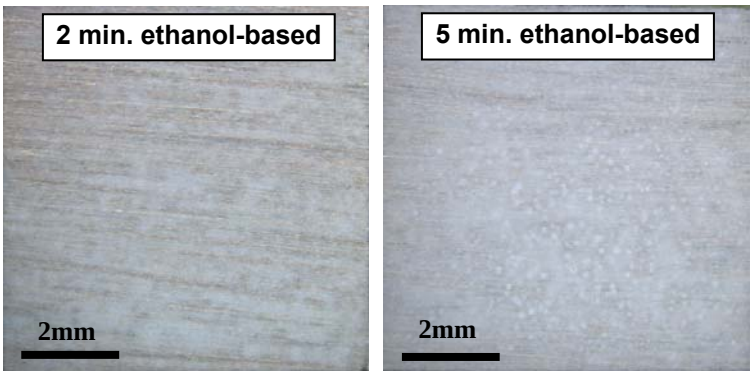

Fig. 6.7 Optical images of the nanocoatings developed in 1 g/l ethanol nanofluid for 2 and 5 min. at 500 kW/m^2.

The pool boiling curve for one of the nanocoatings created with ethanol nanofluids (2 min. development time) is shown in Fig. 6.8 alongside a pool boiling curve for an uncoated heater (plain). The nanocoated heater produced a CHF of about 1930 kW/m^2, which is close to the maximum CHF value obtained using the nanocoatings created using water-based nanofluid. In addition, the nanocoating did not degrade BHT. This combination of maximum CHF enhancement with no BHT degradation was never achieved using the nanocoatings formed in water-based nanofluids as tested in the current study. Thus it seems that boiling performance (CHF and BHT) is not only affected by the thickness of the coating, it is also influenced by the uniformity and/or structure of the nanocoatings.

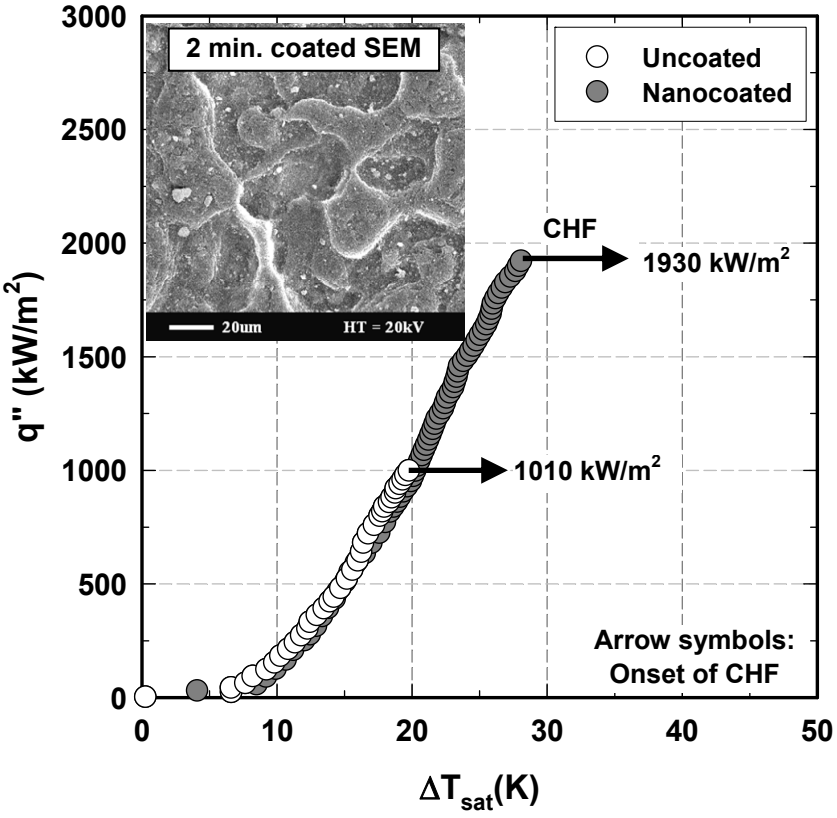

Fig. 6.8 Pool boiling curve of pure water with the nanocoating developed in 1 g/l ethanol nanofluid for 2 min. at 500 kW/m^2.

The pool boiling results of the various nanocoatings created by varying the coating development time (0.5 ~ 5 min.) in the ethanol nanofluid are shown in Fig. 6.9. The developed nanocoatings always show CHF enhancement but BHT appears to degrade as the coating time increases like in the case of nanocoatings developed in water-based nanofluid.

To capture the performance of the various nanocoatings developed in ethanol nanofluid, the CHF and the BHT values obtained are summarized in Fig. 6.10. An optimal nanocoating, which provided the maximum CHF enhancement (~80%) without degrading BHT, is created using a coating development time of 1 ~ 3 min. Shorter development times (< 1 min.) create thinner nanocoatings which likely do not have the surface characteristics (i.e. wetting and wicking) required for maximum CHF enhancement. Longer development times (> 3 min.) create thicker coatings that provide an extra thermal resistance which then degrades BHT.

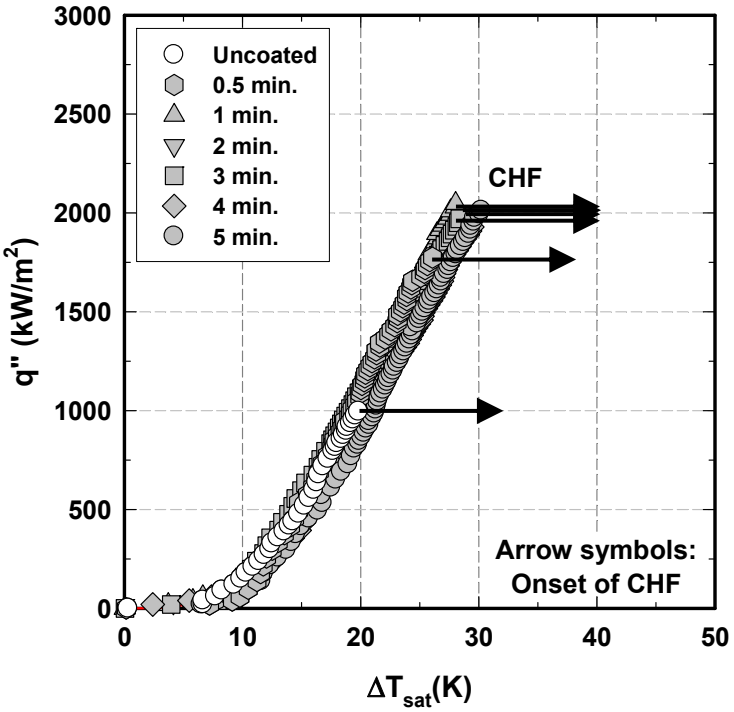

Fig. 6.9 Pool boiling curves of pure water with nanocoated surfaces developed in 1g/l Al_2O_3–ethanol nanofluid for various durations at 500 kW/m^2.

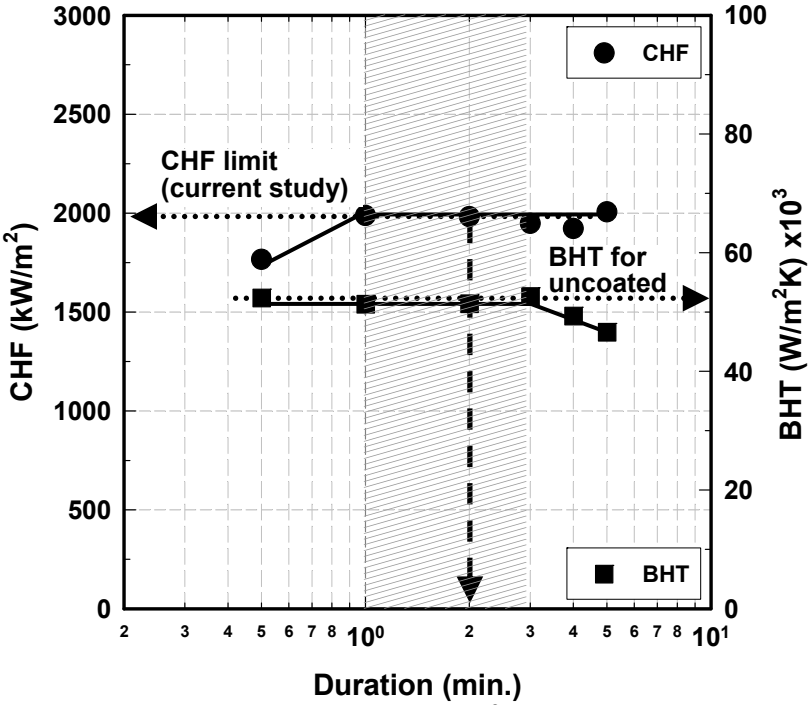

Fig. 6.10 CHF and BHT value (at 1000 kW/m^2) comparison of nanocoatings developed in 1 g/l ethanol nanofluid at 500 kW/m^2 over the duration.

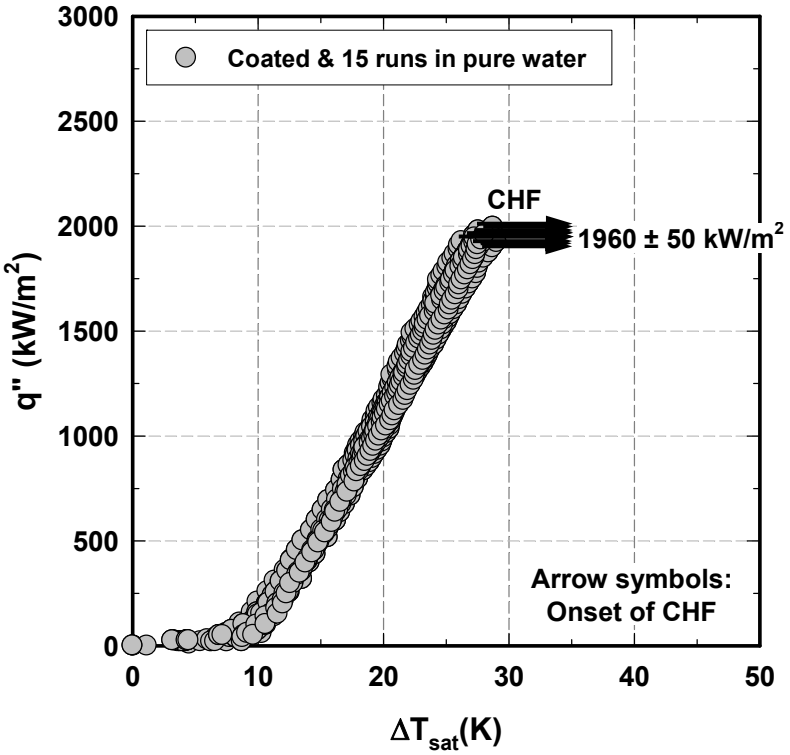

Fig. 6.11 Reliability test of the nanocoated heater developed in 1 g/l alcohol nanofluid for 2 min. (15 runs in pure water).

After finding a methodology for an optimal nanocoating, the reliability of the nanocoating developed in ethanol-based nanofluid was tested. It was performed by conducting 15 consecutive pool boiling tests in pure water with one of the nanocoated heaters (2 min. coating). Reliability was defined as the nanocoating's ability to remain attached to the surface and provide consistent boiling performance. As shown in Fig. 6.11, repeating experiments with the same nanocoated heater gave consistent nucleate BHT and CHF enhancement indicating that the coating has good bonding to the surface.

6.3 Nanocoating Wetting Characteristics

As briefly discussed in Chapter 5.3, it appears that surface wetting characteristics of the nanocoating are responsible for the dramatic CHF enhancement. Thus it is necessary to determine the effect of the various nanocoatings on surface wettability. This was done by measuring the

contact angles between droplets of pure water and the various nanocoated surfaces, as mentioned in Chapter 5.3. To capture any dynamic effects associated with potential fluid wicking (through the nanocoating), contact angles were measured over a 4 min. time span.

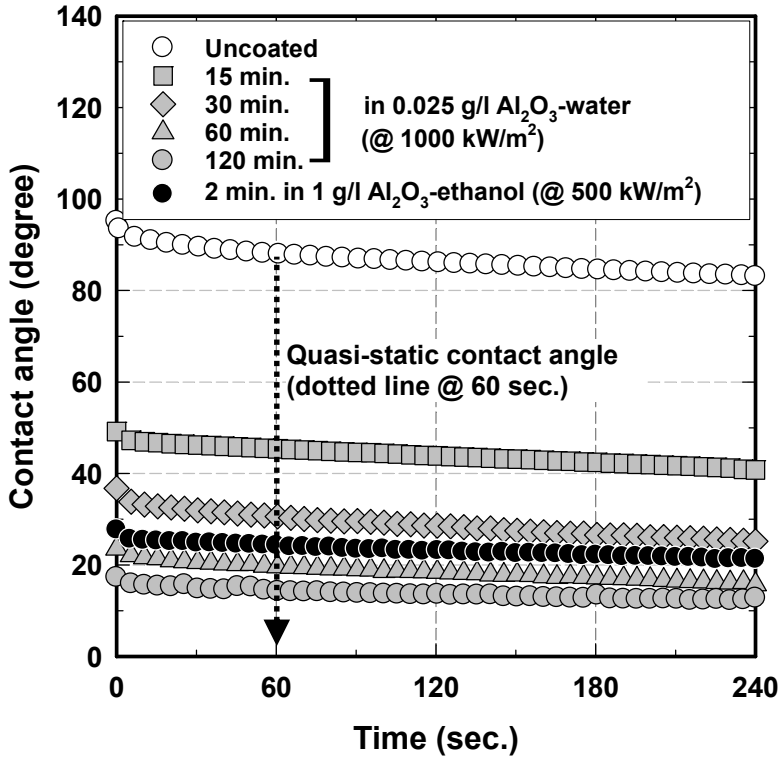

Fig. 6.12 Contact angles of nanocoatings developed in water and ethanol-based nanofluids.

Contact angle measurements for nanocoatings created in water-based nanofluids (15 ~ 120 min. coatings) and ethanol-based nanofluids (2 min. coating) are plotted in Fig. 6.12. As shown in the figure, the effect of all nanocoatings is to increase surface wettability (lower contact angle). The measured contact angles, for the nanocoatings created with water-based nanofluids, are observed to decrease significantly with increasing nanocoating thickness (i.e. increasing coating development time) and then gradually stabilize at about 15 ~ 20°. Increasing the nanocoating development time from 60 min. to 120 min. does not significantly change the surface wettability which indicates that there is a limit to the extent the surface wettability can be modified using nanocoatings (at least those nanocoatings that are produced in this study). The nanocoating generated in ethanol nanofluids, with 2 min. development time, produces contact angles similar

in magnitude to those produced using water nanofluids at relatively long development times (30 ~ 120 min.). This behavior is consistent with pool boiling results where the 2 min. ethanol nanocoating produced CHF values similar to those of nanocoatings created using water nanofluids at higher development times. These results show that the CHF enhancement is directly related to the surface wettability that gets measured by the contact angle produced by the nanocoatings. All other contact angle results for all the developed nanocoatings discussed can be found in Appendix B.

To study the relationship between CHF enhancement and surface wettability, CHF values were plotted as a function of the measured quasi-static contact angle. Although it is a complicated issue to choose the representative contact angle due to the dynamic behavior of the contact angle measurement, observations of the continuous contact angle measurements lead to the value at 60 sec. to be defined as quasi-static contact angle (Chapter 5.3).

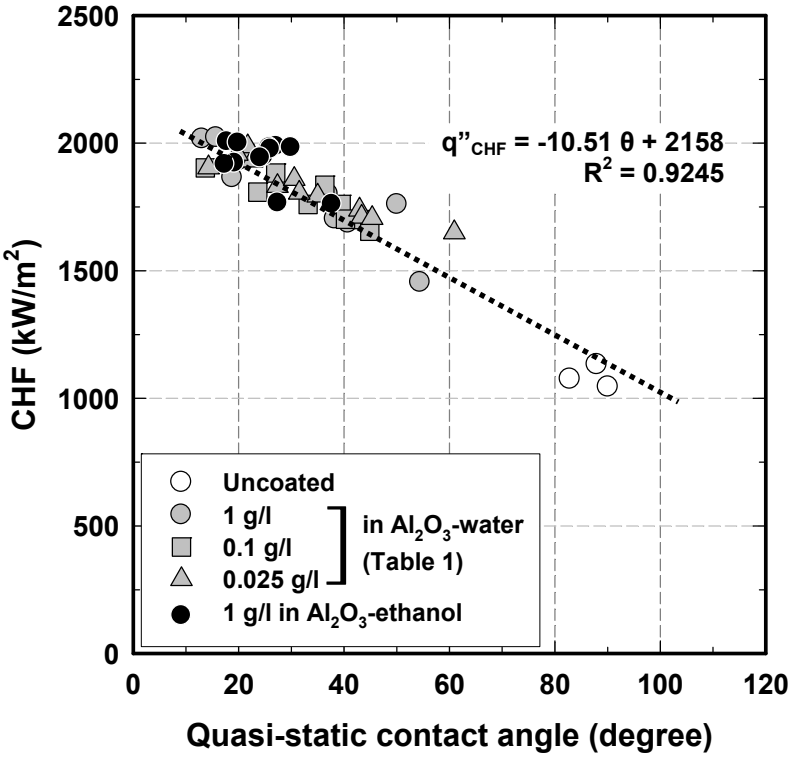

Fig. 6.13 Overall relationship between quasi-static contact angle and CHF for nanocoatings developed in water and ethanol-based nanofluids throughout current study (various heat fluxes, concentrations, and durations).

Fig. 6.13 plots the CHF values produced by all the nanocoatings as a function of the measured quasi-static contact angle. This figure includes all the nanocoatings listed in Table 6.1 and also includes all the nanocoatings generated using ethanol-based nanofluids. There is a clear linear relationship between CHF and surface contact angles where lower contact angles produce higher CHF. A linear regression was performed on the data points which led to the equation shown in Fig. 6.13 which relates the static contact angle to CHF:

$$q''_{CHF} = -10.51\theta + 2158 \quad (6)$$

where θ is a quasi-static contact angle.

In order to further understand the wetting behavior in the nanocoatings a vertical dip test was performed in pure water with the uncoated and nanocoated (2 min. coating in ethanol nanofluid) heaters. Both heaters were vertically oriented and dipped into pure water. Using a high speed camera, the liquid front movement was recorded as the liquid came in contact with the heater surface. Fig. 6.14 provides a series of sequential images taken by high speed camera for the nanocoated heater surface. As soon as the nanocoated surface contacted the liquid, the liquid meniscus was instantly pulled up by ~2.6 mm onto the surface as the result of the hydrophilic nature of the surface. On the other hand, there was no attraction/movement of the liquid when the uncoated heater was used. It should be noted that there appeared no significant wicking head following the observed instantaneous wetting liquid front.

Wicking can generally be defined as the flow of a liquid through the porous medium due to capillary force – see Fig. 6.15(a). However, the present vertical dip test shows that the liquid head on the coated surface stopped at ~1000 ms after it initially pulled the liquid instantaneously by wetting. The liquid meniscus is built up to the measured pulling height within a fraction of second and stayed at that point.

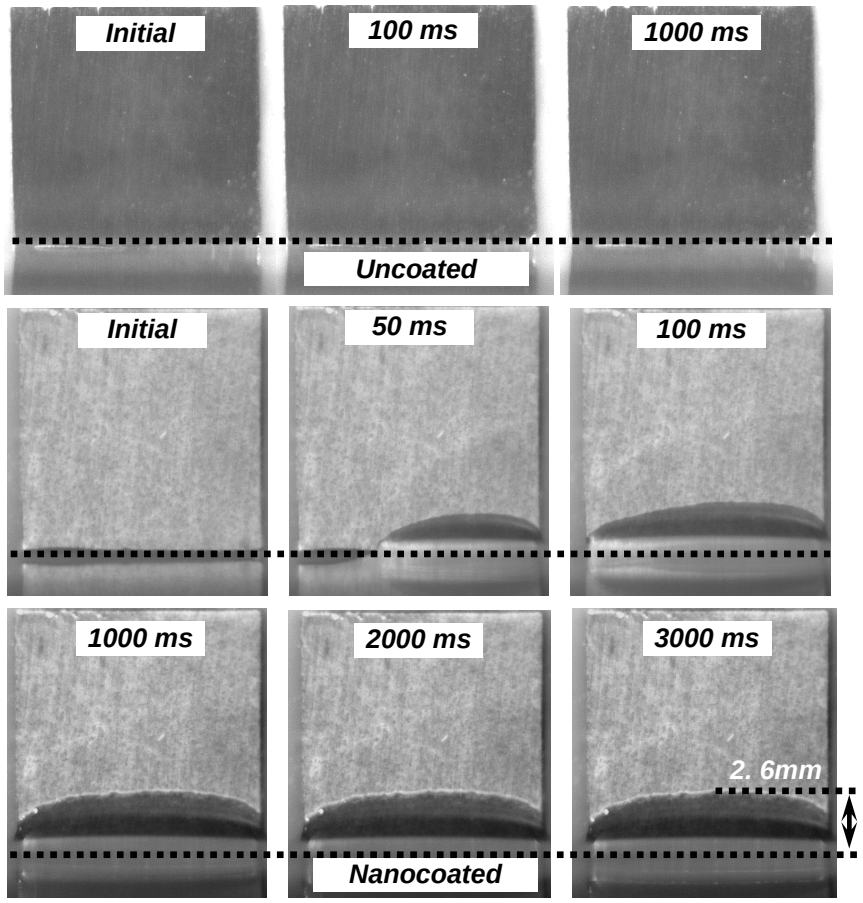

Fig. 6.14 Vertical dip test of plain (uncoated) and nanocoated surfaces.

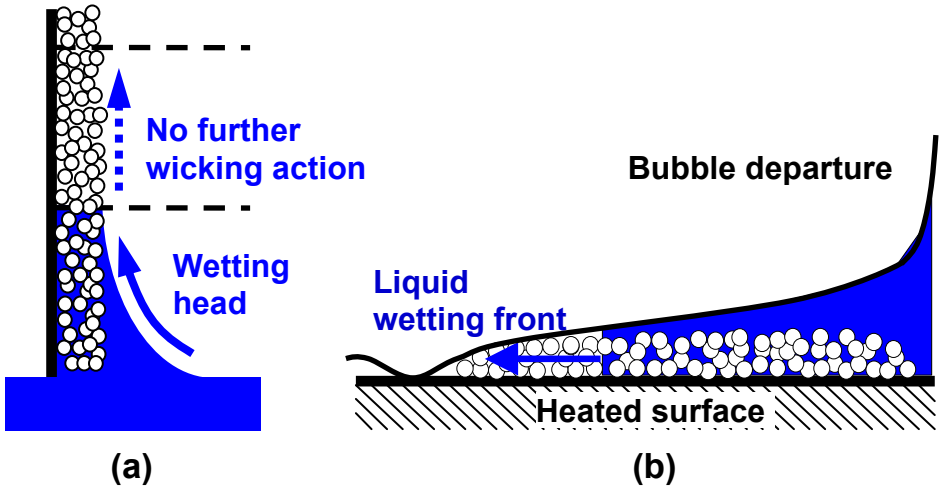

Fig. 6.15 (a) Wetting and wicking mechanisms and (b) CHF enhancement mechanism of nanocoated surface during the boiling process (wetting dominant).

Moreover, the author did not observe behavior indicative of wicking in his sessile drop evaluation on a nanocoated surface. Such a behavior would consist of a significant steady decrease of contact angle as the sessile drop is absorbed by the nanocoating, in comparison to the contact angle behavior of the sessile drop on a plain surface, over the same span of time. Results shown in Fig. 5.8 and Fig. 6.12 indicate that contact angle change over time (4 min) for sessile drops of pure water to be similar in rate and amount between the nanocoated and plain heaters. Kim et al. [8] also compared contact angles of sessile drops of pure water between nanocoated and plain surfaces, and reported values obtained for both surfaces as being static contact angles, thus implying the absence of the dynamic situation that can be expected when the sessile drop wicks for much thicker porous coatings. Therefore, it can be stated that surface wettability dominates over wickability in pulling the liquid front to the equilibrium height of ~2.6 mm on the nanocoated surface (Fig. 6.14). In other words, surface wetting dominates over wicking as the underlying factor in CHF enhancement in the nanocoated surface.

The instantaneous wetting speeds of the liquid front in the first 5 ms were measured during the vertical dipping tests. Fig. 6.16 shows the speeds for various nanocoatings obtained under different generating conditions and the corresponding CHF produced on the same nanocoated surfaces. Each nanocoating was generated under a different combination of heat flux, duration of heat flux, nanofluid concentration, and type of nanofluid, ethanol or water-based (Table 6.2). Fig. 6.16 reveals that, like CHF and contact angle, CHF and instant wetting speed follow a linear relationship with higher CHF corresponding to higher instantaneous wetting speed. A speed of ~0.1 m/s was measured on the nanocoated surface that provided maximum CHF enhancement (~2000 kW/m^2) as compared to almost zero wetting speed on the plain surface.

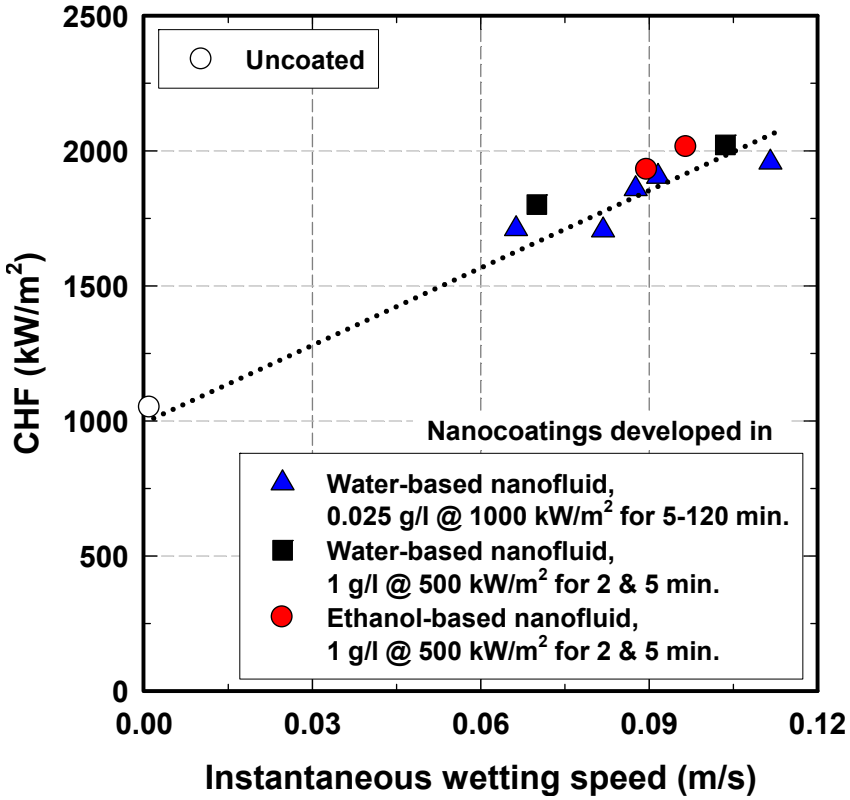

Fig. 6.16 Relationship between CHF and instantaneous wetting speed of developed nanocoatings (Table 6.2).

Table 6.2 Instantaneous wetting speed
and pool boiling performance of nanocoatings with pure water.

	Developed in 0.025 g/l conc. @ 1000 kW/m^2					Developed in 1 g/l conc. @ 500 kW/m^2			
	water nanofluid					water nanofluid		ethanol nanofluid	
Duration (min.)	5	15	30	60	120	2	5	2	5
Instant wetting speed (cm/s)	6.6	8.2	8.8	11.1	9.2	7.0	10.3	9.0	9.7
CHF (kW/m^2)	1710	1710	1860	1950	1900	1820	2050	1930	2020
BHT	U	U	U	D	D	D	D	U	D
Boiling results (Appendix B)	Fig. B1					Fig. B12			
Note - D: Degraded and U: Unchanged									

These effects, lower contact angle and higher instantaneous wetting speed, can be expected to reduce the size of the dry spots at the base of the nucleating bubbles and to continuously rewet the base of the bubbles as the bubbles grow, thereby delaying CHF. To support the idea that rewetting speed in the coating could be sufficient to delay CHF, an estimate of so called superficial vapor velocity on the nanocoated surface was obtained from a single bubble experiment and compared to the estimate of instant wetting speed from the dipping tests. The instantaneous wetting speed required to continuously rewet the base of the bubbles as they grow, and the superficial vapor velocity, may be estimated to be equivalent. The superficial vapor velocity can be obtained from the product of bubble release frequency, f, and bubble departure diameter, d_d. The single bubble was generated on the nanocoated surface at 4 W/cm^2 and 1 atm. Measurements from high speed imaging gave a departure frequency of ~27 Hz and a departure diameter of ~3 mm, yielding a superficial vapor velocity of ~0.081 m/s. The estimates of diameter and frequency matched predictions from correlations of Cole and Shulman's [75] and Cole [76] (will be further discussed later). Additionally, Zuber's [72] expression (eq. (7)) for superficial vapor velocity,

$$fd_d = 0.59[\frac{\sigma g(\rho_l - \rho_v)}{\rho_l^{\,2}}]^{1/4} \tag{7}$$

yielded an estimate of ~0.092 m/s using properties of saturated water at 1 atm. It is interesting that these estimates of superficial vapor velocity are of the same order of magnitude as the measured instantaneous wetting speed (~0.1 m/s). This suggests that the rewetting speed in the nanocoating may be sufficient to continuously rewet the base of the bubbles as they grow and depart. It is believed then that the speed of the micro-thin liquid wetting layer underneath the bubble is a major factor for the CHF enhancement.

CHAPTER 7

PARAMETRIC TESTS ON POOL BOILING OF PURE WATER WITH NANOCOATED HEATER

Discussions from previous sections show that an optimized nanocoated heater provides the same boiling performance as obtained with an optimal nanofluid. A method to obtain an optimized nanocoating was discussed using ethanol nanofluid. This coated heater when used for pure water boiling test shows ~80% CHF enhancement without BHT deterioration. For the fundamental boiling tests, parameters such as nanoparticle size, system pressure, heater orientation, and heater size were varied to see their effects while conducting pool boiling test on nanocoated heater. Until now such a parametric study on the pool boiling of water using a nanoparticle coated flat heater has not been done. Since previous results show that the nanocoating is responsible for a significant CHF enhancement, such a parametric investigation is deemed important. The nanocoating is developed by boiling an Al_2O_3-ethanol nanofluid (1 g/l at 500 kW/m^2 for 2 min.) as discussed previously (Chapter 6.2). The present study carries out the experiments using a flat square heater and the variations in nanoparticle size, system pressure, heater orientation, and heater size are shown in Table 7.1.

Table 7.1 Experimental Parameters.

	Particle size effect	Pressure effect	Orientation effect	Heater size effect
Volume weighted average particle size (nm)	75, 139, & 210	139	139	139
Pressure (kPa)	101	20, 47, 101, & 200	101	101
Orientation (deg.)	0	0	0, 45, 90,135, & 180	0
Heater size (cm x cm)	1	1	1	0.75, 1, 1.5, & 2
Nanocoating	1 g/l Al_2O_3-ethanol at 500 kW/m^2 for 2 min.			

7.1 Effect of Particle Size

All experiments reported so far in this paper were conducted with 139 nm ± 100 nm sized Al_2O_3 nanoparticles obtained from Nanophase Inc. In order to investigate the dependence of nucleate boiling and the CHF value on different nanoparticle sizes, two additional sizes of Al_2O_3 nanoparticles (supplied by Nanoarmor) were tested. The nanoparticle size distribution is shown in Fig. 7.1. Results from Fig. 7.1 show that the volume weighted average particle sizes of additional nanoparticles were measured to be 75 nm ± 50 nm and 210 nm ± 200 nm. Like 139 nm size nanoparticle (Chapter 2.1), the measured 75 nm nanoparticle is larger than the given specification from the manufacturer (~20 nm). This difference, as stated previously, could be due to particle aggregation in solution. However, the 200 nm nanoparticle size from the manufacturer is very close to the measured (210 nm) size. It is believed that the smaller nanoparticle has more aggregation when it is dispersed in water.

Using these nanoparticles (75 nm, 139, nm, and 210 nm), nanocoatings were developed on the heater surface in the manner previously described (1 g/l Al_2O_3-ethanol nanofluid at 500 kW/m^2 for 2 min.). Pool boiling experiments of pure water were then conducted using these nanocoated heaters (1 cm × 1 cm) and the results are shown in Fig. 7.2.

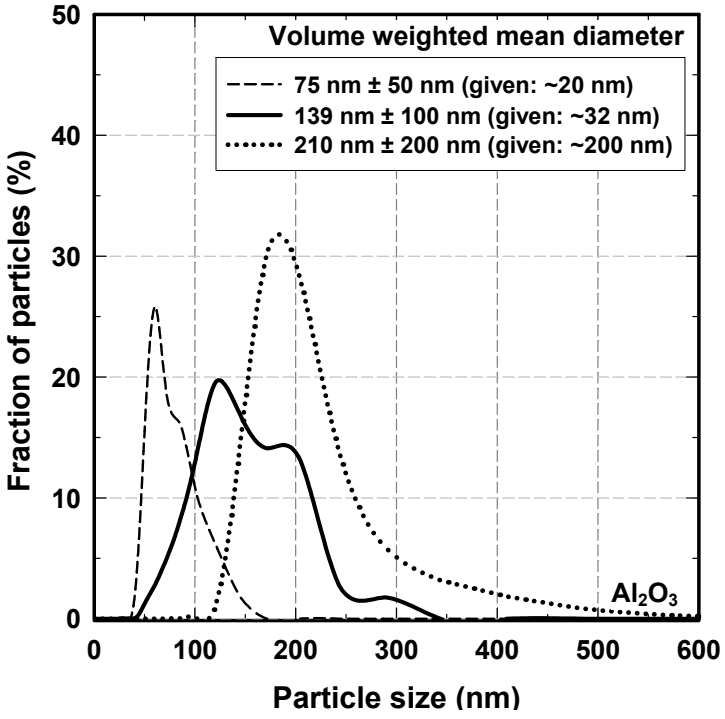

Fig. 7.1 Particle size distribution histogram for various Al_2O_3-water nanofluids (volume weighted mean diameter).

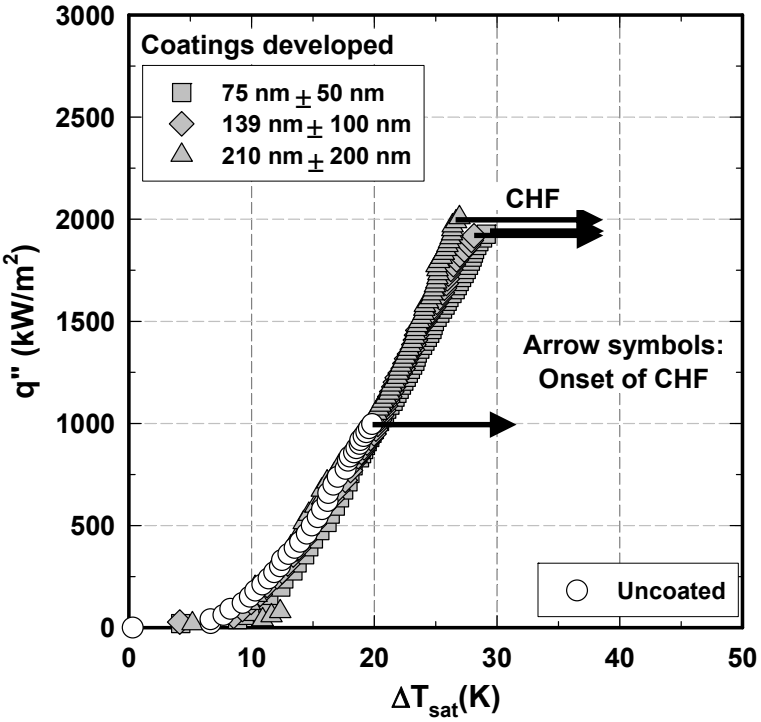

Fig. 7.2 Effect of nanoparticle size on nanocoatings in the pool boiling of pure water (1 cm × 1 cm heater and θ=0° at 1 atm).

The pool boiling curve using the nanocoated surfaces (closed symbols), that were developed using three different nanoparticle sizes, follows the same trend as that for the uncoated surface but extends beyond and shows a dramatic CHF enhancement. Under saturated pool boiling conditions at 1 atm, the magnitude of CHF enhancement is ~80% and the BHT throughout the nucleate boiling region is nearly identical for each nanocoating. This shows that the nanocoating generated in the specified manner using different nanoparticle sizes, still exhibits optimal BHT performance. The SEM images of the nanocoatings in Fig. 7.3 showed no distinctive differences in the coating structures. Thus over the range tested (75 nm ~ 210 nm), there is no significant dependence of the BHT performance and CHF on the average size of the nanoparticles that were used for nanocoating. This trend is similar to previous findings [1, 28, 29] that had used nanofluids, and where the authors had used similar settings and heater size.

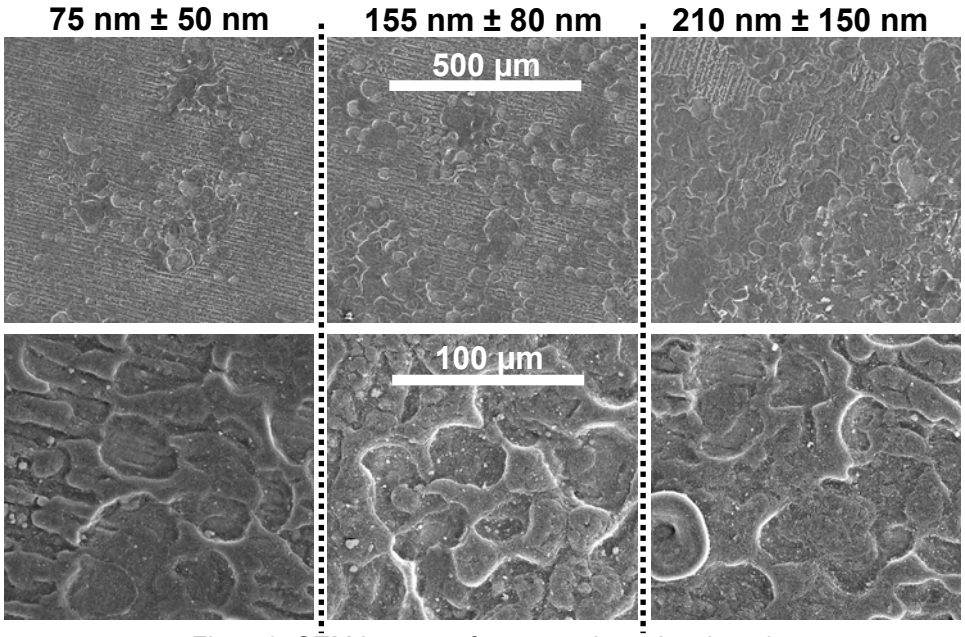

Fig. 7.3. SEM images of nanocoatings developed using different sizes of the nanoparticles.

7.2 Effect of Pressure

Pool boiling tests were conducted at four different saturation pressures (20, 47, 101, and 200 kPa) for both the uncoated and the nanocoated 1 cm × 1 cm heaters in pure water. For the nanocoating development, 139 nm size of the nanoparticle was used. Fig. 7.4 shows the effects of the system pressure on both of these surfaces.

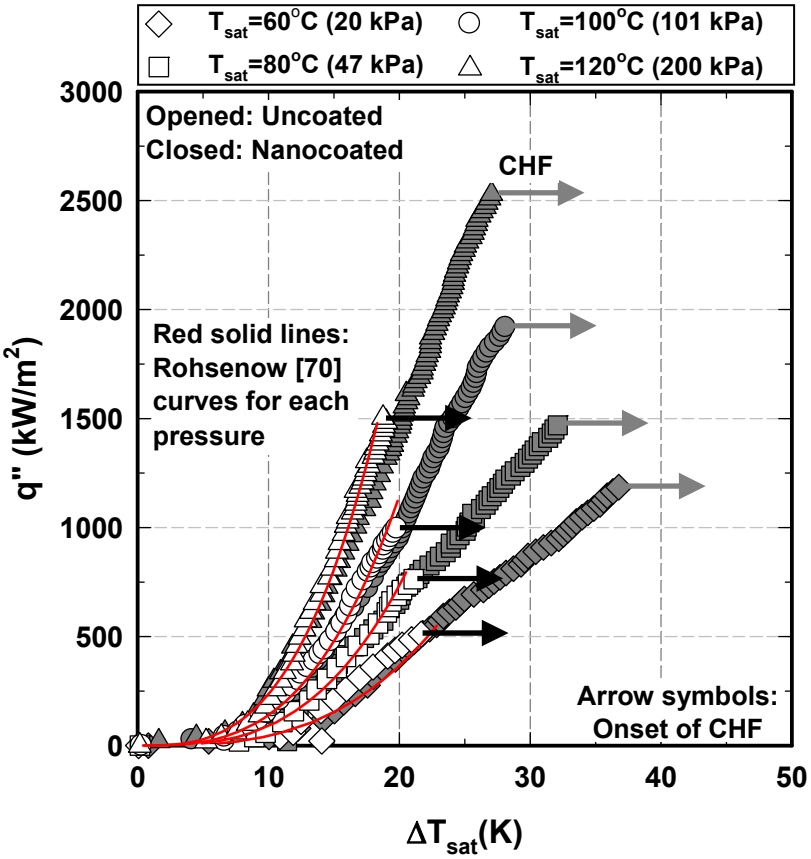

Fig, 7.4 Effect of pressure on the pool boiling curve of pure water
with uncoated and nanocoated heater surfaces (1 cm × 1 cm heater at θ=0°).

The results are in good agreement with previous researchers [41-48], in showing that both the BHT and the CHF increases with increasing pressure. For the uncoated surface at various pressures, the CHF values obtained from Zuber's [72] correlation (eq. (5)) and the nucleate boiling curve from Rohsenow's [70] correlation (eq. (4)) match the experimental results with the given surface factor constant (C_{sf} = 0.0128). However, these well-known relationships

cannot account for heater surface modifications and consequently cannot predict the CHF values correctly over the nanocoated heaters. Tests conducted with nanocoated heaters show a consistent increase in the CHF for each of the tested pressures with no significant effect on the nucleate BHT.

To demonstrate pressure effects on CHF, the CHF enhancement obtained with the nanocoated heater at various pressures is plotted in Fig. 7.5. This CHF enhancement, relative to Zuber's [72] correlation (eq. (5)), is the greatest at the low pressure (~115% at 20 kPa) and gradually decreases as the pressure increases (~70% at 200 kPa). This behavior could be a result of different bubble departure behaviors and wetting characteristics of the nanocoating at different pressures. Bubble departure characteristics at low pressures seem to create an opportunity for the wettability in the nanocoating to reveal more of its influence. As pressure decreases, the bubble's departure size increases but with correspondingly lower frequency.

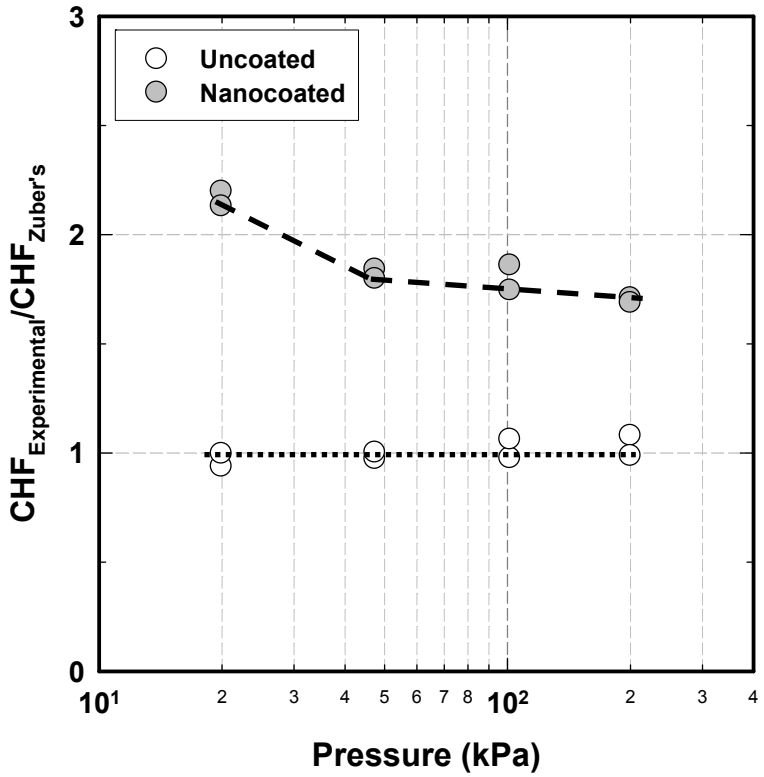

Fig. 7.5 CHF enhancement for uncoated and nanocoated heater surfaces at various pressures (1 cm × 1 cm heater at θ=0°).

Some prevailing correlations of the pressure effects on the departure bubble size and frequency were reviewed. Several investigations have tried to provide analytical correlations for the departure bubble size. Many of these correlations are written in terms of the Bond number (Bo) which is defined as:

$$Bo = \frac{g(\rho_l - \rho_g){d_d}^2}{\sigma} \tag{8}$$

Cole and Shulman [75] proposed a relation in which $Bo^{1/2}$ is simply proportional to the inverse of the absolute pressure:

$$Bo^{1/2} = \frac{1000}{P} \quad \text{(P is pressure in mm Hg)} \tag{9}$$

A year later, Cole [76] provided a modified correlation to include the vapor density through the Jakob number (Ja):

$$Bo^{1/2} = 0.04Ja \tag{10}$$

$$\text{where } Ja = \frac{\rho_l C_{pl}[T_w - T_{sat}(P_\infty)]}{\rho_g h_{fg}} \tag{11}$$

Kutateladze and Gogonin [77] could correlate a large body of data from the literature with the following correlation:

$$Bo^{1/2} = 0.25(1 + 10^5 K_1)^{1/2} \text{ for } K_1 < 0.06 \tag{12}$$

$$\text{where } K_1 = \left(\frac{Ja}{\mathrm{Pr}_l}\right)\left\{\left[\frac{g\rho_l(\rho_l - \rho_g)}{{\mu_l}^2}\right]\left[\frac{\sigma}{g(\rho_l - \rho_g)}\right]^{3/2}\right\}^{-1} \tag{13}$$

Jensen and Memmel [78] proposed an improvement to eq. (12) with their correlation (eq. (14)).

$$Bo^{1/2} = 0.19(1.8 + 10^5 K_1)^{2/3} \tag{14}$$

where K_1 is given by eq. (13)

All the above correlations for departure bubble size at various pressures are plotted in Fig. 7.6. The results clearly show an inverse trend with pressure while showing a considerable scatter. As stated in previously, it is found that Cole and Shulman's [75] (eq. (9)) and Cole's [76] correlations (eq. (10)) predict the bubble departure diameter very well for the single bubble departure measurement in pure water (Chapter 6.3).

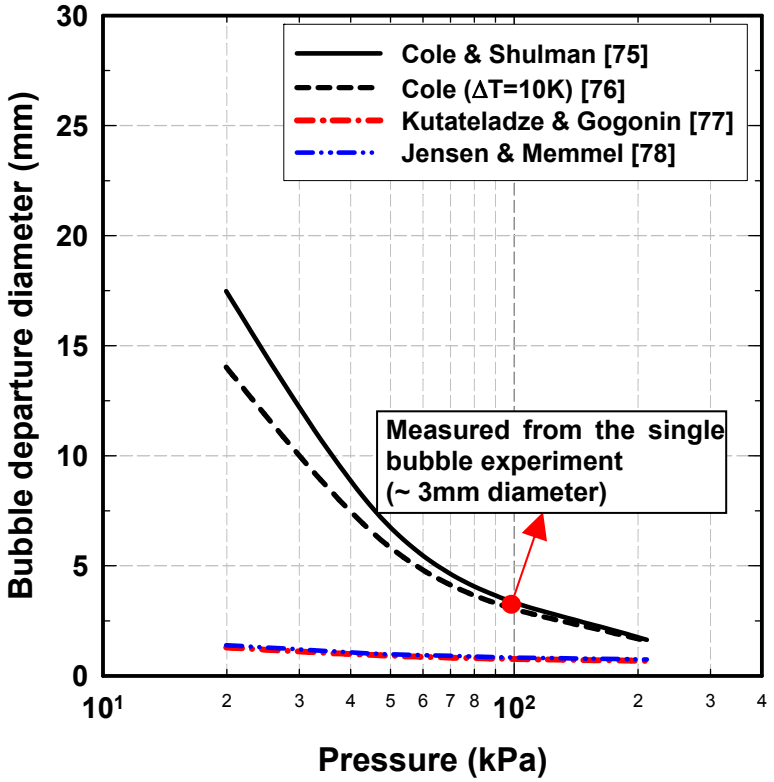

Fig. 7.6 Bubble departure diameters (correlations).

For the bubble departure frequency calculations, Zuber's [72] correlation (eq. (7)) was used. The bubble departure frequency depends on how large the bubble must grow to be

released and on the rate of growth to the departure diameter. Using the bubble departure diameter obtained from the correlations shown in Fig. 7.6 and Zuber's [72] correlation (eq. (7)), the bubble departure frequency was calculated. The results are shown in Fig. 7.7.

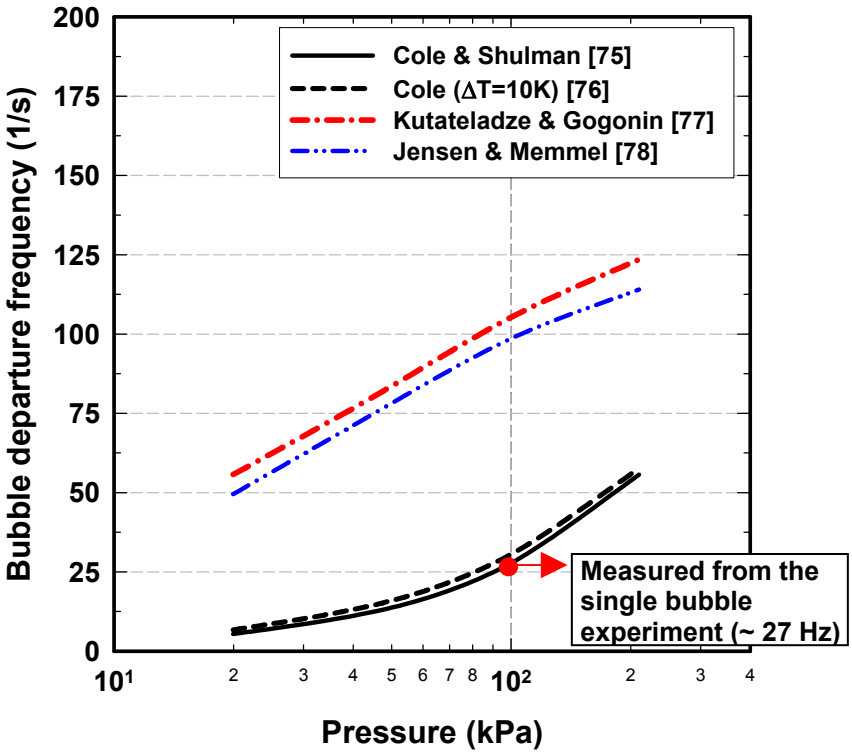

Fig. 7.7 Bubble departure frequency (correlations).

Even though predictions from correlations tend to be valid for the limited cases over which the supporting data have been obtained, Cole and Shulman's [75] and Cole's [76] correlations can be helpful in estimating how the bubble behavior might change with system pressure. According to these correlations, with a decrease from 200 kPa to 101 kPa, the bubble departure size roughly doubles and frequency decreases roughly by half. However, for a further decrease of similar magnitude, that is, to 20 kPa, these correlations predict bubble departure size ~11 times larger, and the departure frequency ~9 times less, relative to 200 kPa. Larger bubbles lead to larger dry spots and lower frequency leads to longer vapor dwelling over the

surface. The increasing relative CHF enhancement with diminishing pressure seen in Fig. 7.5 might be a reflection of the ability of the nanocoating to rewet the bases of bubbles even as they enlarge dramatically at low pressures. The greatest relative CHF enhancement achieved at 20 kPa, could be evidence of this ability coping with departing bubbles that have enlarged by possibly ~11 times relative to the bubbles generated at the highest system pressure.

7.3 Effect of Orientation

The effect of heater surface orientation on the pool boiling of pure water was observed by conducting experiments over a 1 cm × 1 cm heater at 1 atm. The boiling curves obtained using both uncoated and nanocoated heaters at various orientations are shown in Fig. 7.8.

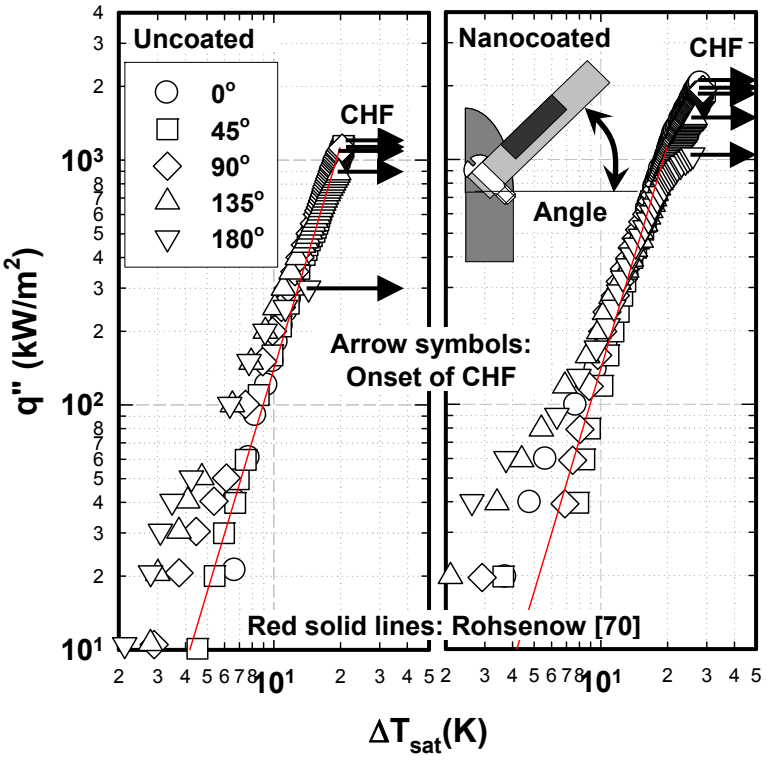

Fig. 7.8 Effect of inclination angle on the pool boiling curve of pure water with uncoated and nanocoated heater surfaces (1 cm × 1 cm heater at 1 atm).

Again, 139 nm sizes of nanoparticles were used to develop the nanocoating. This figure shows that as the inclination angle increases from 0 to 180°, there is a transition heat flux

regime within the nucleate BHT region. At the lower heat fluxes (<100 kW/m^2), the nucleate BHT increases with inclination angle. With further heat flux increases, the heater orientation affects BHT much less or negligibly. This trend is observed for both surfaces (uncoated and nanocoated).

Previous researchers [28, 52-54, 74] have also reported similar findings and Lienhard [74] attributed this to the transition from the isolated bubbles regime to the continuous vapor column regime. Nishikawa et al [54] also reported that the enhancement of BHT (in the low heat flux region) as the inclination angle increases is due to the change in characteristics of bubble behavior and due to the change in the heat transfer mechanism. Higher inclination angle (θ > 90^o) results in longer dwelling time of the bubble. The bubbles formed travel a certain distance on the surface of the heater before departing. During the travel on the surface, the bubbles tend to drag or absorb the entrapment of the other cavities thereby causing an increase in the BHT. The effect of the heater inclination disappears as heat flux further increases since bubble generation is so vigorous that coalesced bubbles prevail all over the heating surface for any inclination angle.

Fig. 7.9 presents the orientation effect on the CHF for both heater surfaces tested. For both surfaces, as the inclination angle changes from 0° to 180°, the CHF values display a decreasing trend beyond a certain angle. This has been also observed in other studies [52, 53, 57, 73]. From 0° to 90°, the effect of inclination angle on CHF seems marginal. Beyond 90° (135° and 180°), the CHF values decrease dramatically. As the inclination angle increases beyond 90°, the bubbles cannot detach freely due to the blockage provided by the inclined heated surface. The bubble residence time against the heated surface therefore increases. As a result, the bubbles flatten, merge with each other becoming large, and slide against the heater surface. This longer dwelling of a vapor blanket results in reaching CHF sooner.

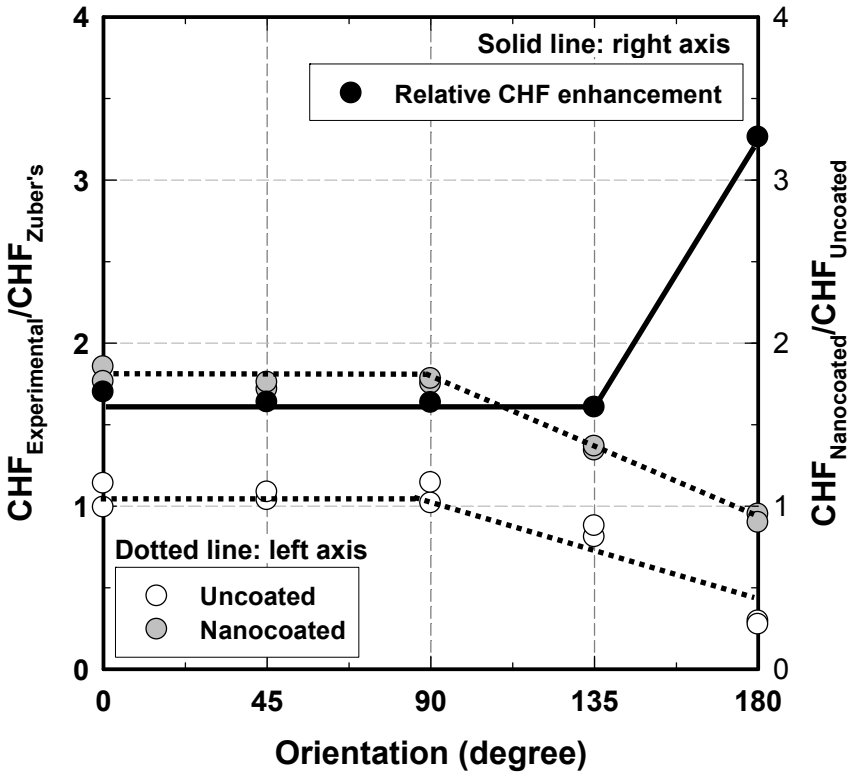

Fig. 7.9 CHF enhancement for uncoated and nanocoated heater surfaces at various inclination angles (1 cm × 1 cm heater at 1 atm).

It should be noted that for all the tested orientations, the nanocoated heater always significantly enhanced the CHF relative to the uncoated heater. Since Zuber's [72] correlation (eq. (5)) does not account for the heater orientation, a direct comparison between the CHF value for an uncoated and nanocoated surface is included in Fig. 7.9 (solid line and right y-axis). For an inclination angle between $0^\circ \leq \theta \leq 135^\circ$, this enhancement in the CHF tends to be flat (~70%). But a dramatic enhancement of CHF (~220%) for the nanocoated surface over the uncoated surface is observed at 180º (downward facing). At this orientation, the merging and flattening of the bubbles is accentuated resulting in larger departure bubbles for both surfaces. Also, the bubble dwelling time is generally longer so that local dry-out occurs much faster, which significantly reduces the CHF. These bubble characteristics resemble those that exist on a horizontal surface at low pressures. It can then be expected that the increased wettability in the coating delays CHF, analogous to the situation with system pressure decreasing. As the

bubbles merge, flatten, and grow, the lower contact angle and relatively high rewetting speed in the nanocoating are sufficient to rewet underneath even the largest bubbles that exist in the face down orientation. Thus the CHF is significantly enhanced at the face down orientation by using nanocoated heater.

7.4 Effect of Heater Size

Four heater sizes (0.75 cm × 0.75 cm, 1 cm × 1 cm, 1.5 cm × 1.5 cm, and 2 cm × 2 cm) were tested at 1 atm (T_{sat} =100°C) in pure water. Fig. 7.10 shows the boiling curves of uncoated and nanocoated (139 nm nanoparticle deposited) surfaces.

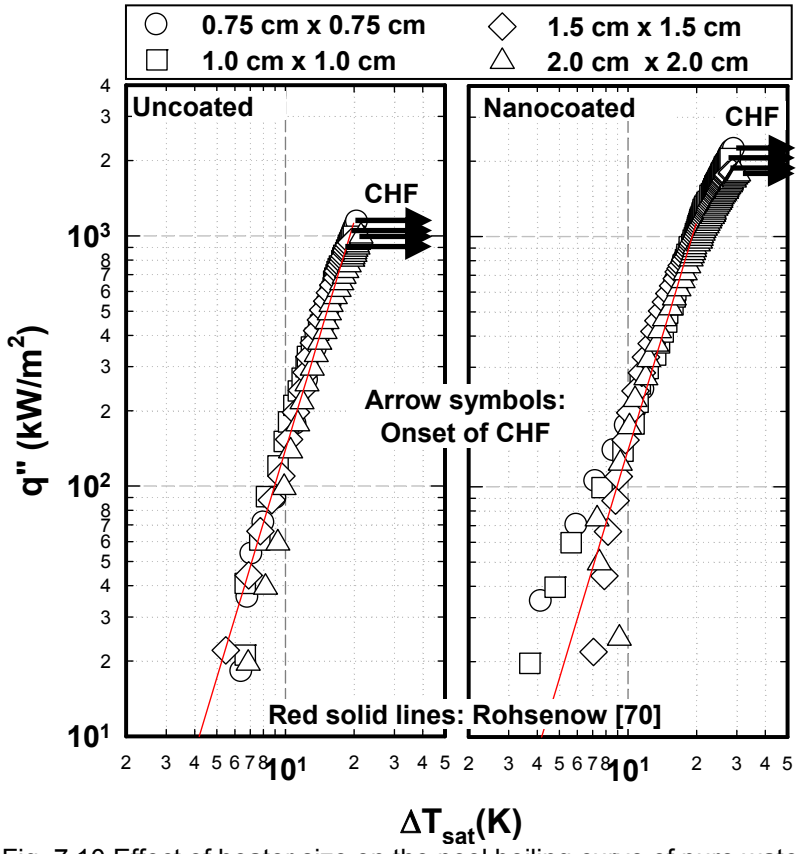

Fig. 7.10 Effect of heater size on the pool boiling curve of pure water with uncoated and nanocoated heater surfaces (θ=0° at 1 atm).

Park and Bergles [59] observed that for a plain heater, size does not affect the nucleate BHT significantly, and a similar inference can be made from the present experiment. Regarding

CHF, a gradual reduction with increasing heater size is observed for both nanocoated and uncoated surfaces. This trend conforms to several other studies [60-62, 73]. However, the CHF was found to be significantly enhanced relative to the uncoated surfaces for all the nanocoated heater sizes.

To further illustrate the effect of heater size on CHF, CHF's obtained for both surfaces were normalized with respect to Zuber's [72] CHF value (eq. (5)) and plotted against dimensionless length *L'* which is given by the following equation:

$$L' = \frac{L}{\sqrt{\frac{\sigma}{g(\rho_l - \rho_g)}}} \tag{15}$$

where *L* is the length of the heater in meters.

Fig. 7.11 shows this normalized data along with Saylor et al.'s [63] CHF data on plain heaters, and Bar-Cohen and McNeil's [48] curve fit of Saylor et al.'s [63] data. The nanocoated heaters clearly show a significant CHF enhancement with decreasing *L'* in Fig. 7.11. The slope of this enhancement is 11 times greater than the slope of Bar-Cohen and McNeil's [48] curve fit. The relative CHF on uncoated heaters follow a similar decreasing trend with increasing *L'* as Saylor et al.'s [63] data and the curve fit. This trend was further confirmed by other studies [60-62, 73]. Bar-Cohen and McNeil's [48] curve fit is based on *L'* values of Saylor et al. [63] which are greater than those of the present study and thus might not reflect CHF enhancement in the smaller *L'* regime. This might explain the slight discrepancy with Bar-Cohen and McNeil's [48] curve fit, seen in Fig. 7.11 for the smallest *L'* (≈ 3) of the uncoated heaters of the present data. Also, shown in Fig. 7.11 is a transition point not reached in the present data. Researchers [48, 73, 74] have shown that the CHF reduction relative to Zuber's [72] (eq. (5)) stabilizes after a certain point. Analysis based on these researchers suggests this point to be at $L' \approx 22$.

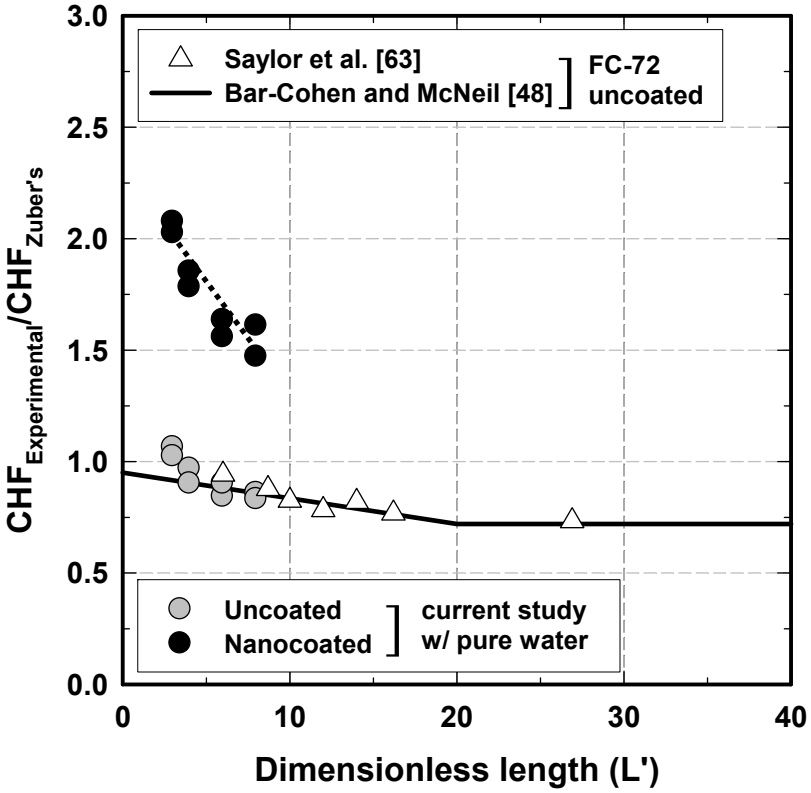

Fig. 7.11 CHF enhancement for uncoated and nanocoated heater surfaces at various heater sizes (θ=0° at 1 atm).

Lienhard [74] stated that the decrease in CHF was influenced by the number of "vapor jets" present on the surface of the heater. He suggested that the number of vapor jets that can exist on a heater changes at critical heater areas that are related to the vapor wavelength. The transitions would be from 1 to 4 jets, 4 to 5 jets, and 5 to 9 jets at these critical areas. The actual number of vapor jets present on the heater can be calculated using:

$$\frac{q''_{CHF}}{q''_{CHF\ Zuber}} = 1.14 \frac{N_j}{A_H / \lambda_d{}^2} \tag{16}$$

where N_j is the number of vapor jets, A_H is heater size, and λ_d is the wavelength of the vapor jets. The λ_d is given by:

$$\lambda_d = 2\pi\sqrt{\frac{3\sigma}{g(\rho_l - \rho_g)}} \tag{17}$$

Furthermore, Lienhard et al. [74] reported that heater size area (A_H) varied as a function of the wavelength of the vapor jets (λ_d) and suggested the following correlations for the transition point of the number of vapor jets:

From 1 to 4 jets: $A_H = (2\lambda_d)^2$ (18)

From 4 to 5 jets: $A_H = (1+\sqrt{2})^2 \lambda_d{}^2$ (19)

From 5 to 9 jets: $A_H = (3\lambda_d)^2$ (20)

According to the correlations given by Lienhard et al. [74], it was determined that all heater sizes tested lied on the one jet regime and that the transition heater size from 1 to 4 jets would be ~30 cm^2 ($L' \approx 22$) for pure water at saturated atmospheric pressure. This particular case was beyond the scope of the present investigation due to power supply limitations.

Regarding the trend of CHF reduction observed for the L' range studied, Rainey and You [73] attribute it to the rewetting resistance of fluid. For a small surface, unlike an infinite flat plate case, a majority of the rewetting fluid is supplied from the sides rather than from above. As the heat flux increases, the vapor dwelling time and amount covering the surface increase. This, in turn, increases the rewetting resistance to the cooler bulk liquid advancing over the heater surface. Thus the rewetting resistance should be a function of flow path distance parallel to the heater surface. The larger surface offers a longer resistive distance to the hot spots at its center and this leads to lower CHF with increasing area. As previously stated, the current data for uncoated heaters follows this trend and agrees well with Saylor's [63] data and Bar-Cohen and McNeil's [48] curve fit as shown in Fig. 7.11.

The CHF enhancement in Fig. 7.11 can again be attributed to the capacity of the nanocoating to rewet the base of the growing bubbles and to reduce the size of the dry spots. This in turn creates a less resistive path for the cooler bulk fluid to advance over the heater and cool the base of the bubbles and thus delay the CHF. Because of, better wettability and the resulting less resistive path, not only a significant relative CHF enhancement is obtained, but a steepening of the slope of CHF enhancement with reduced heater size, can also be observed (Fig. 7.11).

CHAPTER 8

CONCLUSIONS AND RECOMMENDATIONS

Pool boiling experiments were conducted with uncoated/nanocoated surfaces in nanofluids/pure water under saturated conditions using flat square heaters. A critical nanofluid concentration and transient characteristics of nanofluid during pool boiling heat transfer were discussed. Also an investigation was conducted to elicit what causes the deposition of nanoparticles onto the heater surface and how this deposition changes the wetting behavior of the heater surface. Additionally, the boiling performance of artificially developed nanocoatings was evaluated in the pure water to see if this BHT phenomenon is solely due to surface characteristics. Finally, work on optimizing the nanocoating on the heater surface was done and a parametric investigation (pressure, orientation, and heater size variations) was performed with the optimum coating. Below is a summary of the major findings through this present investigation.

8.1 Conclusions of Chapter 3

1. Within the experimental range, the results show only a marginal change in the thermal property (≤ 5%) of low concentration nanofluids (≤ 1 g/l) when compared to those of the base fluid. Therefore, it is assumed that nanofluids thermo-physical properties (thermal conductivity, viscosity, and surface tension) at the low concentrations (0.001 ~ 1 g/l), do not play a major role in altering the pool boiling characteristics.

8.2 Conclusions of Chapter 4

1. Increasing nanoparticle concentration is found to increase CHF, with no detriment to the BHT coefficients, up until a concentration of about 0.025 g/l (0.0007% vol.) is reached. Further concentration increment produced no additional CHF enhancement but degraded the BHT. Similar results were observed using water-based nanofluids composed of other nanoparticles (CuO and diamond).
2. Results show that heater surfaces are continuously being modified, during the nanofluid boiling process, making nanofluid pool boiling performance dependant on both the duration of experiments (transient characteristics) and the applied heat flux. The longer a heater is subjected to nanofluid pool boiling process, the thicker the nanoparticle coating gets generated on its surface. The thickness of this nanoparticle coating can then dictate both CHF and BHT.
3. It appears that there is an upper limit to the nanoparticle deposition thickness that can form on the heater surface during nanofluid pool boiling. The BHT curves show a tendency to merge together when this deposition is relatively large. This indicates that there is a limiting deposition thickness observed during the pool boiling of nanofluids.

8.3 Conclusions of Chapter 5

1. Tests confirm that microlayer evaporation (underneath bubble), during nanofluid boiling, is the mechanism that forms the nanoparticle coatings on heater surfaces. These nanocoatings change the heater surface wetting characteristics which in turn significantly increase the CHF during nanofluid boiling.
2. Results also indicate that there is an optimal nanocoating thickness/structure which can produce the maximum CHF enhancement while not degrading BHT. Increasing the nanocoating thickness beyond this optimal thickness produces no further changes in surface wetting characteristics and thus no further CHF enhancement is observed.

However, thicker coatings create an additional thermal resistance and can degrade BHT.

3. From the repeating tests in pure water, the nanocoating developed during boiling process appears to be reliable for quite a good duration (16 runs).

8.4 Conclusions of Chapter 6

1. When tested in water, developed nanocoatings have the ability to enhance CHF. However, the boiling performance of the coatings is influenced by the thickness and structure of the nanocoating degrading nucleate boiling heat transfer.
2. The nanocoatings developed in ethanol nanofluids appear to be more uniform as compared to those developed in water nanofluids. The uniformity of the coatings is attributed to ethanol's smaller bubble diameters, a result of ethanol's lower surface tension. These relatively uniform nanocoatings were found to outperform nanocoating created in water nanofluids, by significantly enhancing CHF while not affecting the nucleate boiling heat transfer.
3. A linear relationship between the CHF enhancement and the quasi-static contact angles of the nanocoatings is revealed, confirming a strong CHF dependence on surface wettability. Additionally, the measured speed of the liquid meniscus is found to be on the order of the bubble departure superficial velocity. The speed of the wetting front, advancing in on growing bubbles, is believed to be the source for the dramatic CHF enhancement of nanocoatings.

8.5 Conclusions of Chapter 7

1. The CHF enhancement was found to be nearly identical for three nanocoatings formed from three different average nanoparticle sizes each., Over the range of average nanoparticle size tested (75 ~ 210 nm), there is no significant dependence of nucleate BHT and CHF on the nanoparticle size.
2. The relatively high wetting speeds, associated with the hydrophilic nature of the nanocoating, allow for more efficient rewetting underneath the growing bubbles. This is believed to be the mechanism driving CHF enhancement in nanocoated surfaces. This CHF enhancement mechanism is believed to be more prominent at lower system pressures where larger bubble departure diameters are produced. This is the reason CHF enhancement, in the nanocoatings, is highest at the lowest pressure and gradually decreases as the pressure increases.
3. Both surfaces, (uncoated and nanocoated), show a similar decreasing trend of CHF as the heater inclination angle increased from 0° to 180°. However, the nanocoated surface showed a significant CHF enhancement ratio at all the tested orientations. In particular, the enhancement ratio is best at the downward facing orientation (180°). At this orientation, the bubble dwelling time is generally longer so that the local dry-out occurs much faster, which significantly reduces the CHF. The rewetting speed in the nanocoating is believed sufficient to wet underneath even the largest bubbles which occur in the downward facing orientation, resulting in the increase of CHF at all orientations.
4. A similar CHF decreasing trend is observed, for both coated and uncoated surfaces, as heater size increases from 0.75 cm × 0.75 cm to 2 cm × 2 cm. This CHF reduction could be due to the longer resistive path offered to the cooler bulk fluid with increasing heater size. However, the better wettability of the nanocoating is believed to reduce the

path's resistance, and significantly enhancing CHF (~90%) compared to the uncoated surface.

8.6 Recommendations

The following are recommendations for future research put forth by the author in order to better understand boiling heat transfer with nanofluid / nanocoated surface.

1 Even though the nanocoating developed appears to be reliable during pool boiling experiments, the bonding strength of nanocoated structures is physically weak so that it needs to find a better coating/bonding methodology.

2. It is suggested to conduct the nanocoating experiments in alternative working fluids (relatively different wetting characteristics) so that it can be determined whether the significant CHF enhancement of nanocoatings can be replicated with a variety of working fluids.

3. Current study mainly relied on existing correlations to explain the bubble characteristics. Therefore, experimental bubble characterization (departure size and frequency) would be an interesting topic over the nanocoating with various working fluids.

4. All contact angles were measured at room temperature. However, the actual contact angle at the saturated condition could be different. Therefore, it will be valuable to conduct the contact angle measurement at tested conditions.

APPENDIX A

PROPERTY MEASUREMENT EQUIPMENTS

1. Thermal conductivity measurement (KD2Pro-C)

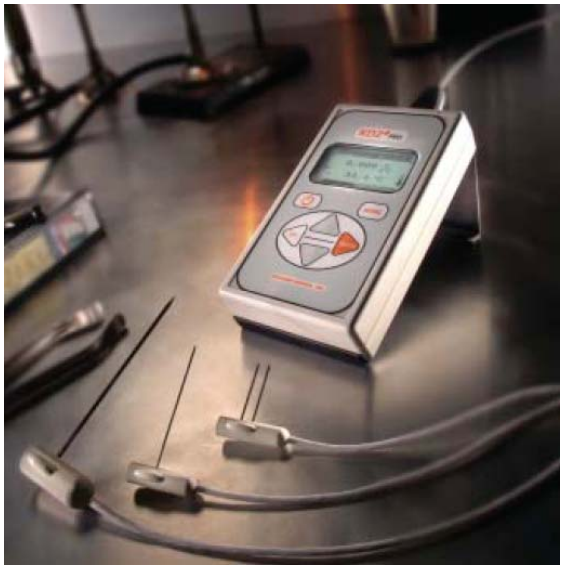

- Operating temperature : 50 ~ 150°C
- range of K: 0.02 ~ 2 W/mK
- Precision : ± 2.5%

$$\Delta T(r,t) = \frac{q}{4\pi k} \ln \frac{4at}{r^2 C}$$

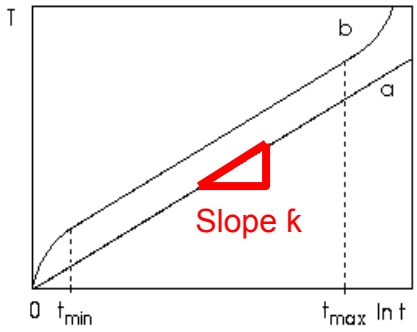

Typical temperature rise curve

where

k: thermal conductivity (W/mK)
a: thermal diffusivity [m^2/s] ~ $a=k/\rho Cp$
ρ: density (kg.m-3)
Cp: heat capacity (J/kgK)

$C=\exp(\gamma)$,
$\gamma=0.5772157$ (Euler's constant)

2. Surface tension and contact angle measurement (FTA 1000)

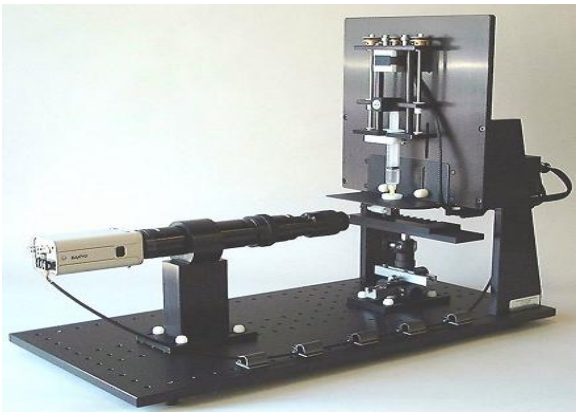

- Max operating temperature : 100°C
- Range of angle : 5 ~ 175°
- Precision : ± 1%

Surface Tension
(Laplace-Young equation)

$$\Delta\rho g h = \gamma(\frac{1}{R_1} + \frac{1}{R_2})$$

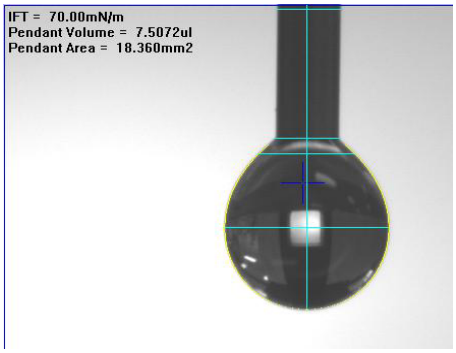

where

$\Delta\rho$: the difference in δensities
h: the height in the drop
γ: surface tension
R_1 and R_2: radii of curvature
g: the acceleration of gravity

Contact angle
(Optical Goniometer)

$$\tan\theta_1 = \frac{2h}{d} \quad \& \quad \theta_2 = 2\theta$$

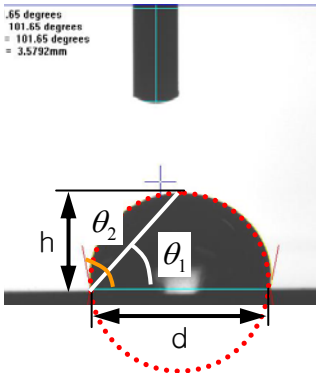

where

θ : measured angle
h: the height in the drop
d: diameter

3. Viscosity measurement (glass capillary viscometer)

- Max operating temperature : 200°C
- Range of angle : 0.1 to 100,000 cSt
- Precision : ± 0.2%

$$\nu = Ct$$

where

ν : kinematic viscosity [cSt, mm^2/s]
C : Viscometer constant
t : time [sec.]

Conversion
(kinematic -dynamic viscosity)

$$\mu = \rho\nu$$

where

μ : dynamic viscosity [cP, Pa·s]
ρ : density
Ex) 10 P = 1 Pa·s = 1000 Cp = 1000 mPa·s

APPENDIX B

ADDITIONAL RESULTS

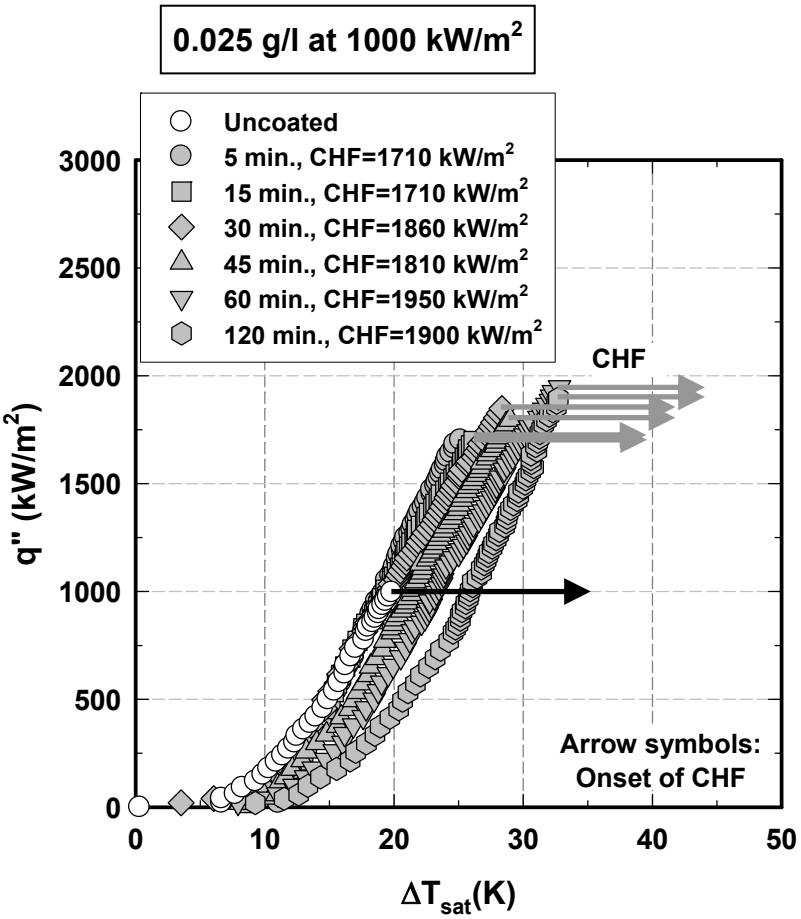

Fig. B1 (a) Pool boiling curves of nanocoated surfaces developed in 0.025 g/l Al_2O_3 nanofluid at heat flux of 1000 kW/m^2 for various durations.

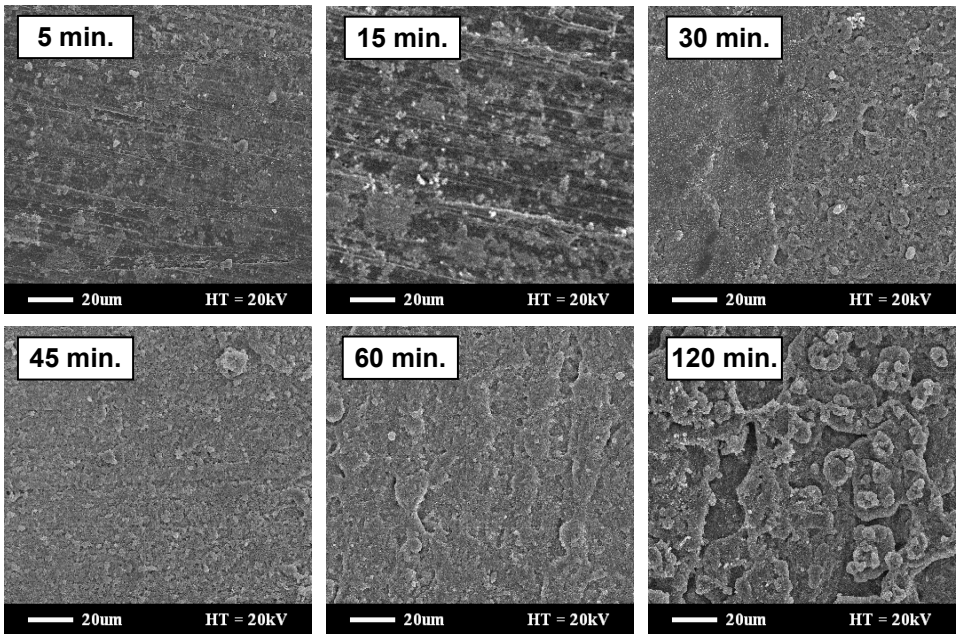

Fig. B1 (b) SEM Images of developed coatings after boiling experiments in pure water.

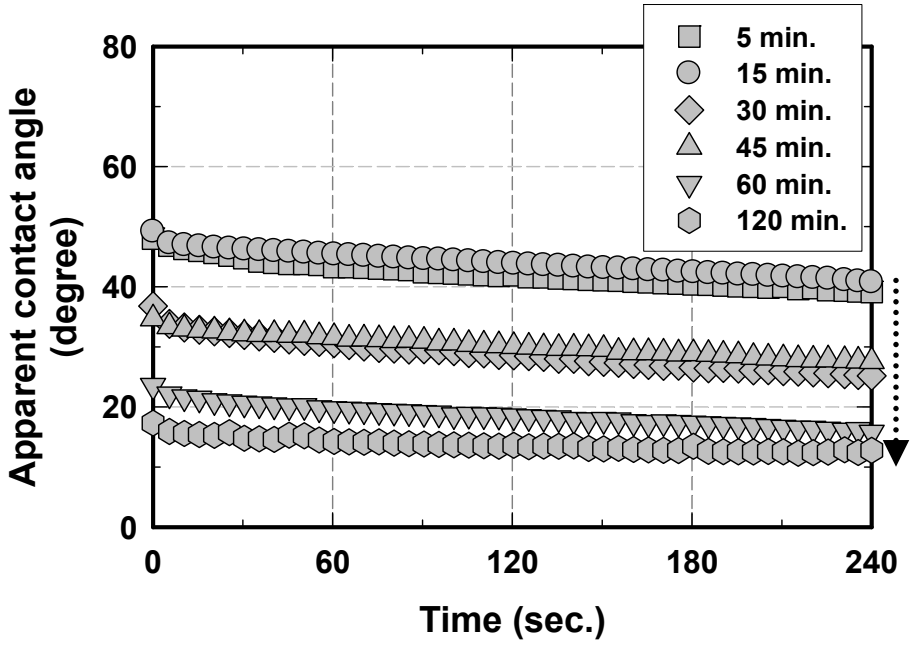

Fig. B1 (c) Apparent contact angle measurement of nanocoated surfaces developed in Al_2O_3 0.025 g/l nanofluid at heat flux of 1000 kW/m^2 for various durations.

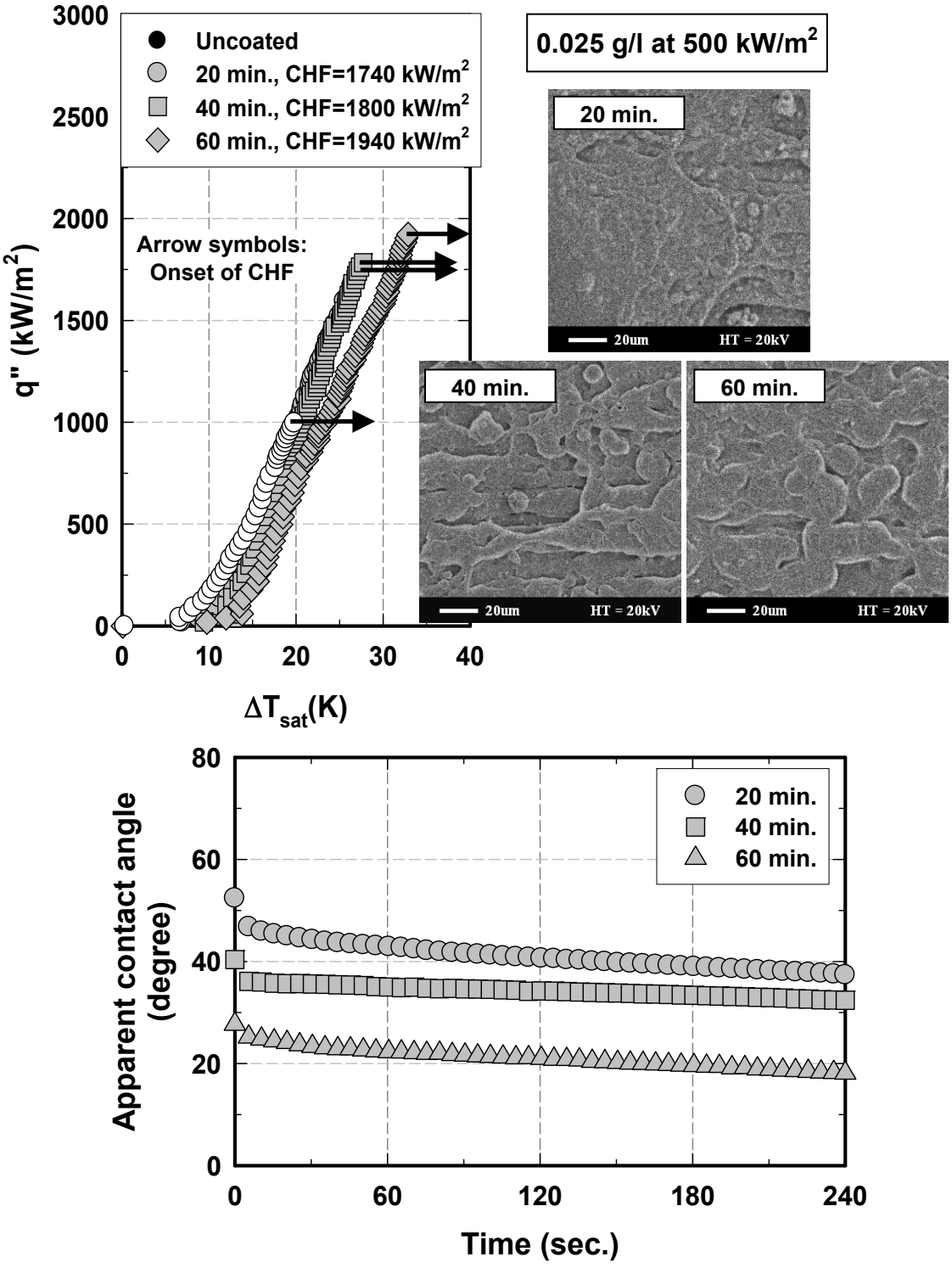

Fig. B2 Pool boiling curves, SEM images, and apparent contact angles of nanocoated surfaces developed in Al_2O_3 0.025 g/l nanofluid at heat flux of 500 kW/m^2 for various durations.

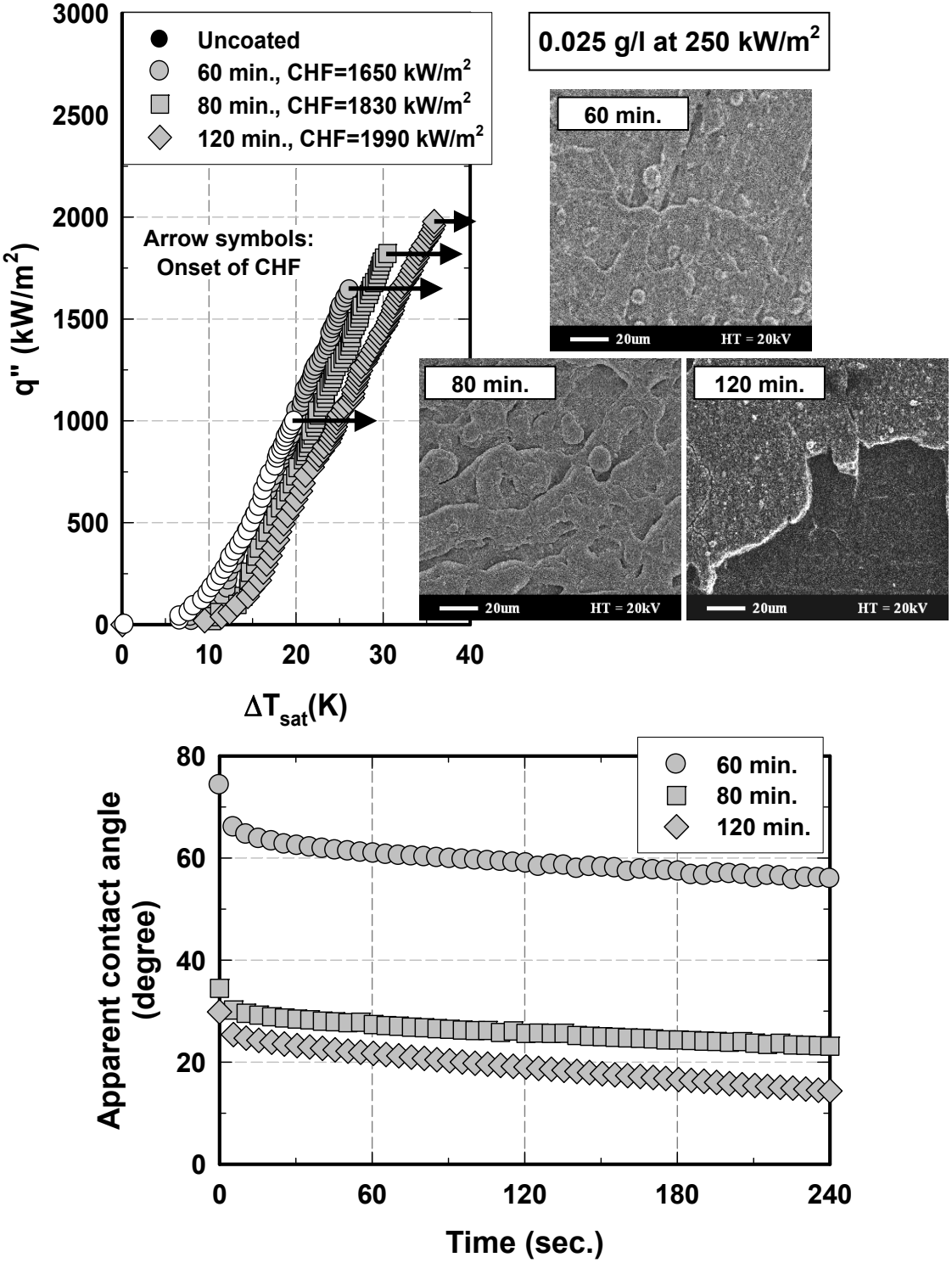

Fig. B3 Pool boiling curves, SEM images, and apparent contact angles of nanocoated surfaces developed in Al_2O_3 0.025 g/l nanofluid at heat flux of 250 kW/m^2 for various durations.

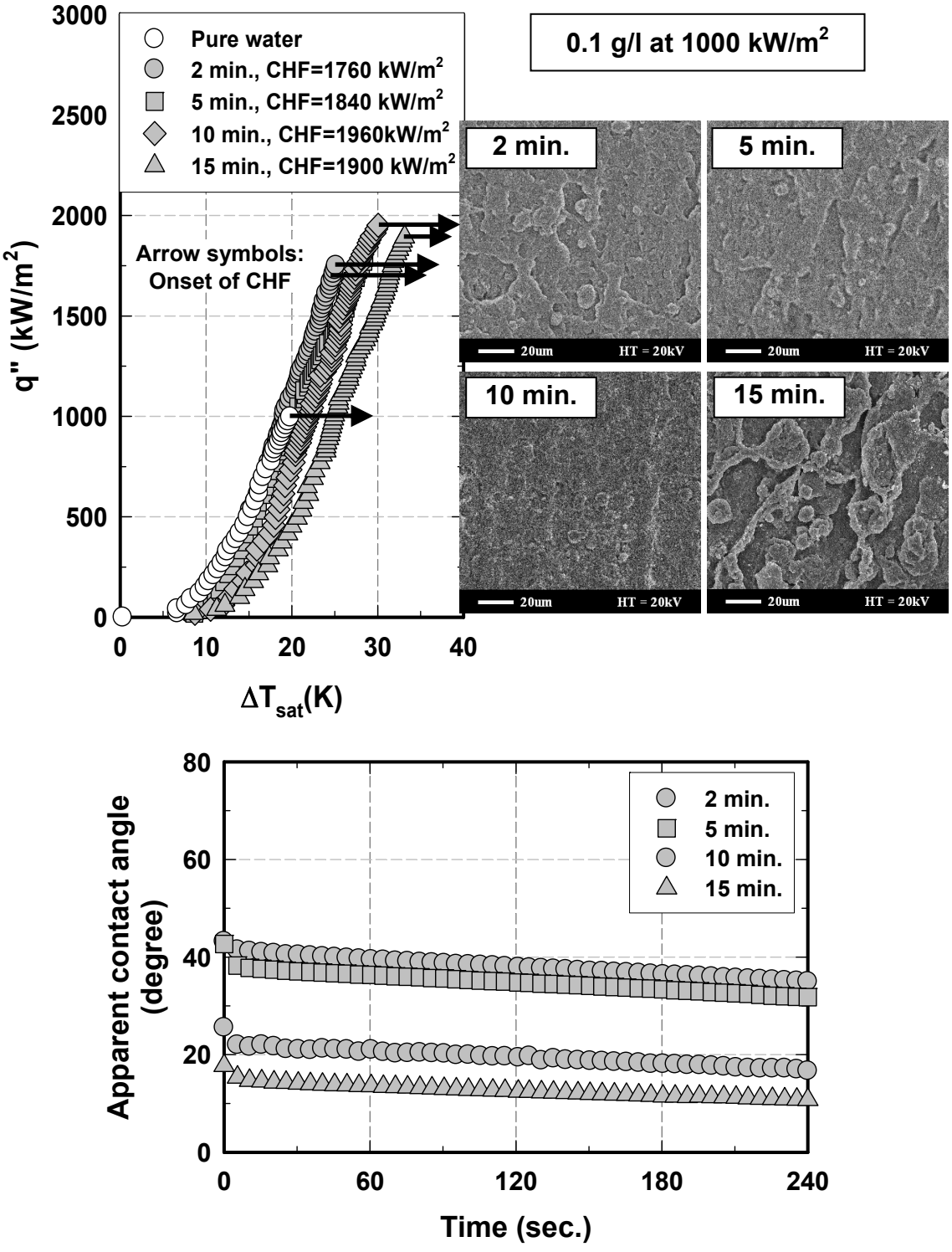

Fig. B4 Pool boiling curves, SEM images, and apparent contact angles of nanocoated surfaces developed in Al_2O_3 0.1g/l nanofluid at heat flux of 1000 kW/m^2 for various durations.

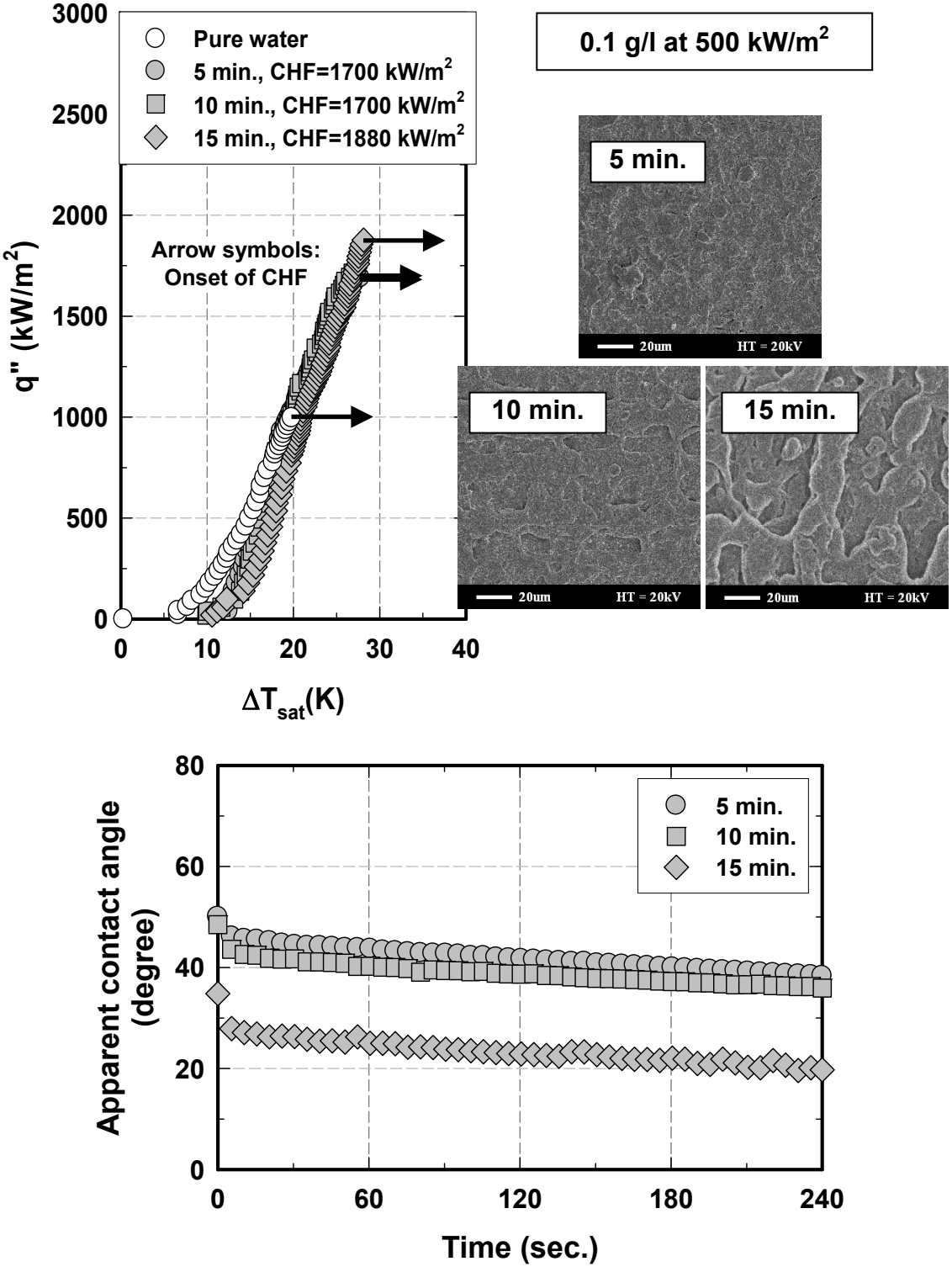

Fig. B5 Pool boiling curves, SEM images, and apparent contact angles of nanocoated surfaces developed in Al_2O_3 0.1 g/l nanofluid at heat flux of 500 kW/m^2 for various durations.

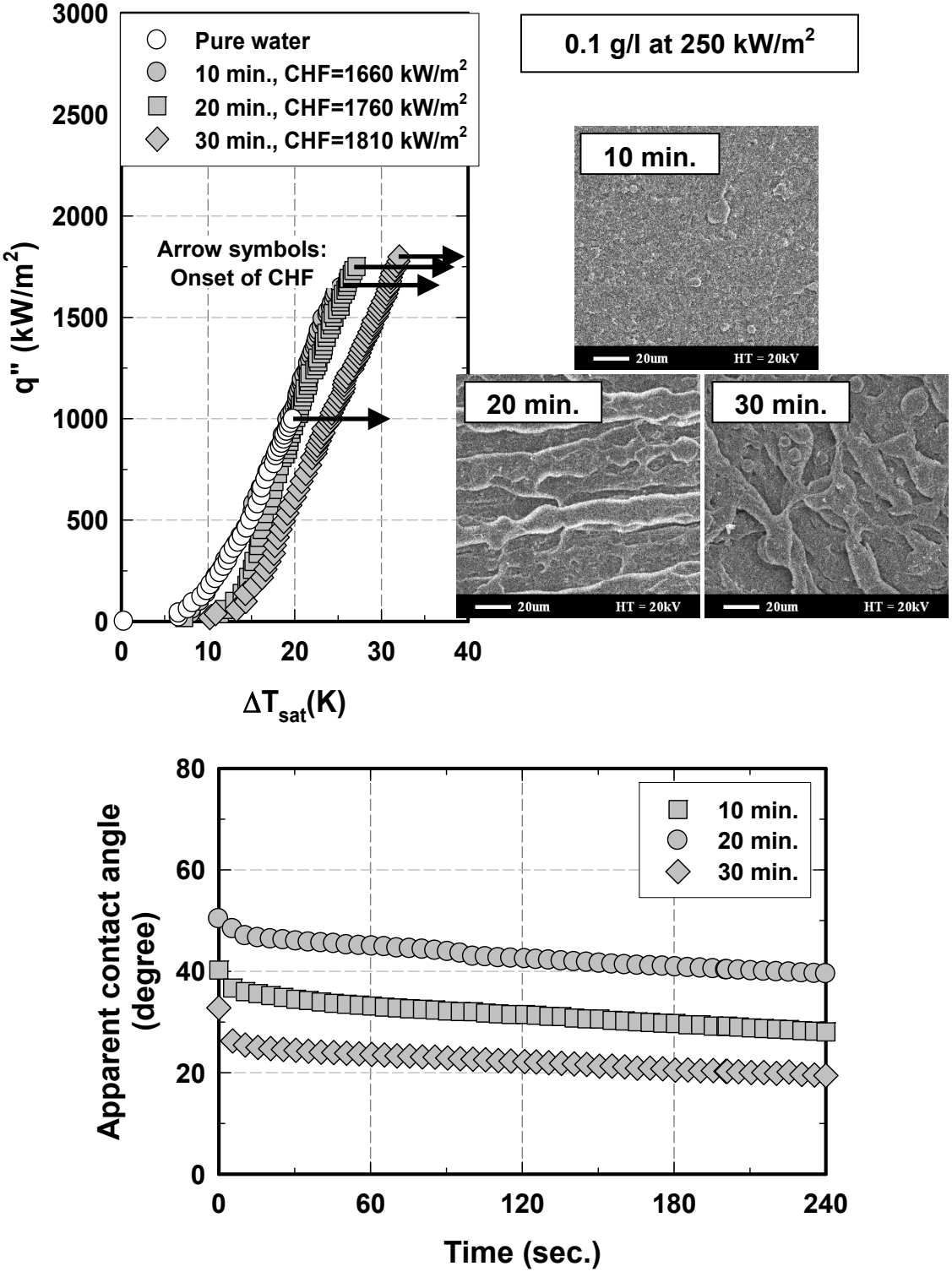

Fig. B6 Pool boiling curves, SEM images, and apparent contact angles of nanocoated surfaces developed in Al_2O_3 0.1 g/l nanofluid at heat flux of 250 kW/m^2 for various durations.

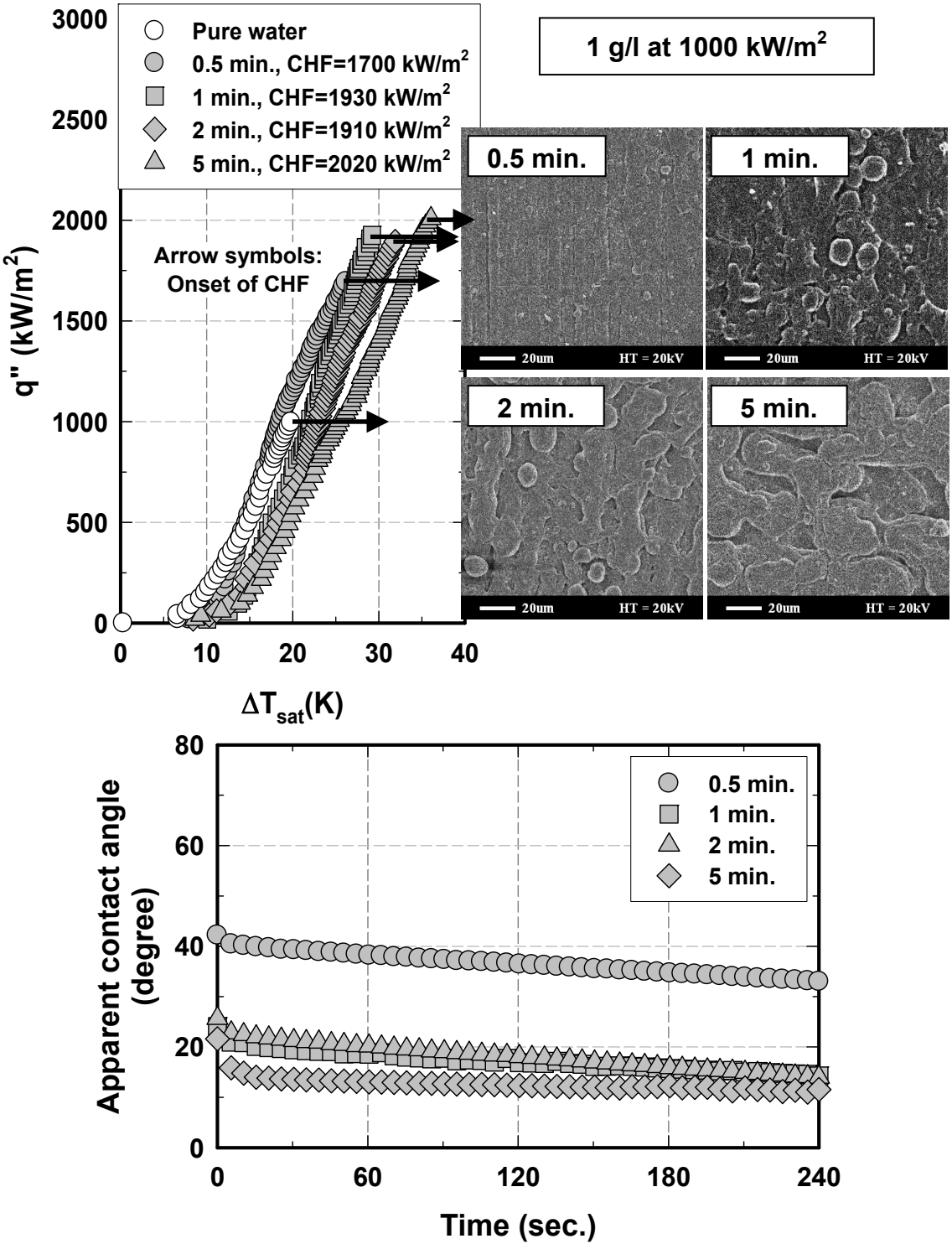

Fig. B7 Pool boiling curves, SEM images, and apparent contact angles of nanocoated surfaces developed in Al_2O_3 1 g/l nanofluid at heat flux of 1000 kW/m^2 for various durations.

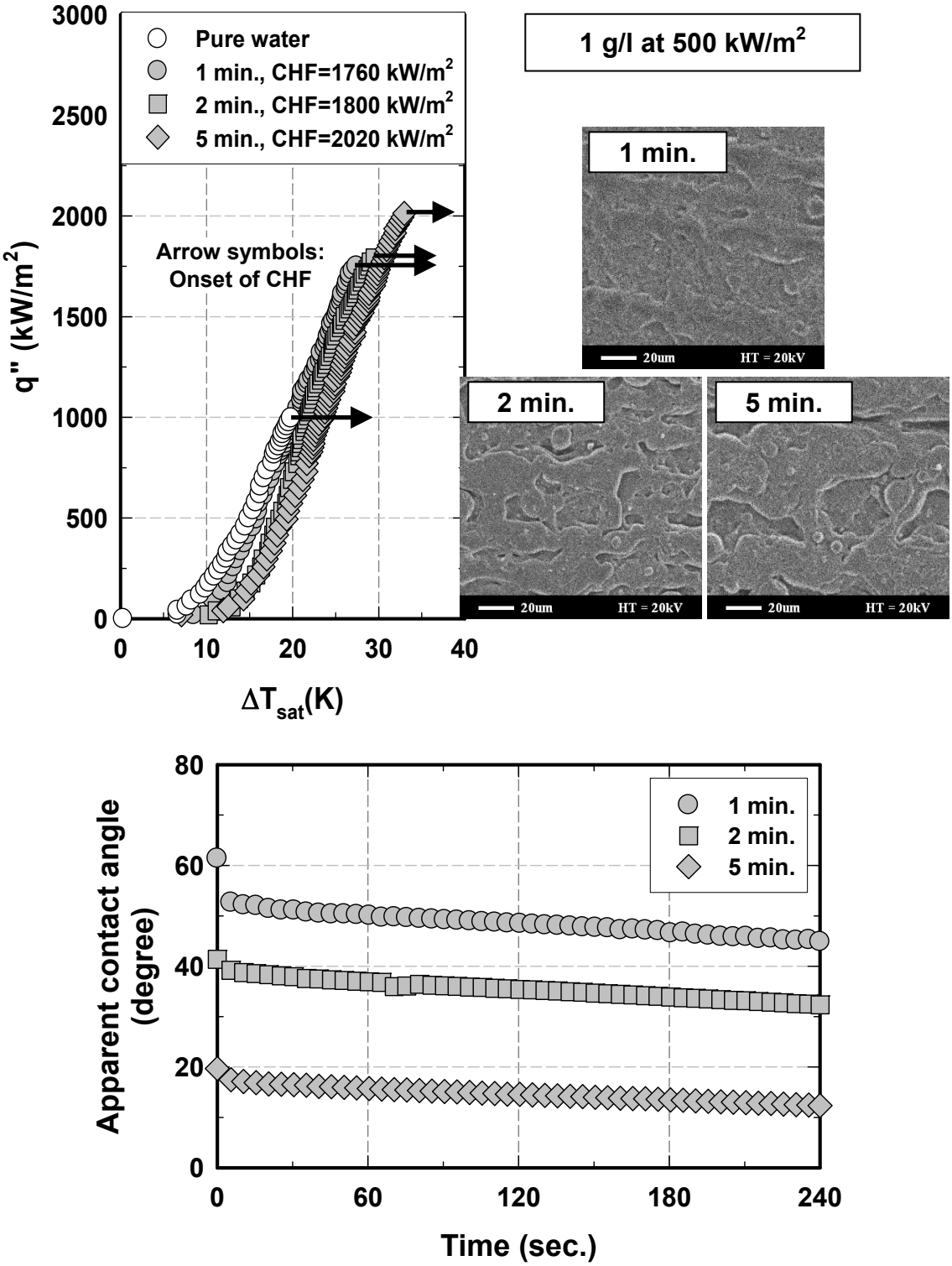

Fig. B8 Pool boiling curves, SEM images, and apparent contact angles of nanocoated surfaces developed in Al_2O_3 1 g/l nanofluid at heat flux of 500 kW/m^2 for various durations.

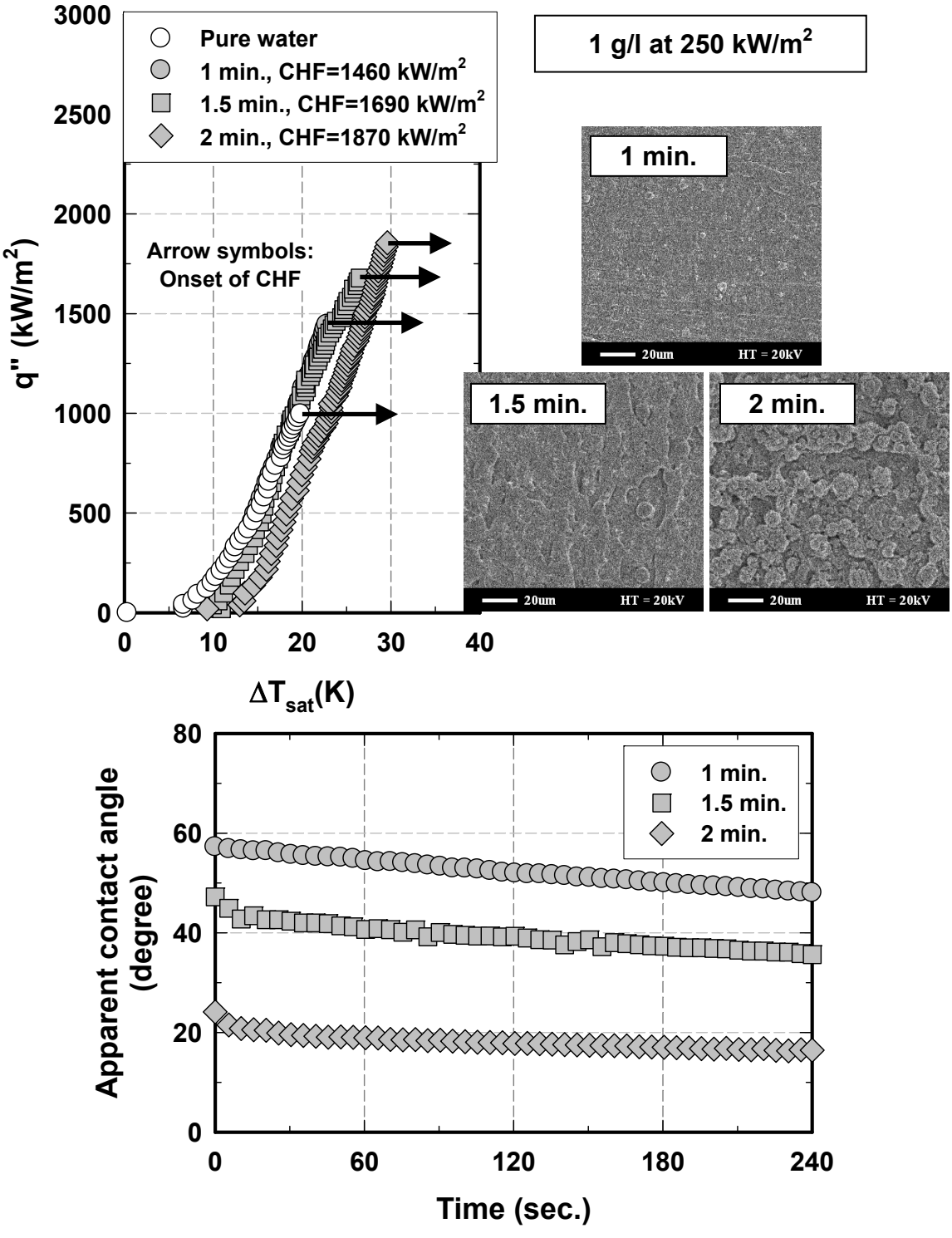

Fig. B9 Pool boiling curves, SEM images, and Apparent Contact Angles of nanocoated surfaces developed in Al_2O_3 1 g/l nanofluid at heat flux of 250 kW/m^2 for various durations.

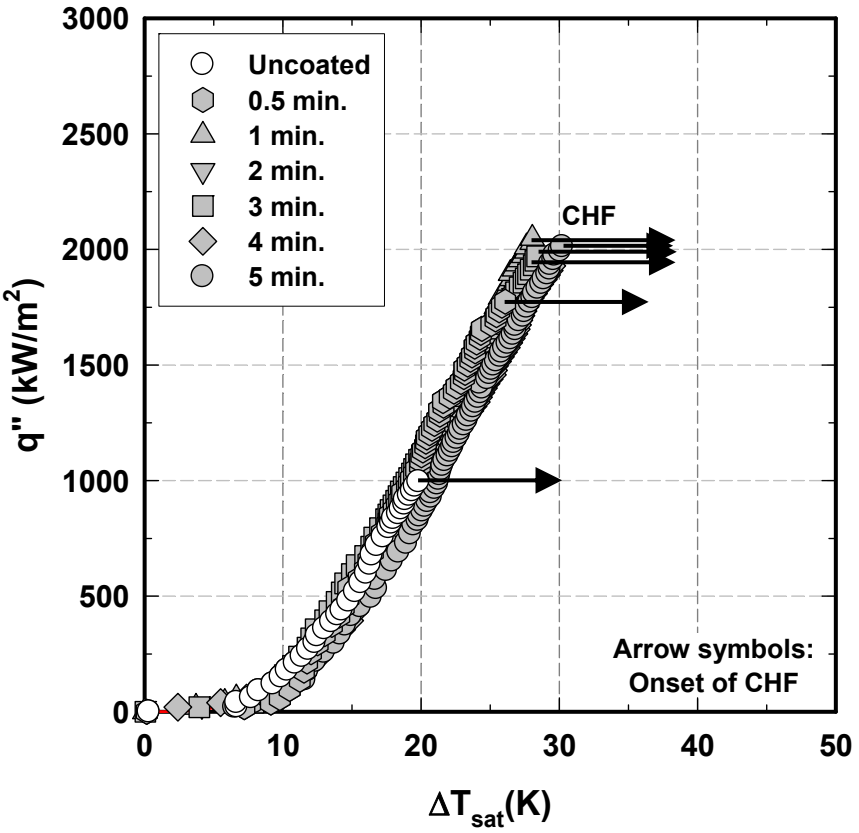

Fig. B10 Pool boiling curves of nanocoated surfaces developed in 1g/l Al_2O_3–ethanol nanofluid at heat flux of 500 kW/m^2 for various durations.

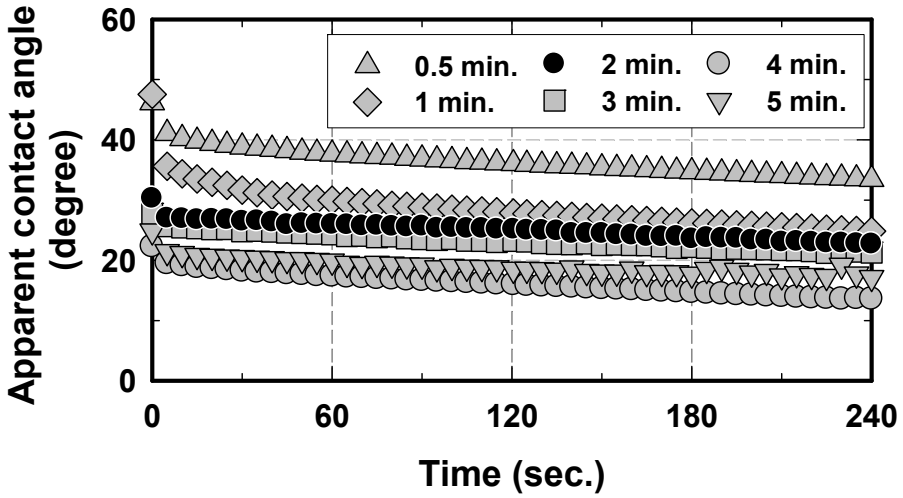

Fig. B11 Apparent Contact Angles of nanocoated surfaces developed in 1 g/l Al_2O_3-ethanol nanofluid at heat flux of 500 kW/m^2 for various durations (0.5 min. ~ 5 min.).

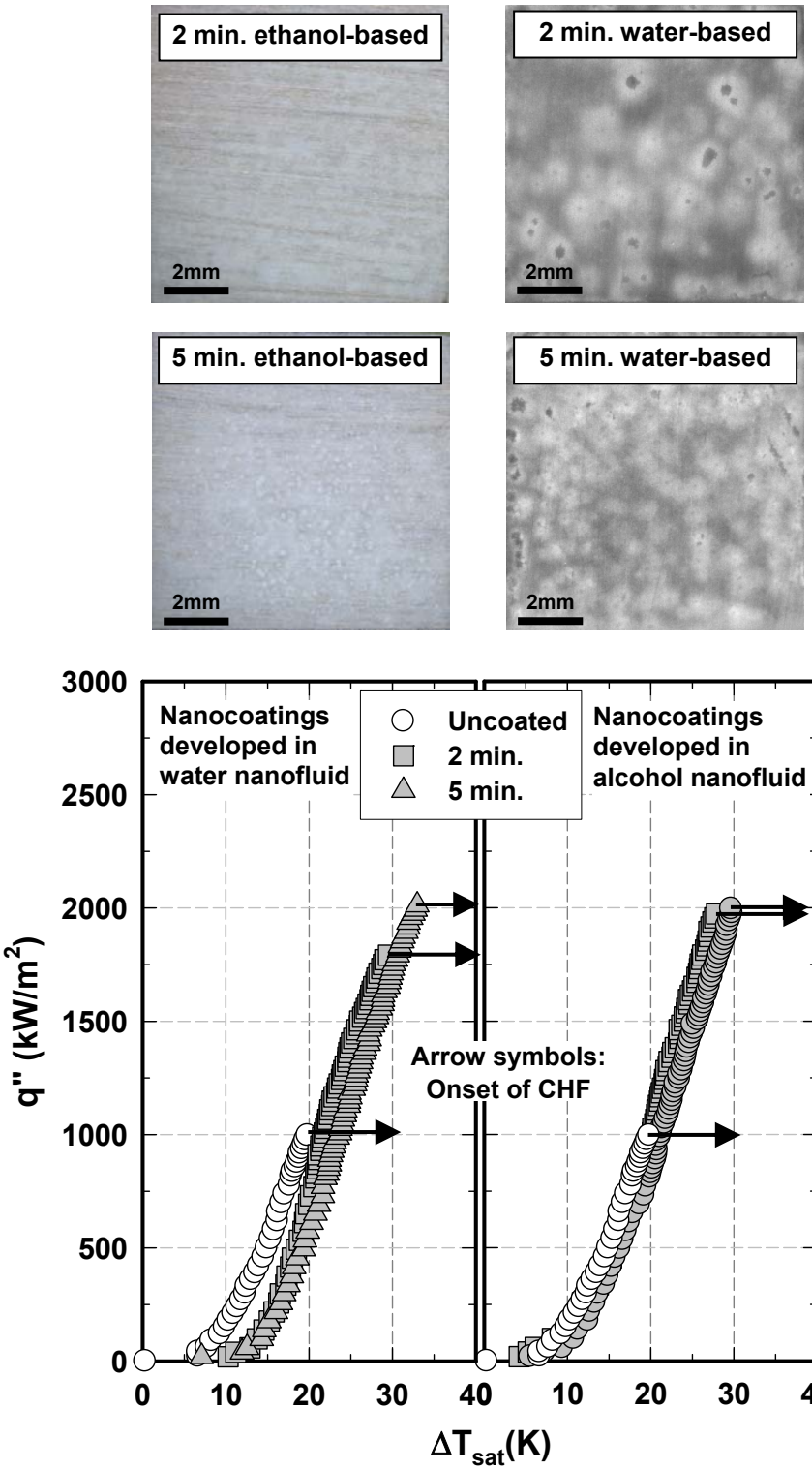

Fig. B12 Optical images and pool boiling curves of nanocoated surfaces developed in 1g/l Al_2O_3–water/ethanol nanofluid for 2 and 5 min. at heat flux of 500 kW/m^2.

APPENDIX C

EXPERIMENTAL DATA

A plain (uncoated) in pure water expeiments,
1 cm × 1 cm at various pressures

Tsat=60°C (20kPa)	
[kW/m^2]	[°C]
0.00	0.09
20.99	14.09
40.88	10.89
60.51	11.89
110.54	12.50
160.74	14.02
210.92	15.05
260.94	15.97
311.23	16.99
360.47	17.99
410.50	19.12
460.70	20.23
510.40	21.67

Tsat=80°C (47kPa)	
[kW/m^2]	[°C]
0.01	0.18
18.66	7.76
38.55	8.93
58.45	9.78
107.61	11.06
157.31	11.94
207.20	13.12
257.14	13.68
306.29	14.48
355.84	15.22
406.22	15.93
456.70	16.83
508.85	17.72
560.40	18.38
610.53	19.05
661.14	19.41
712.83	20.21
763.74	21.11

Tsat=100°C (101kPa)	
[kW/m^2]	[°C]
0.00	0.32
21.10	6.67
40.80	6.65
60.80	7.71
90.80	8.26
120.40	9.28
150.70	9.87
180.60	10.31
210.20	10.89
239.80	11.39
270.10	11.84
299.90	12.32
329.90	12.48
359.90	13.00
389.90	13.51
419.60	13.96
440.00	14.27
459.50	14.50
479.30	14.75
499.50	14.90
520.20	15.23
539.50	15.40
559.20	15.64
579.50	15.75
599.90	16.03
619.20	16.19
638.40	16.29
658.10	16.26
678.20	16.45
698.50	16.66
718.90	16.81
738.00	17.02
757.20	17.24
776.60	17.66
796.40	17.66
816.30	17.85
836.50	18.00
856.90	18.36
877.60	18.55
898.40	18.81
917.60	18.86
936.80	19.13
956.20	19.35
975.70	19.57
995.60	19.83

Tsat=120°C (210kPa)	
[kW/m^2]	[°C]
0.00	0.19
19.80	5.25
39.80	6.40
60.10	7.50
99.70	8.42
139.20	9.34
178.90	9.80
218.60	10.17
258.20	10.52
297.80	10.97
337.90	11.26
377.60	11.81
417.40	11.95
457.40	12.15
496.10	12.40
534.60	12.76
575.20	12.85
613.50	13.25
654.40	13.54
692.90	14.03
731.60	14.06
771.10	14.63
811.90	14.85
851.40	15.16
890.30	15.25
929.70	15.44
971.20	15.75
1008.80	15.93
1028.70	16.06
1049.00	16.07
1069.40	16.44
1090.10	16.64
1110.20	16.67
1132.30	16.80
1150.70	16.83
1168.40	16.66
1187.60	17.04
1207.40	17.20
1225.80	17.30
1245.90	17.43
1265.20	17.48
1284.00	17.69
1305.10	17.54
1324.90	18.04
1344.80	18.17
1365.50	18.19
1386.30	18.37
1405.70	18.54
1427.90	18.59
1448.50	18.81
1466.60	18.85
1484.80	19.01
1503.90	18.77
1522.00	19.01
1540.50	19.29
1560.60	19.39
1578.00	19.20
1597.90	19.53

A plain (uncoated) in pure water expeiments,
1 cm × 1 cm at various orientations

0°		45°		90°		135°		180°	
[kW/m^2]	[°C]	[kW/m^2]	[°C]	[kW/m^2]	[°C]	[kW/m^2]	[°C]	[kW/m^2]	[°C]
0.00	0.32	0.00	0.08	0.00	0.12	0.00	0.09	0.00	-0.03
21.10	6.67	10.10	4.53	10.50	2.89	10.60	2.78	10.50	2.13
40.80	6.65	20.00	5.41	20.60	3.74	20.50	3.00	20.60	2.79
60.80	7.71	29.90	5.96	30.40	4.47	30.50	3.74	30.50	3.09
90.80	8.26	39.80	6.70	40.40	5.38	40.50	4.10	40.40	3.48
120.40	9.28	49.70	6.95	50.30	6.11	50.50	4.74	50.30	4.25
150.70	9.87	59.60	7.47	100.50	7.46	100.00	6.51	100.50	6.34
180.60	10.31	109.70	8.55	150.20	8.92	149.50	7.90	150.30	7.74
210.20	10.89	159.40	9.87	200.00	9.88	199.80	9.17	200.20	9.13
239.80	11.39	209.20	10.78	250.20	10.82	249.40	10.11	250.10	11.27
270.10	11.84	259.10	11.67	299.90	11.62	299.60	11.04	300.00	14.35
299.90	12.32	309.60	12.24	350.20	12.44	349.00	11.98		
329.90	12.48	359.40	13.05	400.40	13.12	399.20	12.76		
359.90	13.00	410.20	13.78	450.40	13.86	448.60	13.60		
389.90	13.51	429.90	14.05	501.20	14.57	468.30	14.00		
419.60	13.96	449.30	14.19	550.80	15.22	488.10	14.24		
440.00	14.27	469.60	14.53	600.30	15.73	508.60	14.62		
459.50	14.50	488.80	14.84	621.40	15.94	527.90	14.87		
479.30	14.75	509.40	15.23	641.00	16.20	547.30	15.13		
499.50	14.90	529.30	15.47	660.80	16.37	567.50	15.47		
520.20	15.23	548.60	15.72	680.70	16.59	587.90	15.83		
539.50	15.40	567.60	15.89	700.80	16.75	608.50	16.08		
559.20	15.64	588.80	16.01	721.90	16.94	627.40	16.31		
579.50	15.75	608.80	16.23	742.00	17.11	647.10	16.59		
599.90	16.03	627.80	16.36	761.50	17.20	667.10	16.79		
619.20	16.19	646.60	16.53	781.30	17.37	686.90	17.05		
638.40	16.29	665.40	16.67	800.20	17.54	707.70	17.28		
658.10	16.26	686.00	16.82	819.50	17.72	728.00	17.54		
678.20	16.45	707.10	17.00	839.70	17.84	747.30	17.75		
698.50	16.66	727.10	17.10	860.00	18.04	766.60	18.07		
718.90	16.81	746.90	17.36	880.70	18.22	786.10	18.35		
738.00	17.02	765.60	17.48	901.90	18.36	805.90	18.59		
757.20	17.24	785.00	17.71	921.10	18.53	826.30	18.87		
776.60	17.66	805.70	17.85	938.90	18.60	846.30	19.18		
796.40	17.66	825.80	18.03	958.50	18.90	867.10	19.43		
816.30	17.85	845.50	18.20	977.70	19.05	887.40	19.64		
836.50	18.00	865.70	18.13	997.60	19.18				
856.90	18.36	887.10	18.33	1018.10	19.27				
877.60	18.55	905.20	18.52	1038.30	19.46				
898.40	18.81	925.30	18.70	1058.50	19.73				
917.60	18.86	943.30	18.82	1078.70	19.77				
936.80	19.13	963.10	19.19	1098.90	20.08				
956.20	19.35	983.50	19.38	1119.10	20.32				
975.70	19.57	1003.10	19.50						
995.60	19.83	1022.90	19.76						
		1043.00	19.83						
		1063.80	19.96						
		1084.30	20.14						
		1105.20	20.35						
		1124.70	20.57						
		1142.40	20.55						

A plain (uncoated) in pure water expeiments,
1 atm using various heater sizes

0.75 cm x 0.75 cm	
[kW/m^2]	**[^{o}C]**
0.00	0.03
18.13	6.42
35.91	6.83
53.51	7.11
71.29	8.03
89.24	9.07
176.71	11.12
264.89	12.48
353.24	13.65
439.82	14.87
526.93	15.79
615.11	16.66
702.93	17.39
789.16	17.92
822.58	18.19
856.71	18.58
891.56	18.81
927.11	19.04
963.20	19.24
1000.18	19.51
1033.42	19.75
1067.38	20.04
1101.69	20.37
1136.53	20.65

1 cm x 1 cm	
[kW/m^2]	**[^{o}C]**
0.00	0.32
21.10	6.67
40.80	6.65
60.80	7.71
90.80	8.26
120.40	9.28
150.70	9.87
180.60	10.31
210.20	10.89
239.80	11.39
270.10	11.84
299.90	12.32
329.90	12.48
359.90	13.00
389.90	13.51
419.60	13.96
440.00	14.27
459.50	14.50
479.30	14.75
499.50	14.90
520.20	15.23
539.50	15.40
559.20	15.64
579.50	15.75
599.90	16.03
619.20	16.19
638.40	16.29
658.10	16.26
678.20	16.45
698.50	16.66
718.90	16.81
738.00	17.02
757.20	17.24
776.60	17.66
796.40	17.66
816.30	17.85
836.50	18.00
856.90	18.36
877.60	18.55
898.40	18.81
917.60	18.86
936.80	19.13
956.20	19.35
975.70	19.57
995.60	19.83

1.5 cm x 1.5 cm	
[kW/m^2]	**[^{o}C]**
0.00	-0.61
22.04	5.47
43.96	6.90
66.04	7.76
87.87	8.71
109.60	9.59
153.64	10.37
197.11	11.12
241.24	11.80
284.71	12.37
328.89	12.72
373.64	13.33
417.87	13.75
461.42	14.29
505.42	14.64
548.58	15.23
592.04	15.67
635.96	16.19
679.16	16.82
722.40	16.96
744.89	17.34
766.62	17.49
788.31	17.80
810.27	17.94
831.91	18.15
853.91	18.52
875.24	18.49
897.47	18.76
919.69	18.96
940.76	19.43

2 cm x 2 cm	
[kW/m^2]	**[^{o}C]**
0.00	-1.48
19.58	6.86
39.40	8.16
59.18	9.25
98.65	9.86
138.10	10.52
177.18	11.31
216.85	11.82
256.18	12.41
295.55	13.10
335.38	13.64
374.88	14.13
414.13	14.90
453.60	15.19
492.43	15.56
531.73	15.84
570.75	16.53
609.85	17.17
648.95	17.63
688.15	18.06
726.63	18.55
765.38	19.03
804.70	19.73
823.78	19.78
842.98	20.16
862.45	20.17
882.20	20.36
901.43	20.77
920.13	20.61
940.08	20.90
958.93	21.25
978.35	21.46
997.75	21.44

Al_2O_3 nanofluids experiments, 1 cm × 1 cm, (0.001-0.025 g/l)
at T_{sat}=100°C (101 kPa) w/ various concentrations

0.001g/l	
[kW/m^2]	**[°C]**
0.00	0.24
10.00	6.63
30.10	13.86
50.20	8.70
89.70	9.45
129.50	10.40
169.40	10.96
209.00	11.62
248.50	12.33
287.80	13.07
327.60	13.36
366.80	13.93
407.40	14.42
446.40	14.84
486.00	15.21
525.90	15.76
565.30	16.14
604.40	16.57
645.10	16.88
684.70	17.30
724.20	17.54
764.30	17.79
803.80	18.27
823.85	18.47
843.90	18.67
863.55	18.83
883.20	19.00
903.30	19.21
923.40	19.41
942.80	19.50
962.20	19.59
982.15	19.71
1002.10	19.82
1022.30	19.98
1042.50	20.14
1063.05	20.30
1083.60	20.47
1103.40	20.72
1123.20	20.97
1141.95	21.04
1160.70	21.11
1180.15	21.25
1199.60	21.39
1209.30	21.48
1219.00	21.57
1228.75	21.80
1238.50	22.04
1248.50	21.97
1258.50	21.90
1268.40	22.03
1278.30	22.16
1288.65	22.12
1299.00	22.09

0.005 g/l	
[kW/m^2]	**[°C]**
0.00	0.04
19.80	5.68
39.90	6.56
59.70	7.23
109.80	8.45
159.50	9.45
209.60	10.40
259.00	11.42
308.30	12.46
358.30	13.08
407.80	13.98
457.40	14.53
506.80	15.25
556.80	15.74
606.40	16.27
655.40	16.61
705.30	16.98
754.90	17.77
803.70	18.18
828.75	18.38
853.80	18.59
878.65	18.82
903.50	19.05
928.25	19.26
953.00	19.47
977.75	19.86
1002.50	20.25
1027.00	20.45
1051.50	20.66
1077.00	20.96
1102.50	21.27
1127.10	21.47
1151.70	21.66
1176.75	21.94
1201.80	22.21
1226.40	22.47
1251.00	22.73
1275.65	22.97
1300.30	23.21
1324.60	23.45
1348.90	23.69
1372.95	23.88
1397.00	24.08
1422.05	24.42
1447.10	24.76
1471.50	24.90
1495.90	25.04
1520.40	25.25
1544.90	25.46
1569.80	25.69
1594.70	25.91
1619.95	26.65
1645.20	27.38

0.01 g/l	
[kW/m^2]	**[°C]**
0.00	0.02
20.10	6.76
39.90	7.57
59.70	8.41
109.80	9.27
159.50	10.10
209.10	10.72
258.60	11.20
308.30	11.81
358.30	12.39
407.80	13.00
457.60	13.62
506.80	14.26
556.80	14.84
606.60	15.27
655.80	15.78
704.80	16.21
754.20	16.67
803.00	17.31
828.00	17.65
853.00	17.99
878.15	18.24
903.30	18.50
927.90	18.68
952.50	18.87
977.35	19.23
1002.20	19.59
1026.85	19.89
1051.50	20.20
1076.85	20.46
1102.20	20.72
1126.80	20.87
1151.40	21.02
1176.30	21.33
1201.20	21.65
1225.65	21.94
1250.10	22.22
1275.00	22.34
1299.90	22.46
1324.40	22.74
1348.90	23.02
1373.45	23.14
1398.00	23.27
1422.85	23.64
1447.70	24.01
1471.80	24.19
1495.90	24.37
1520.25	24.79
1544.60	25.21
1569.10	25.50
1593.60	25.79
1619.05	26.20
1644.50	26.61
1654.00	26.81
1663.50	27.00
1673.35	27.16
1683.20	27.33
1692.95	27.47
1702.70	27.61
1712.90	27.78
1723.10	27.94
1732.40	28.01
1741.70	28.07
1752.20	28.27
1762.70	28.47
1773.30	28.59
1783.90	28.70
1794.50	28.72
1805.10	28.75
1815.70	28.92
1826.30	29.10

0.025 g/l	
[kW/m^2]	**[°C]**
0.00	0.33
20.30	5.89
40.20	6.41
60.10	7.35
100.10	8.73
150.20	10.04
200.60	10.96
250.20	12.03
300.40	12.48
349.80	13.10
400.20	13.21
440.40	13.79
479.50	14.35
520.40	14.74
559.50	15.13
600.00	15.77
638.40	16.00
678.00	16.41
718.70	16.68
758.70	16.77
797.80	17.41
837.80	17.72
858.30	17.82
878.90	17.98
899.70	18.18
918.70	18.42
937.90	18.57
957.40	18.88
976.90	19.09
996.80	19.29
1016.80	19.34
1036.90	19.71
1057.20	19.80
1077.70	20.13
1098.50	20.23
1119.40	20.39
1138.40	20.33
1157.20	20.66
1176.20	20.95
1195.50	21.14
1214.90	21.41
1234.50	21.56
1252.50	21.65
1272.20	21.86
1291.90	21.92
1312.00	22.40
1332.40	22.65
1352.90	22.78
1373.30	23.01
1393.90	23.15
1415.00	23.02
1435.90	23.43
1454.30	23.87
1473.10	24.20
1491.70	24.30
1510.70	24.60
1529.50	24.59
1548.90	24.85
1567.90	24.96
1587.30	25.14
1606.60	25.54
1626.20	25.51
1645.90	25.80
1665.60	26.01
1685.60	26.10
1705.50	26.40
1725.50	26.54
1746.10	26.61
1766.10	26.98
1786.40	27.19
1807.10	27.66
1827.80	27.75
1848.60	27.88
1869.40	28.15
1890.30	28.77
1911.40	29.15
1929.40	29.52
1947.80	29.75
1965.80	30.26

Al_2O_3 nanofluids experiments, 1 cm × 1 cm, (0.05-1 g/l)
at T_{sat}=100°C (101 kPa) w/ various concentrations

0.05 g/l	
[kW/m^2]	**[°C]**
0.00	0.11
20.10	5.61
39.90	7.05
59.70	8.09
109.80	8.89
159.50	10.00
209.20	10.03
258.60	10.92
308.40	11.70
358.50	12.41
407.90	13.18
448.50	13.36
488.20	14.08
527.40	14.19
566.80	14.53
608.30	15.10
646.60	15.52
686.80	16.22
727.60	16.78
765.80	16.97
805.50	17.58
825.00	17.74
845.80	17.97
866.10	18.30
886.70	18.63
905.40	18.88
924.80	19.10
944.10	19.38
963.90	19.51
983.10	19.98
1002.50	20.13
1022.60	20.29
1042.60	20.53
1063.50	20.81
1083.90	21.11
1104.50	21.22
1123.30	21.63
1141.30	21.92
1161.30	22.25
1180.20	22.64
1199.60	23.00
1219.50	23.13
1238.60	23.41
1257.80	23.66
1278.80	23.86
1298.40	24.15
1317.70	24.57
1338.50	24.89
1358.90	25.34
1379.40	25.63
1400.60	26.10
1420.80	26.41
1442.00	26.66
1461.10	27.18
1479.60	27.42
1498.30	28.06
1516.70	28.54
1535.60	29.19
1554.60	29.51
1574.40	29.87
1593.30	30.21
1612.60	30.48
1632.40	30.87
1652.40	31.21
1672.10	31.67
1692.60	31.95
1712.50	32.29
1731.90	33.07
1752.00	33.50
1773.10	33.69
1792.70	33.86
1813.20	34.22
1834.60	34.01
1854.20	34.32
1876.60	34.22
1897.20	34.36
1918.30	34.76

0.1 g/l	
[kW/m^2]	**[°C]**
0.00	0.20
19.90	5.07
40.10	6.03
59.90	6.83
109.90	9.17
159.60	10.09
209.30	10.91
258.90	11.58
308.50	11.98
358.80	12.52
408.30	13.03
449.10	13.34
488.90	13.68
528.20	14.23
567.60	14.70
608.80	15.24
647.50	15.66
688.10	16.19
728.80	16.52
766.80	16.89
806.70	17.25
827.00	17.40
847.40	17.69
867.20	17.95
888.00	18.30
907.20	18.66
925.60	18.68
944.90	19.16
965.00	19.28
984.50	19.58
1003.90	19.83
1023.70	19.80
1044.40	20.04
1065.50	20.23
1085.10	20.56
1106.00	20.60
1125.10	20.58
1143.70	21.09
1162.20	21.22
1182.70	21.45
1201.50	22.19
1220.40	22.53
1240.10	22.81
1260.30	23.26
1279.70	23.47
1299.60	23.66
1320.60	23.77
1339.80	24.36
1360.50	24.85
1382.60	25.49
1402.60	26.01
1423.80	26.33
1442.70	26.48
1460.40	26.56
1479.30	26.78
1497.60	27.08
1517.10	27.38
1534.90	28.00
1554.90	28.16
1573.30	28.75
1593.60	29.18
1612.60	29.78
1632.40	29.96
1653.10	30.44
1672.10	30.83
1690.80	31.33
1712.20	31.75
1731.90	32.04
1752.40	32.34
1771.90	33.19
1792.70	33.56
1812.10	33.72
1834.60	34.12
1853.80	34.17
1875.80	34.13
1898.00	33.66
1918.30	33.45

0.5 g/l	
[kW/m^2]	**[°C]**
0.00	1.34
20.10	8.03
39.90	8.78
59.70	9.57
109.90	9.67
159.50	10.38
209.20	11.29
258.70	12.31
308.30	12.94
358.40	13.72
408.10	14.49
457.40	15.19
506.80	15.85
557.00	16.70
605.90	17.08
655.60	17.82
705.30	18.55
754.20	19.06
802.70	19.32
827.85	19.69
853.00	20.05
877.75	20.23
902.50	20.42
927.10	20.84
951.70	21.26
976.65	21.61
1001.60	21.96
1026.10	22.21
1050.60	22.47
1076.25	22.86
1101.90	23.25
1126.35	23.64
1150.80	24.02
1175.85	24.34
1200.90	24.66
1225.00	25.09
1249.10	25.53
1274.05	26.05
1299.00	26.57
1324.40	26.88
1349.80	27.19
1374.40	27.44
1399.00	27.70
1423.35	28.20
1447.70	28.70
1473.50	29.13
1499.30	29.57
1523.65	30.13
1548.00	30.69
1572.75	31.08
1597.50	31.46
1622.80	31.85
1648.10	32.23
1657.55	32.42
1667.00	32.60
1676.70	32.86
1686.40	33.12
1696.90	33.34
1707.40	33.57
1717.45	33.77
1727.50	33.97
1737.00	34.11
1746.50	34.26
1757.00	34.46
1767.50	34.66
1777.85	34.69
1788.20	34.71
1798.45	34.88
1808.70	35.05
1819.20	35.03
1829.70	35.01
1840.25	35.07
1850.80	35.12
1861.25	35.13
1871.70	35.15
1881.75	35.25
1891.80	35.35
1902.75	35.50
1913.70	35.66
1920.60	35.76
1927.50	35.86

1 g/l	
[kW/m^2]	**[°C]**
0.00	0.15
20.10	7.61
39.90	9.93
59.70	11.10
109.80	10.15
159.40	10.90
209.00	11.84
258.50	12.31
308.20	13.02
358.00	13.39
407.50	14.15
457.20	14.39
506.20	14.77
556.40	15.42
605.30	16.22
655.40	16.99
704.60	17.81
753.20	18.45
802.00	19.37
827.10	19.78
852.20	20.19
877.20	20.52
902.20	20.86
926.40	21.39
950.60	21.92
975.85	22.47
1001.10	23.01
1025.55	23.53
1050.00	24.05
1075.50	24.60
1101.00	25.16
1125.45	25.73
1149.90	26.31
1174.75	26.97
1199.60	27.62
1224.05	28.12
1248.50	28.61
1273.10	29.24
1297.70	29.87
1323.25	30.48
1348.80	31.09
1373.25	31.29
1397.70	31.48
1422.70	31.68
1447.70	31.88
1472.80	32.11
1497.90	32.35
1522.25	32.55
1546.60	32.75
1571.35	33.02
1596.10	33.30
1621.35	33.45
1646.60	33.61
1670.15	33.88
1693.70	34.15
1719.00	34.26
1744.30	34.36
1768.70	34.29
1793.10	34.22
1818.20	34.04
1843.30	33.86
1853.50	33.77
1863.70	33.68

Al_2O_3 -0.025 g/l nanofluid experiments, 1 cm × 1 cm at various pressures

Tsat=60°C (20kPa)	
[kW/m^2]	[°C]
0.01	0.37
18.46	11.05
38.21	21.12
57.96	12.59
107.81	13.17
156.80	14.35
206.01	15.42
255.61	16.27
304.96	17.73
354.24	18.67
403.78	19.86
453.01	20.68
502.06	22.04
529.60	22.26
558.70	22.68
589.20	23.38
618.70	23.83
648.70	24.74
677.60	25.34
707.10	25.78
737.60	26.32
766.20	27.24
795.80	28.05
825.70	28.39
856.40	29.10
885.40	29.67
914.90	30.03
944.70	30.82
975.20	31.49
1004.00	32.50
1032.90	33.16
1062.60	33.54
1092.20	34.29
1122.40	34.56
1153.40	34.98
1182.30	35.83
1210.80	36.31
1230.50	36.79
1250.00	37.26
1269.50	37.14
1289.90	37.92
1309.70	38.22
1330.30	38.80
1350.90	39.30
1371.40	39.87
1391.70	40.35
1412.20	40.68
1433.20	41.20
1451.80	42.08
1470.30	42.56
1488.90	43.06
1508.50	43.18
1527.30	43.89
1546.30	44.28
1566.00	44.75
1584.50	45.42

Tsat=80°C (47kPa)	
[kW/m^2]	[°C]
0.00	-0.27
20.40	7.46
40.30	10.32
60.30	10.64
100.30	11.42
150.50	12.34
200.90	13.52
250.50	13.93
300.60	14.56
349.90	15.30
400.30	16.02
440.90	16.36
480.10	17.06
521.00	18.01
560.10	18.28
600.90	18.81
620.05	19.03
639.20	19.25
658.95	19.53
678.70	19.81
699.15	20.15
719.60	20.49
738.55	20.77
757.50	21.04
776.95	21.30
796.40	21.56
816.45	21.89
836.50	22.22
856.85	22.51
877.20	22.81
897.10	23.12
917.00	23.44
936.30	23.67
955.60	23.90
975.25	24.26
994.90	24.63
1014.80	24.88
1034.70	25.12
1055.10	25.45
1075.50	25.78
1096.30	26.02
1117.10	26.27
1135.95	26.61
1154.80	26.96
1173.90	27.12
1193.00	27.28
1212.55	27.65
1232.10	28.02
1251.75	28.25
1271.40	28.48
1291.30	28.76
1311.20	29.04
1331.55	29.19
1351.90	29.33
1372.60	29.72
1393.30	30.10
1414.15	30.28
1435.00	30.47
1453.65	30.76
1472.30	31.06
1491.05	31.44
1509.80	31.81
1528.90	32.08
1548.00	32.21
1567.20	32.35
1586.50	32.63
1606.00	32.73
1625.20	32.81
1645.20	32.93

Tsat=100°C (101kPa)	
[kW/m^2]	[°C]
0.00	0.33
20.30	5.89
40.20	6.41
60.10	7.75
100.10	8.73
150.20	10.04
200.60	10.96
250.20	12.03
300.40	12.48
349.80	13.10
400.20	13.21
420.10	13.54
440.40	13.79
459.80	13.99
479.50	14.35
499.80	14.52
520.40	14.74
539.80	14.91
559.50	15.13
579.60	15.43
600.00	15.77
619.00	15.90
638.40	16.00
658.00	16.17
678.00	16.41
698.10	16.50
718.70	16.68
739.60	16.75
758.70	16.77
778.20	17.26
797.80	17.41
817.80	17.69
837.80	17.72
858.30	17.82
878.90	17.98
899.70	18.18
918.70	18.42
937.90	18.57
957.40	18.88
976.90	19.09
996.80	19.29
1016.80	19.34
1036.90	19.71
1057.20	19.80
1077.70	20.13
1098.50	20.23
1119.40	20.39
1138.40	20.33
1157.20	20.66
1176.20	20.95
1195.50	21.14
1214.90	21.41
1234.50	21.56
1252.50	21.65
1272.20	21.86
1291.90	21.92
1312.00	22.40
1332.40	22.65
1352.90	22.78
1373.30	23.01
1393.90	23.15
1415.00	23.02
1435.90	23.43
1454.30	23.87
1473.10	24.20
1491.70	24.30
1510.70	24.60
1529.50	24.59
1548.90	24.85
1567.90	24.96
1587.30	25.14
1606.60	25.54
1626.20	25.51
1645.90	25.80
1665.60	26.01
1685.60	26.10
1705.50	26.40
1725.50	26.54
1746.10	26.61
1766.10	26.98
1786.40	27.19
1807.10	27.66
1827.80	27.75
1848.60	27.88
1869.40	28.15
1890.30	28.77
1911.40	29.15
1929.40	29.52
1947.80	29.75
1965.80	30.26

Tsat=120°C (210kPa)	
[kW/m^2]	[°C]
0.00	1.95
20.00	3.72
39.80	4.63
59.50	5.62
99.60	6.40
139.90	7.22
180.00	8.23
219.90	9.05
257.70	9.65
297.90	10.62
338.20	11.43
377.90	12.15
417.00	12.56
456.30	13.03
495.60	13.16
535.30	13.66
575.20	14.11
613.50	14.42
653.80	14.71
694.60	15.03
732.40	15.26
772.90	15.34
811.90	15.93
852.50	16.30
891.40	16.39
932.30	16.75
969.10	16.82
1008.00	17.09
1047.70	17.24
1086.80	17.59
1125.30	17.82
1166.40	17.94
1205.10	18.14
1243.20	18.37
1282.80	18.58
1322.50	18.70
1361.70	19.06
1401.20	19.27
1440.00	19.62
1479.20	19.88
1518.30	19.93
1537.60	20.18
1556.20	20.22
1575.30	20.24
1593.90	20.25
1613.90	20.48
1633.40	20.48
1652.60	20.80
1669.80	20.85
1689.90	21.06
1709.90	21.15
1731.00	21.10
1748.90	21.41
1767.70	21.21
1788.80	21.71
1809.30	21.72
1829.50	21.99
1850.30	22.01
1870.70	22.04
1892.40	22.08
1912.00	22.34
1932.80	22.31
1950.20	22.35
1970.00	22.14
1987.60	22.39
2005.20	22.41
2023.80	22.48
2042.40	22.39
2059.90	22.82
2078.70	23.05
2097.10	23.11
2116.00	23.18
2134.70	23.20
2153.00	23.35
2172.60	23.62
2191.00	23.74
2211.20	23.86
2228.60	23.92
2248.50	23.95
2268.20	24.06
2287.40	24.09
2306.40	24.07
2326.70	24.14
2346.20	24.33
2366.20	24.37
2385.90	24.43
2406.10	24.58
2424.70	24.70
2445.00	24.88
2466.40	25.11
2486.50	25.25
2505.80	25.38
2526.40	25.63
2545.90	25.75
2566.80	25.88

Al_2O_3 nanocoating-2min. experiments, 1 cm × 1 cm at various pressures

Tsat=60°C (20kPa)	
[kW/m²]	[°C]
0.00	0.81
19.75	5.42
39.50	10.03
59.20	11.15
78.90	12.27
118.40	14.17
157.90	15.04
198.10	15.75
237.30	16.64
276.60	17.57
316.30	18.03
355.90	18.66
395.20	19.70
435.00	20.35
455.30	20.73
475.60	21.11
494.95	21.44
514.30	21.78
534.20	22.32
554.10	22.86
574.20	23.11
594.30	23.37
614.10	23.85
633.90	24.33
653.35	24.65
672.80	24.97
693.40	25.70
714.00	26.43
733.25	26.84
752.50	27.25
772.00	27.70
791.50	28.15
811.55	28.73
831.60	29.30
850.55	29.57
869.50	29.83
889.00	30.43
908.50	31.02
928.85	31.60
949.20	32.19
968.75	32.54
988.30	32.89
1007.95	33.21
1027.60	33.53
1047.80	33.97
1068.00	34.40
1087.40	34.87
1106.80	35.33
1126.15	35.61
1145.50	35.88
1165.40	36.33
1185.30	36.77

Tsat=80°C (47kPa)	
[kW/m²]	[°C]
0.10	-0.54
19.90	11.42
39.60	7.33
59.20	9.76
98.60	10.84
138.10	11.88
177.60	12.31
216.80	13.04
256.60	13.55
296.10	14.28
335.70	14.90
375.00	15.30
415.10	15.89
454.30	16.56
493.80	17.31
533.40	18.02
572.70	18.79
611.10	19.06
630.40	19.25
649.50	19.70
668.70	19.99
689.30	20.10
709.30	20.17
729.50	20.53
748.60	20.87
767.50	21.39
786.80	21.53
806.20	21.80
826.30	22.31
846.30	22.80
866.90	23.10
886.90	23.54
907.70	23.95
926.90	23.94
945.70	24.38
964.40	24.60
984.70	25.07
1004.10	25.16
1023.70	25.36
1043.50	25.77
1063.70	25.56
1085.00	26.24
1105.10	26.59
1125.00	26.82
1143.90	27.06
1163.00	27.45
1181.70	27.65
1200.80	27.92
1220.00	28.10
1238.80	28.53
1258.40	28.81
1278.40	29.26
1297.00	29.57
1316.10	29.83
1334.80	30.13
1353.90	30.34
1373.10	30.65
1391.90	30.88
1411.50	31.38
1431.50	31.65
1450.10	31.85
1469.20	32.11

Tsat=100°C (101kPa)	
[kW/m²]	[°C]
0.00	0.00
19.70	3.71
39.70	5.79
59.80	6.63
99.30	8.69
138.80	9.49
178.30	10.62
217.50	11.06
257.30	11.31
296.70	12.26
336.20	13.21
375.30	13.74
415.30	14.26
454.60	14.79
494.00	14.93
533.80	15.74
573.10	16.11
611.50	16.20
651.70	16.46
691.60	16.87
730.00	17.47
770.10	17.49
808.40	17.87
828.80	18.08
849.40	18.14
869.20	18.58
889.50	18.71
910.90	18.56
929.50	19.03
948.90	19.31
967.90	19.31
987.20	19.54
1006.90	19.71
1027.30	19.75
1047.10	19.98
1066.80	20.10
1087.90	20.20
1108.20	20.26
1128.50	20.44
1147.80	20.57
1166.60	20.64
1185.00	20.78
1204.70	20.93
1224.00	21.12
1242.80	21.17
1263.00	21.31
1282.10	21.34
1301.70	21.61
1322.10	21.70
1341.60	22.04
1362.00	22.14
1382.50	22.44
1402.80	22.83
1423.90	23.03
1444.90	23.00
1462.70	22.90
1481.90	23.22
1500.20	23.52
1519.00	23.54
1537.50	23.76
1556.20	23.82
1576.00	24.09
1595.20	24.03
1613.90	24.26
1633.30	24.52
1653.30	24.72
1671.90	25.06
1692.80	25.06
1710.90	25.25
1731.70	25.37
1751.80	25.43
1772.90	25.63
1792.10	25.73
1813.40	26.08
1832.90	26.25
1854.00	26.37
1873.70	26.55
1895.80	26.47
1915.80	26.73

Tsat=120°C (210kPa)	
[kW/m²]	[°C]
0.10	-1.09
20.00	1.61
39.90	4.49
59.50	6.68
98.90	8.02
138.20	8.87
177.50	9.48
217.60	9.71
257.30	9.99
296.60	10.41
336.00	10.92
375.10	11.43
415.30	11.80
454.20	11.86
493.60	12.38
532.80	12.75
571.80	13.23
610.40	13.45
650.80	13.95
689.70	14.23
728.80	14.46
768.40	14.77
807.10	15.15
846.80	15.42
885.30	15.75
925.20	16.07
965.40	16.34
1004.00	16.66
1043.90	16.84
1084.30	17.35
1123.10	17.76
1162.60	17.89
1202.80	18.13
1241.20	18.46
1280.20	18.68
1319.80	18.99
1339.60	19.19
1360.30	19.32
1379.80	19.47
1400.70	19.47
1420.90	19.75
1441.80	19.86
1463.20	20.03
1480.70	20.10
1499.40	20.14
1518.50	20.22
1537.00	20.40
1555.70	20.38
1574.80	20.57
1593.30	20.71
1612.30	20.53
1633.20	21.05
1651.00	21.11
1671.40	21.27
1690.80	21.53
1710.80	21.74
1729.70	21.75
1750.60	21.93
1769.80	22.02
1790.50	22.12
1810.20	22.30
1831.60	22.37
1850.80	22.37
1871.70	22.39
1892.60	22.62
1913.70	22.74
1934.50	22.88
1955.40	23.00
1973.70	23.14
1992.10	23.31
2010.20	23.42
2028.70	23.56
2046.50	23.63
2064.90	23.75
2083.70	23.88
2102.90	24.01
2122.30	24.12
2140.20	24.12
2159.30	24.21
2178.50	24.31
2197.40	24.44
2216.00	24.52
2235.50	24.64
2254.60	24.76
2273.80	24.95
2293.50	25.05
2312.90	25.22
2332.40	25.49
2351.50	25.64
2372.40	25.74
2392.60	25.88
2411.80	25.93
2431.50	26.15
2450.90	26.33
2470.40	26.56
2489.50	26.68
2510.40	26.91
2530.60	27.05

Al_2O_3 nanocoating-2min. experiments, 1 cm × 1 cm at various orientations

0°		45°		90°		135°		180°	
[kW/m^2]	[°C]	[kW/m^2]	[°C]	[kW/m^2]	[°C]	[kW/m^2]	[°C]	[kW/m^2]	[°C]
0.00	0.00	0.00	0.00	0.00	0.00	0.00	0.00	0.00	0.00
19.70	3.71	19.80	3.63	19.60	2.92	19.80	2.10	20.20	1.99
39.70	4.79	39.60	7.91	39.20	6.89	39.60	3.40	40.00	2.62
59.80	5.63	59.55	8.42	59.05	7.47	59.40	4.40	60.00	3.74
99.30	7.69	79.50	8.92	78.90	8.05	79.20	5.39	90.10	6.34
138.80	9.49	119.00	10.17	118.20	8.87	118.70	6.87	129.90	7.97
178.30	10.62	158.40	10.82	158.40	9.69	158.00	8.71	169.60	9.55
217.50	11.06	198.40	11.40	198.30	10.19	197.90	9.78	209.10	10.78
257.30	11.31	238.50	12.05	238.50	10.66	236.80	10.41	249.00	11.44
296.70	12.26	277.70	12.47	277.70	11.61	275.60	11.13	288.00	12.03
336.20	13.21	317.40	12.89	317.30	12.22	314.70	12.05	328.00	12.56
375.30	13.74	357.00	13.10	356.90	12.76	353.10	13.08	367.40	13.24
415.30	14.26	396.00	13.86	396.00	13.53	390.90	13.71	407.70	13.84
454.60	14.79	435.60	14.43	435.60	13.85	429.40	14.29	446.90	14.33
494.00	14.93	475.60	14.86	475.80	14.40	467.90	15.21	486.30	15.10
533.80	15.74	516.10	15.51	516.10	14.94	506.50	15.23	526.20	15.82
573.10	16.11	556.40	15.93	556.40	15.43	544.10	15.93	565.70	16.37
611.50	16.20	596.40	16.01	596.40	16.11	581.60	16.40	605.20	16.95
651.70	16.46	636.10	16.44	636.10	16.59	618.10	16.78	645.50	17.48
691.60	16.87	675.00	16.81	675.00	16.99	655.30	17.19	685.20	17.94
730.00	17.47	715.10	17.27	715.10	17.45	690.80	17.45	725.00	18.52
770.10	17.49	754.40	17.67	753.90	17.85	728.10	17.73	765.10	19.24
808.40	17.87	793.00	18.04	793.00	18.26	765.80	18.19	804.70	19.77
828.80	18.08	832.80	18.32	832.80	18.85	803.90	18.65	824.40	20.14
849.40	18.14	852.80	18.65	852.55	18.99	822.60	18.80	844.30	20.47
869.20	18.58	872.80	18.98	872.30	19.13	841.30	18.95	864.30	20.93
889.50	18.71	892.75	19.22	892.50	19.33	859.95	19.21	884.10	21.41
910.90	18.56	912.70	19.46	912.70	19.54	878.60	19.48	904.00	21.77
929.50	19.03	932.85	19.70	932.40	19.70	897.25	19.57	924.20	22.09
948.90	19.31	953.00	19.95	952.10	19.86	915.90	19.67	943.90	22.81
967.90	19.31	972.00	20.18	971.55	20.06	934.90	19.97	963.80	23.09
987.20	19.54	991.00	20.41	991.00	20.26	953.90	20.28	983.80	24.07
1006.90	19.71	1011.15	20.56	1011.15	20.41	972.65	20.38	1003.60	24.69
1027.30	19.75	1031.30	20.71	1031.30	20.55	991.40	20.47	1023.50	25.38
1047.10	19.98	1051.05	20.91	1051.35	20.75	1010.35	20.68	1043.70	25.97
1066.80	20.10	1070.80	21.11	1071.40	20.96	1029.30	20.89		
1087.90	20.20	1090.25	21.30	1090.85	21.08	1048.35	21.12		
1108.20	20.26	1109.70	21.49	1110.30	21.21	1067.40	21.35		
1128.50	20.44	1129.35	21.75	1129.65	21.46	1086.10	21.61		
1147.80	20.57	1149.00	22.01	1149.00	21.71	1104.80	21.87		
1166.60	20.64	1169.40	22.11	1169.40	21.82	1123.45	21.90		
1185.00	20.78	1189.80	22.21	1189.80	21.93	1142.10	21.93		
1204.70	20.93	1208.90	22.37	1209.20	22.28	1160.75	22.19		
1224.00	21.12	1228.00	22.53	1228.60	22.62	1179.40	22.46		
1242.80	21.17	1247.70	22.61	1247.85	22.76	1198.40	22.81		
1263.00	21.31	1267.40	22.69	1267.10	22.90	1217.40	23.15		
1282.10	21.34	1286.95	22.88	1286.65	23.03	1236.15	23.47		
1301.70	21.61	1306.50	23.08	1306.20	23.16	1254.90	23.80		
1322.10	21.70	1326.50	23.35	1326.15	23.37	1273.85	24.01		
1341.60	22.04	1346.50	23.61	1346.10	23.58	1292.80	24.23		
1362.00	22.14	1365.45	23.81	1365.25	23.66	1311.85	24.30		
1382.50	22.44	1384.40	24.02	1384.40	23.74	1330.90	24.37		
1402.80	22.83	1403.85	24.14	1403.85	23.98	1349.60	24.60		
1423.90	23.03	1423.30	24.26	1423.30	24.21	1368.30	24.83		
1444.90	23.00	1443.15	24.53	1442.80	24.52	1386.95	25.25		
1462.70	22.90	1463.00	24.79	1462.30	24.83	1405.60	25.67		
1481.90	23.22	1482.80	24.95	1482.25	24.94	1424.25	25.95		
1500.20	23.52	1502.60	25.11	1502.20	25.05	1442.90	26.23		
1519.00	23.54	1522.45	25.23	1522.80	25.24	1461.90	26.41		
1537.50	23.76	1542.30	25.34	1543.40	25.43	1480.90	26.60		
1556.20	23.82	1561.05	25.70	1561.60	25.65				
1576.00	24.09	1579.80	26.06	1579.80	25.87				
1595.20	24.03	1599.10	26.31	1599.10	26.02				
1613.90	24.26	1618.40	26.56	1618.40	26.18				
1633.30	24.52	1638.15	26.73	1638.15	26.41				
1653.30	24.72	1657.90	26.90	1657.90	26.64				
1671.90	25.06	1677.15	27.04	1676.95	26.87				
1692.80	25.06	1696.40	27.18	1696.00	27.10				
1710.90	25.25	1716.40	27.43	1716.00	27.23				
1731.70	25.37	1736.40	27.68	1736.00	27.36				
1751.80	25.43	1756.65	27.78	1756.25	27.59				
1772.90	25.63	1776.90	27.89	1776.50	27.83				
1792.10	25.73	1797.00	28.12	1797.00	27.85				
1813.40	26.08	1817.10	28.36	1817.50	27.88				
1832.90	26.25	1835.90	28.59	1836.70	27.96				
1854.00	26.37	1854.70	28.82	1855.90	28.05				
1873.70	26.55	1874.30	29.14	1875.30	28.22				
1895.80	26.47	1893.90	29.46	1894.70	28.39				
1915.80	26.73			1913.50	28.62				
1937.80	26.95			1932.30	28.85				
1955.60	27.18								
1973.90	27.39								
1992.70	27.63								
2011.10	27.62								
2030.10	28.02								
2048.30	28.04								

Al_2O_3 nanocoating-2min. experiments w/ various heater sizes

0.75 cm x 0.75 cm	
[kW/m^2]	[^{o}C]
0.00	-3.11
34.84	4.16
70.22	5.96
105.07	7.21
139.38	8.65
175.11	9.81
209.07	11.06
244.09	11.72
279.64	12.09
315.38	12.41
350.40	12.96
384.71	13.38
418.31	13.89
453.87	14.11
486.76	14.51
521.42	14.87
558.04	15.34
591.64	15.56
626.13	15.91
662.40	16.21
695.64	16.75
730.13	17.05
765.16	17.30
800.36	17.59
833.78	18.03
867.38	18.45
901.33	18.85
936.18	19.24
971.73	19.58
1008.18	19.79
1040.71	20.24
1073.24	20.57
1107.02	20.96
1141.51	21.07
1175.64	21.28
1211.02	21.64
1246.76	21.92
1282.67	22.11
1319.29	22.34
1351.47	22.60
1384.36	22.59
1417.42	22.82
1451.02	22.95
1485.33	23.18
1519.29	23.47
1554.49	23.72
1589.16	23.81
1624.00	24.14
1659.56	24.38
1694.93	24.55
1731.91	24.96
1767.82	25.12
1800.36	25.59
1832.53	25.76
1864.53	25.83
1896.53	26.27
1930.13	26.41
1962.67	26.81
1996.09	26.97
2029.16	27.32
2062.22	27.66
2096.18	27.76
2129.96	27.95
2164.09	28.33
2199.64	28.59
2233.07	29.23

1 cm x 1 cm	
[kW/m^2]	[^{o}C]
0.00	0.00
19.70	3.71
39.70	4.79
59.80	5.63
99.30	7.69
138.80	9.49
178.30	10.62
217.50	11.06
257.30	11.31
296.70	12.26
336.20	13.21
375.30	13.74
415.30	14.26
454.60	14.79
494.00	14.93
533.80	15.74
573.10	16.11
611.50	16.20
651.70	16.46
691.60	16.87
730.00	17.47
770.10	17.49
808.40	17.87
828.80	18.08
849.40	18.14
869.20	18.58
889.50	18.71
910.90	18.56
929.50	19.03
948.90	19.31
967.90	19.31
987.20	19.54
1006.90	19.71
1027.30	19.75
1047.10	19.98
1066.80	20.10
1087.90	20.20
1108.20	20.26
1128.50	20.44
1147.80	20.57
1166.60	20.64
1185.00	20.78
1204.70	20.93
1224.00	21.12
1242.80	21.17
1263.00	21.31
1282.10	21.34
1301.70	21.61
1322.10	21.70
1341.60	22.04
1362.00	22.14
1382.50	22.44
1402.80	22.83
1423.90	23.03
1444.90	23.00
1462.70	22.90
1481.90	23.22
1500.20	23.52
1519.00	23.54
1537.50	23.76
1556.20	23.82
1576.00	24.09
1595.20	24.03
1613.90	24.26
1633.30	24.52
1653.30	24.72
1671.90	25.06
1692.80	25.06
1710.90	25.25
1731.70	25.37
1751.80	25.43
1772.90	25.63
1792.10	25.73
1813.40	26.08
1832.90	26.25
1854.00	26.37
1873.70	26.55
1895.80	26.47
1915.80	26.73
1937.80	26.95
1955.60	27.18
1973.90	27.39
1992.70	27.63
2011.10	27.62
2030.10	28.02
2048.30	28.04

1.5 cm x 1.5 cm	
[kW/m^2]	[^{o}C]
0.00	-0.86
21.87	7.06
44.04	7.88
66.18	8.17
88.00	8.82
109.87	9.11
153.60	9.75
197.56	10.22
241.56	10.79
285.29	11.50
329.64	11.98
373.29	12.72
417.24	13.04
461.20	13.59
504.44	14.10
548.13	14.66
591.42	15.18
635.51	15.78
678.53	16.36
722.13	16.70
744.49	17.00
765.87	17.22
787.42	17.67
809.16	17.86
831.56	18.30
852.40	18.54
874.27	18.81
896.58	19.01
918.76	19.17
939.20	19.33
961.64	19.67
983.24	19.94
1004.40	20.17
1026.84	20.40
1049.91	20.64
1071.07	20.79
1092.44	21.00
1114.36	21.31
1135.78	21.68
1157.33	21.89
1179.82	22.11
1201.42	22.38
1223.91	22.51
1244.71	22.72
1265.60	22.81
1287.38	22.90
1309.33	23.10
1331.73	23.37
1354.18	23.60
1375.47	23.94
1396.36	24.21
1417.60	24.55
1439.16	24.71
1461.02	24.96
1482.40	25.13
1504.04	25.13
1526.40	25.44
1548.80	25.64
1571.38	25.80
1592.18	25.98
1613.78	26.11
1634.22	26.43
1655.20	26.65
1675.91	26.73
1698.36	27.19
1719.33	27.23
1741.82	27.37
1763.91	27.44
1784.89	28.53
1805.60	28.69

2 cm x 2 cm	
[kW/m^2]	[^{o}C]
0.00	-2.90
24.80	9.16
49.63	7.49
74.33	7.32
124.08	9.26
173.60	10.16
223.10	10.75
272.30	11.98
321.53	12.32
370.85	13.35
420.23	13.74
469.08	14.46
518.30	15.40
568.15	15.97
617.18	16.72
666.13	17.45
715.18	17.81
764.13	18.44
813.08	18.93
837.58	19.14
861.38	19.37
885.68	19.55
910.15	19.62
934.03	20.33
958.33	20.79
982.88	20.93
1006.70	21.03
1030.80	21.33
1054.90	21.50
1079.80	21.84
1103.60	22.20
1127.50	22.43
1152.25	22.79
1177.35	22.95
1200.98	23.44
1224.83	23.74
1249.50	23.90
1273.60	23.80
1297.30	24.28
1320.90	24.59
1345.58	24.88
1369.65	25.27
1393.80	25.56
1418.70	25.59
1442.08	25.85
1465.93	26.20
1489.48	26.55
1514.10	27.01
1538.05	27.16
1562.68	27.41
1586.18	27.69
1609.50	28.17
1633.25	28.38
1657.90	28.44
1681.13	29.24
1706.03	29.17
1729.40	29.69
1753.25	30.09
1776.80	30.53

REFERENCES

[1] S. M. You, J. H. Kim, and K. H. Kim, Effect of Nanoparticles on Critical Eat Flux of Water in Pool Boiling Heat Transfer, Applied Physics Letters 83 (16) (2003) 3374-3376.

[2] H. Masuda, A. Ebata, K. Teramae, and N. Hishinuma, Alteration of Thermal Conductivity and Viscosity of Liquid by Dispersing Ultra-Fine Particles (Dispersion of γ-Al2O3, SiO2, and TiO2 Ultra-Fine Particles), Netsu Bussei 7 (1993) 227-233.

[3] S. Lee, S. U. S. Choi, S. Li, and J. A. Eastman, Measuring Thermal Conductivity of Fluids Containing Oxide Naanoparticles, Transactions of the ASME, Journal of Heat Transfer 121 (1999) 280-289.

[4] H. J. Xie, T. X. Wang, and F. Ai. Thermal Conductivity Enhancement of Suspensions Containing Nanosized Alumina Particles, Journal of Applied Physics 91 (2002) 4568-4572.

[5] S. K. Das, N. Putra, P. Thiesen, and W. Roetzel, Temperature Dependence of Thermal Conductivity Enhancement for Nanofluids, Transactions of the ASME, Journal of Heat Transfer 125 (2003) 567-574.

[6] Y. H. Jeong, W. J. Chang, and S. H. Chang, Wettability of Heated Surfaces under Pool Boiling using Surfactant Solutions and Nano-fluids, International Journal of Heat and Mass Transfer 51 (2008) 3025-3031.

[7] H. E. Patel, S. K. Das, T. Sundararajan, A. S. Nair, B. George, and T. Pradeep, Thermal Conductivities of Naked and Monolayer Protected Metal Nanoparticle Based Nanofluids: Manifestation of Anomalous Enhancement and Chemical Effects, Applied Physics Letter 83 (2003) 2931-2933.

[8] S. J. Kim, I. C. Bang, J. Buongiorno, and L. W. Hu, Surface Wettability Change During Pool Boiling of Nanofluids and Its Effect on Critical Heat Flux, International Journal of Heat and Mass Transfer 50 (2007) 4105-4116.

[9] J. C. Maxwell, A Treatise on Electricity and Magnetism, unabridged 3rd ed. Clarendon Press, Oxford UK (1891).

[10] R. L. Hamilton, and O. K. Crosser, Thermal Conductivity of Heterogeneous Two Component Systems, Industrial and Engineering Chemistry Fundamentals 1 (1962) 187-191.

[11] D. J. Jeffrey, Conduction Through a Random Suspension of Spheres, The Proceedings of Royal Society of London 335 (1973) 355-367.

[12] P. M. Hui, X. Zhang, A. J. Markworth, and D. Stroud, Thermal Conductivity of Graded Composites: Numerical Simulations and an Effective Medium Approximation, Journal of Materials Science 34 (1999) 5497–5503.

[13] Y. Xuan, and Q. Li, Heat Transfer Enhancement of Nanofluids, International Journal of Heat and Fluid Flow 21 (2000) 58–64.

[14] K. C. Leong, C. Yang, and S.M.S. Murshed, A Combined Static and Dynamic Mechanisms-based Model for the Effective Thermal Conductivity of Nanofluids: Fundamentals and Applications Conference, Copper Mountain Colorado (2007) 16–20.

[15] M. S. Liu, M. C. C. Lin, I. T. Huang, and C. C. Wang, Enhancement of Thermal Conductivity with CuO for Nanofluids, Chemical Engineering Technology 29 (1) (2006) 72-77.

[16] R. Prasher, A. D. Song, and J. Wang, Measurements of Nanofluid Viscosity and Its Implications for Thermal Applications, Applied Physics Letters 89 (2006) 133108.

[17] S. M. S. Murshed, K. C. Leong, and C. Yang, Enhanced Thermal Conductivity of TiO2-Water Based Nanofluids, International Journal of Thermal Sciences 44 (2005) 367-373.

[18] A. Einstein, Investigations on the Theory of the Brownian Movement, Dover Publications Inc. New York (1956).

[19] I. M. Krieger, and T. J. Dougherty, A Mechanism for Non-Newtonian Flow In Suspensions of Rigid Spheres. Transactions of the Society of Rheology 3 (1959) 137–152.

[20] L. E. Nielsen, Generalized Equation for the Elastic Moduli of Composite Materials, Journal of Applied Physics 41 (1970) 4626–4627.

[21] G. K. Batchelor, The Effect of Brownian Motion on the Bulk Stress in a Suspension of Spherical Particles, Journal of Fluid Mechanics 83 (1977) 97–117.

[22] M. N. Golubovic, H. D. M. Hettiarachchi, W. M. Worek , and W. J. Minkowycz, Nanofluids and Critical Heat Flux, Experimental and Analytical Study, Applied Thermal Engineering (2008).

[23] D. Milanova, and R. Kumar, Role of Ions in Pool Boiling Heat Transfer of Pure and Silica Nanofluids, Applied Physcis Letters 87 (233107) (2005).

[24] Y. M. Yang, and J. R. Maa, Boiling of Suspension of Solid Particles in Water, Pool Boiling Charecteristics of Nano-Fluids, International Journal of Heat and Mass Transfer 27 (1) (1984) 145-147.

[25] P. Vassallo, R. Kumar, and S. D'Amico, Pool Boiling Heat Transfer Experiments in Silica-Water Nano-Fluids, International Journal of Heat and Mass Transfer 47 (2003) 407-411.

[26] H. Kim, and M.H. Kim, Experimental study of the Characteristics and Mechanism of Pool Boiling CHF Enhancement Using Nanofluids, Journal of Heat and Mass Transfer 45 (7) (2007) 991-998.

[27] D. Milanova, and R. Kumar, Heat Transfer Behavior of Silica Nanoparticles in Pool Boiling Experiment, Journal of Heat Transfer 130 (2008) 1-16.

[28] J. H. Kim, K. H. Kim, and S. M. You, Pooling Boiling Heat Transfer in Saturated Nanofluids, Proceedings of IMECE: ASME Int. Mechanical Engineering Congress and RD&D Expo, Anaheim, California (2004).

[29] G. Moreno Jr, S.J. Oldenberg, and S.M. You, Pool Boiling Heat Transfer of Alumina-Water, ZincOxide-Water and Alumina-Water+Ethylene Glycol Nanofluid, Proceedings of HT2005, ASME Summer Heat Transfer Conference (2005).

[30] S. K. Das, N. Putra, and W. Roetzel, Pool Boiling Characteristics of Nano-Fluids, International Journal of Heat and Mass Transfer 46 (2003) 851-862.

[31] I. C. Bang, and S. H. Chang, Boiling Heat Transfer Performance and Phenomena of Al2O3–water Nano-fluids from a Plain Surface in a Pool. International Journal of Heat and Mass Transfer 48 (2005) 2407-2419.

[32] S. K. Das, N. Putra, and W. Roetzel, Pool Boiling of Nano-Fluids on Horizhontal Narrow Tubes, International Journal of Multiphase Flow 29 (2003) 1237-1247.

[33] I. C. Bang, J. Buongiorno, L. Hu, and H. Wang, Measurement of Key Pool Boiling Parameters in Nanofluids for Nuclear Applications, Journal of Power and Energy Systems 2 (1) (2008) 340-351.

[34] Z. Liu, and L. Liao, Sorption and Agglutination Phenomenon of Nanofluids on a Plain Heating Surface During Pool Boiling, International Journal of Heat and Mass Transfer 51 (2008) 2593-2602.

[35] M. Chopkar, A. K. Das, and I. Manna, Pool Boiling Heat Transfer Characteristics of ZrO2-Water Nanofluids from a Flat Surface in a Pool, Heat Mass Transfer 44 (2008) 999-1004.

[36] J. P. Tu, N. Dinh, and T. Theofanous, An Experimental Study of Nnofluid Boiling Heat Transfer, in Proceedings of 6th International Symposium on Heat Transfer, Beijing, China (2004).

[37] D. Wen, and Y. Ding, Experimental Investigation into the Pool Boiling Heat Transfer of Aqueous based γ-alumina Nanofluids, Journal of Nanoparticle Research 7 (2005) 265–274.

[38] K. Park, and D. Jung, Enhancement of Nucleate Boiling Heat Transfer Using Carbon Nanotubes, International Journal of Heat and Mass Transfer 50 (2007) 4499-4502.

[39] S. C. Johnathan, and J. Kim, Nanofluid boiling: The Effect of Surface Wettability, International Journal of Heat and Fluid Flow 29 (6) (2008) 1577-1585.

[40] K. Sefiane, On the Role of Structural Disjoining Pressure and Contact Line Pinning in Critical Heat Flux Enhancement During Boiling of Nanofluids, Applied Physics Letters 89 (44106) (2006).

[41] M. T. Cichelli, and C. F. Bonilla, Heat Transfer to Liquids Boiling Under Pressure, AIChE (1945) 755-787.

[42] K. Nishikawa, Y. Fujita, and H. Ohta, Effect of System Pressure and Surface Roughness on Nucleate Boiling Heat Transfer, Memoirs of the Faculty of Engineering Kyushu University 42 (2) (1982) 95-111.

[43] W. R. McGillis, V. P. Carey, J. S. Fitch, and W. R. Hamburgen, Pool Boiling Enhancement Techniques for Water at Low Pressure, in: Proceedings, Seventh Annual IEEE Semiconductor Thermal Measurement and Management Symposium, IEEE, New York (1991) 64–72.

[44] A. A. Watwe, A. Bar-Cohen, and A. McNeil, Combined Pressure and Subcooling Effects on Pool Boiling From a PPGA Chip Package, ASME Journal of Electronic Packaging 119 (1997) 95–105.

[45] K. N. Rainey, S. M. You, and S. Lee, Effect of Pressure, Subcooling, and Dissolved Gas on Pool Boiling Heat Transfer from Microporous, Square Pin-Finned Surfaces in FC-72, International Journal of Heat and Mass Transfer 46 (2003) 23-35.

[46] I. Mudawar, and T. M. Anderson, Parametric Investigation into the Effect of Pressure, Subcooling, Surface Augmentation and Choice of Coolant on Pool Boiling in the Design of Cooling Systems for High-Power-Density Electronic Chips. Journal of Electronic Packaging 112 (1990) 375-382.

[47] N. Abuaf, S. H. Balck, and F. W. Staub, Pool Boiling Performance of Finned Surfaces in R-113, International Journal of Heat and Fluid Flow 6 (1) (1985) 23-30.

[48] A. Bar-Cohen, and A. McNeil, Parametric Effects on Pool Boiling Critical Heat Flux in Dielectric Liquids, Proceedings of the Engineering Foundation Conference on Pool and External Flow Boiling, ASME, Santa Barbara, CA (1992) 171–175.

[49] E. A. Kazakova, Maximum heat transfer to boiling water at high pressures, The Engineers' Digest 12 (3) (1951) 81–85

[50] A. T. Storr, The Effect of Heating Surface Geometry and Orientatin on Nucleate Boiling of Subcooled Water, M.S Thesis, Washington University, Sever Institute of Technology, Department of Chemical Engineering (1958).

[51] B. D. Marcus, and D. Dropkin, The Effect of Surface Configuration on Nucleate Boiling Heat Transfer, International Journal of Heat and Mass Transfer 6 (1963) 863-867.

[52] P. M. Githinji, and R. H. Sabersky, Some Effect of the Orientation of the Heating Surface in Nucleate Boiling, ASME Journal of Heat Transfer 85 (1963) 379.

[53] J. Y. Chang, and S. M. You, Heater Orientation Effect on Pool Boiling of Micro-Porous-Enhanced Surfaces in Saturated FC-72, ASME Journal of Heat Transfer 118 (1996) 937-943.

[54] K. Nishikawa, Y. Fujita, S. Uchida, and H. Ohta, Effect of Surface Configuration on Nucleate Boiling Heat Transfer, International Journal of Heat and Mass Transfer 27 (9) (1984) 1559-1571.

[55] D. S. Jung, J.E.S. Venart, and A.C.M. Sousa, Effects of Enhanced Surfaces and Surface Orientation on Nucleate and Film Boiling Heat Traansfer in R-11," International Journal of Heat and Mass Transfer 30 (1987) 2627-2639.

[56] C. Beduz, R. G. Scurlock, and A. J. Sousa, Angular Dependence of Boiling Heat Transfer Mechanisms in Liquid Nitrogen, Advances Cryogenic Engineering 33 (1988) 363-370.

[57] S. J. Reed, and I. Mudawar, Elimination of Boling Incipience Temperature Drop in Highly Wetting Fluids Using Spherical Contact with a Flat Surface, International Journal of Heat and Mass Transfer 42 (1999) 2439-2454.

[58] E. Baker, Liquid Cooling of Microelectronic Devices by Free and Forced Convection, Microelectronics and Reliability 11 (1972) 213-222.

[59] K. A. Park, and A. E. Bergles, Effects of Size of Simulated Microelectronic Ships on Boiling and Critical Heat Flux, ASME Journal of Heat Transfer 110 (1988) 728-734.

[60] S. S Kutateladze, and I. I. Gogonin, Critical Heat Flux as a Function of Heater Size for Liquid Boiling in Large Enclosure, Journal of Engineering Physics 33 (1977) 1286-1289.

[61] S. Ishigai, K. Inoue, Z. Kiwaki, and T. Inai, Boiling Heat Transfer from a Flat Surface Facing Downward, In Proceedings of the International Heat Transfer Conference, Boulder, CO (1961) 224-229.

[62] J. H Lienhard, V.K. Dhir, and D.M. Riherd, Peak Pool boiling Heat Flux Measurement on Finite Horizontal Flat Plates, Journal of Heat Transfer 95 (4) (1973) 477-482.

[63] J. R. Saylor, T. W. Simon, and A. Bar-Cohen, The Effect of a Dimensionless Length Scale on the Critical Heat Flux in Saturated, Pool Boiling. ASME Publication HTD 108 (1989) 71-80.

[64] S. J. Kline, and F. A. McClintock, Describing Uncertainties in Single-Sample Experiments, Mechanical Engineering 75 (1953) 3-8.

[65] F. P. Incropera, D. P. Dewitt, T. L. Bergman, and A. S. Lavine, Fundamentals of Heat and Mass Transfer, 6th edition, Wiley, New York (2005) 949-950.

[66] I. L. Pioro, W. Rohsenow, and S. S. Doerffer, Nucleate Pool-boiling Heat Transfer. I: Review of Parametric Effects of Boiling Surface, International Journal of Heat and Mass Transfer 47 (2004) 5033-5044.

[67] K. H. Sun, and J. H. Lienhard, The Peak Pool Boiling Heat Flux on Horizontal Cylinders, International Journal of Heat and Mass Transfer 13 (1970) 1425-1435.

[68] N. Barkhru, and J. H. Lienhard, Boiling from Small Cylinders, International Journal of Heat and Mass Transfer 15 (1972) 2011-2025.

[69] F. Tachibana, and M. Akiyama, Non-Hydrodynamic Aspects of Pool Boiling Burnout, Journal of Nuclear Science and Technology 4 (3) (1967) 121-130.

[70] W. M. Rohsenow, A Method of Correlating Heat Transfer Data for Surface Boiling of Liquids, Tansaction, ASME 84 (1962) 969-975.

[71] V. P. Carey, Liquid-Vapor Phase Change Phenomena: An Introduction to the Thermophysics of Vaporization and Condensation Process in Heat Transfer Equipment, Taylor & Francis, Hebron, KY (1992).

[72] N. Zuber, Hydrodynamic Aspects of Boiling Heat Transfer, AECU (1959) 4439.

[73] K. N. Rainey, and S. M. You, Effect of Heater Size and Orientation on Pool Boiling Heat Transfer from Microporous Coated Surface, International Journal of Heat and Mass Transfer 44 (2001) 2589-2599.

[74] J. H. Lienhard, On the Two Regimes of Nucleate Boiling, ASME Journal of Heat Transfer 118 (1985) 262-264.

[75] R. Cole, and H. L. Shulman, Bubble Departure Diameters at subatmospheric pressure, Chemical Engineering Program Symposium Series 62 (64) (1966) 6-16.

[76] R. Cole, Bubble Frequencies and Departure Volumes at Subatmospheric Pressures, AIChE Journal 13 (1967) 779-783.

[77] S. S. Kutateladze, and I. I. Gogonin, Growth Rate and Detachment Diameter of a Vapor Bubble in Free Convection Boiling of a Saturated Liquids, High Temperature 17 (1979) 667-671.

[78] M. K. Jensen, and G. J. Memmel, Evaulation of Bubble Departure Diameter Correlations, Proceeding 8th International Heat Transfer Conference 4 (1986) 1907-1912.

BIOGRAPHICAL INFORMATION

Sang Muk Kwark received his B.S in Mechanical Engineering at Chungnam National University, Daejeon, Korea in Feb. 2002. He received his M.S. in Mechanical Engineering from The University of Texas at Arlington, Arlington TX in December 2005. He has continued to work for the doctorate degree in the Micro-Scale Heat Transfer Laboratory at the University of Texas at Arlington under Dr. Seung Mun You, focusing on the nanofluid boiling heat transfer.